

https://dspace.org/

Investigation into the microstructure and tensile properties of unalloyed titanium and Ti-6Al-4V alloy produced by powder metallurgy, casting and layered manufacturing

Masikane, Muziwenhlanhla Arnold

2016

http://hdl.handle.net/10539/20060

Downloaded from a DSpace repository. https://dspace.org/

Investigation into the microstructure and tensile properties of unalloyed titanium and Ti-6Al-4V alloy produced by powder metallurgy, casting and layered manufacturing

Muziwenhlanhla Arnold Masikane

A dissertation submitted to the Faculty of Engineering and the Built Environment, University of the Witwatersrand, Johannesburg, in fulfilment of the requirements for the degree of Master of Science in Engineering.

Johannesburg, 2015

DECLARATION

I declare that this dissertation is my own unaided work. It is being submitted for the degree of Master of Science in Engineering to the University of the Witwatersrand, Johannesburg. It has not been submitted before for any degree or examination in any other University.

Muziwenhlanhla Arnold Masikane

-------- day of ----------, 2015

ABSTRACT

Solid titanium (Ti) and Ti-6Al-4V (wt.%) materials were fabricated from powders using spark plasma sintering (SPS), cold isostatic press (CIP) and sinter, layered (rapid) manufacturing, centrifugal and vacuum casing. ASTM Grade 4 Ti, Al and V, 60Al-40V (wt.%) and the pre-alloyed Ti-6Al-4V powders were used as starting materials. The solid Ti and Ti-6Al-4V materials produced by the SPS were compared to the CIP and sinter method on the basis of density, microstructure and chemistry. The materials produced by the CIP and sinter method were also compared to those produced by vacuum casting method on the basis of microstructure, oxygen pick-up, chemistry and room temperature tensile properties. Centrifugal casting was compared to the vacuum casting technique on the basis of microstructural homogeneity. Rapid manufacturing was compared to SPS and CIP and sinter on the basis of microstructural homogeneity, density and tensile properties. The tensile properties of all materials were also compared to their commercial counterparts to investigate the effect of interstitial oxygen. The technology resulting in materials with superior properties was finally identified as most promising for commercial production of Ti-based materials.

On the basis of densification, the SPS method appears superior compared to the CIP and sinter and rapid manufacturing method due to the benefit of pressure aided sintering, while the rapid manufacturing method is superior to the CIP and sinter method due to the use of a high power laser resulting in high densification rates. In cases where microstructural homogeneity is the key requirement, the CIP and sinter and rapid manufacturing methods appear superior compared to the SPS method due to longer isothermal holding time and higher sintering temperature and the use of pre-alloyed Ti-6Al-4V powder, respectively. On the basis of oxygen pick-up and additional contamination, the vacuum casting route is inferior due to the tendency of melt-crucible interaction, resulting in the dissociation of ZrO_2 and subsequent pick-up of O and Zr. Based on the homogeneity of the microstructure, centrifugal casting is better than vacuum casting. The ductility of vacuum cast Ti was better than that of CIP and sintered Ti, possibly due to limited diffusion of oxygen from the crucible compared to oxygen absorbed from the controlled atmosphere during CIP and sinter.

The vacuum casting of the Ti-6Al-4V alloy resulted in dissolution of oxygen and Zr due to melt-crucible interaction. Hence the ductility was worse compared to the alloy produced by CIP and sinter. The rapidly manufactured Ti-6Al-4V specimens exhibited superior ductility and strength compared to all alloys produced by other methods due to the use of high purity starting powder. The tensile properties of these specimens were also comparable to standard requirements. The similarity of the tensile properties of wrought Ti-6Al-4V alloy reported in the literature was an indication of limited oxygen pick-up during rapid manufacturing. Therefore based on low oxygen pick-up, microstructural homogeneity, high density and superior tensile properties, the rapid manufacturing route appears to be the most promising approach for commercial processing of titanium based materials.

DEDICATION

This work would have not been completed if it was not for God's mercy to sustain my life until this time and the support I received from those close to my heart. Therefore I wish to dedicate this work to them.

ACKNOWLEDGEMENTS

The research work of this magnitude is usually almost impossible to complete alone. Therefore I wish to extend my sincere gratitude to a number of people for their support. Professor I. Sigalas, I would have never considered enrolling for postgraduate studies if it was not for his persuasion and the generous financial assistance received from the School of Chemical and Metallurgical Engineering. I also wish to thank him for initiating contact with a number of professionals in the emerging South African titanium industry. I got to meet Pierre Rossouw from the department of Materials Science and Manufacturing (MSM) at the Council for Scientific and Industrial Research (CSIR), whom I wish to thank for offering his expertise on vacuum casting, heat treatment, machining and tensile testing of unalloyed titanium and the Ti-6Al-4V alloy. The additional discussions we had on this subject really helped me to modify some of my experiments to give my work some meaning.

Tapiwa David Mutava, whose friendship and counsel gave me strength during this time, sacrificed a lot of time off his doctoral studies to assist me with centrifugal casting experiments and tension testing of the Ti-6Al-4V specimens obtained by rapid manufacturing. To my love Asiphe Nkolongwane and dear brother Philani Masikane, thank you for taking me in and supporting me emotionally and financially when the bursary ran out. I also wish to acknowledge my other brothers, Ntuthuko Masikane and Sphamandla Masikane, whom the submission of their theses gave me inspiration to complete this work. To my parents, Thulasizwe Masikane and Jabulile Masikane, your love and patience inspired me in more ways than you can imagine. I also wish to extend my appreciation to Dr Olugbenga Johnson who spent long hours on the SEM to examine my specimens. Finally, Doctor Mbense, Xolani Mdletshe and the workshop staff at the School of Chemical and Metallurgical Engineering for transportation to and from various suppliers and service providers which were crucial for this work.

TABLE OF CONTENTS

DECLARATION ii
ABSTRACT iii
DEDICATION v
ACKNOWLEDGEMENTS vi
TABLE OF CONTENTS vii
LIST OF FIGURES x
LIST OF TABLES xv
CHAPTER 1: INTRODUCTION 1
CHAPTER 2: LITERATURE REVIEW 4
2.1 Classification and properties of titanium alloys 4
2.2 Production of pure titanium and titanium alloy powders 6
2.3 Titanium powder metallurgy 7
2.3.1 Compaction of titanium powders 8
2.3.2 Sintering of titanium powders 9
2.3.3 Hot isostatic pressing of titanium and α+β titanium alloys 11
2.4 Casting of titanium 12
2.5 Rapid manufacturing 13
2.6 Heat treatment 13
2.6.1 Heat treatment of pure titanium 13
2.6.2 Heat treatment of α+β titanium alloys 15
2.7 Thermomechanical processing of the α+β titanium alloys 18
2.7.1 Processing route for fully lamellar microstructures 18
2.7.2 Processing route for bi-modal microstructures 20
2.7.3 Processing of fully equiaxed microstructures 21
2.8 Microstructure and mechanical properties of a+ß titanium alloys 22
2.8.1 Effect of lamellar microstructures on the mechanical properties 22
2.8.2 Effect of bi-modal microstructures on the mechanical properties 24
2.8.3 Effect of fully equiaxed microstructures on the mechanical properties 26
2.9 Effect of aging and oxygen content on the mechanical properties 27
CHAPTER 3: EXPERIMENTAL PROCEDURE 29
3.1 Raw materials 29
3.2 Equipment and consumables 30
3.2.1 Milling and blending of raw powders 31
3.2.2 Powder compaction 31

3.2.3 Sintering 32
3.2.4 Casting 33
3.2.5 Hot Isostatic Pressing 34
3.2.6 Heat treatment 34
3.2.7 Characterization techniques 34
3.2.8 Metallographic specimen preparation 35
3.3 Experimental procedures 36
3.3.1 Milling of titanium and Ti-6Al-4V powder mix 36
3.3.2 Blending of titanium powder with a 60Al:40V master alloy powder 37
3.3.3 Compaction of powders 37
3.3.4 Cold isostatic pressing 38
3.3.5 Sintering of titanium powder and Ti-6Al-4V powder mixture 40
3.3.6 Hot isostatic pressing 41
3.3.7 Fabrication of tensile specimens from sintered materials 41
3.3.8 Fabrication of tensile specimens from cast materials 42
3.3.9 Fabrication of tensile specimens using rapid manufacturing 44
3.3.10 Heat treatment 45
3.3.11 Tension testing 46
3.3.12 Metallography 46
CHAPTER 4: RESULTS 48
4.1 Characterization of as-received powders 48
4.2 Milling of pure Ti and blended elemental Ti-6Al-4V powders 54
4.3 Pressing and sintering of titanium powder and Ti-6Al-4V powder 59
4.4 Rapid manufacturing of the Ti-6Al-4Valloy tensile specimens 74
4.5 Casting of pure titanium 76
4.6 Casting of blended Ti-6Al-4V alloy 78
4.7 HIP of Ti and Ti-6Al-4V tensile specimens 79
4.8 Heat treatment 81
4.9 Tension testing 82
4.9.1 Cast titanium tensile specimens 83
4.9.2 Pressed and sintered titanium tensile specimens 86
4.9.3 Cast Ti-6Al-4V tensile specimens 89
4.9.4 Pressed and sintered blended Ti-6Al-4V alloy specimens 90
4.9.5 Rapid manufactured Ti-6Al-4V tensile specimens 92
CHAPTER 5: DISCUSION 96
5.1 Characterization of as-received powders 96
5.2 Attrition milling of titanium powder and blended Ti-6Al-4V powder 97

5.3 Cold compaction of titanium and blended Ti-6Al-4V powder 99
5.4 Sintering of titanium powder and blended Ti-6Al-4V powder 101
5.5 Rapid manufacturing 107
5.6 Casting 108
5.6.1 Centrifugal casting 108
5.6.2 Vacuum casting 109
5.7 Hot isostatic pressing 110
5.8 Heat treatment 111
5.9 Tension testing 112
5.9.1 Cast and sintered titanium 112
5.9.2 Cast and sintered blended elemental Ti-6Al-4V alloy 114
5.9.3 Rapidly manufactured pre-alloyed Ti-6Al-4V alloy 114
CHAPTER 6: CONCLUSIONS AND RECOMMENDATIONS 116
6.1 Conclusions 116
6.2 Recommendations 118
REFERENCES 120

LIST OF FIGURES

Figure 2.1: Pseudo-Binary phase diagram of Ti-6Al-4V alloy [2012Wan] 17
Figure 2.2: Diagram of a fully lamellar microstructure of α+ β titanium alloy [2001Chr] 18
Figure 2.3: Bi-modal microstructure of the Ti-6Al-4V alloy [2002Nal] 20
Figure 2.4: Fully equiaxed microstructure of the Ti-6Al-4V alloy [2002Bie] 21
Figure 3.1: Spark plasma sintering (SPS) furnace 32
Figure 3.2: Leybolt Heraeus ISPIII/Ds three chamber vacuum furnace 34
Figure 3.3: Titanium rods produced by cold isostatic pressing at a pressure of 700 MPa 39
Figure 3.5: A 2 kg titanium billet formed by cold isostatic pressing at a pressure of 400 MPa. 39
Figure 3.4: Exterior appearance of the tensile specimens machined from pressureless sintered titanium rod 42
Figure 3.6: Cylindrical ingot obtained by vacuum casting of the cold isostatically pressed CP-Ti billet 43
Figure 3.7: Cylinders cut out from the (a) top section and (b) bottom section of the titanium ingot obtained by conventional casting under vacuum 44
Figure 3.8: Cast titanium tensile specimen 44
Figure 3.9: Exterior appearance of the fine polished Ti-6Al-4V specimen produced by rapid manufacturing 45
Figure 4.1: Particle size distribution of as-received commercial grade titanium powder 48
Figure 4.2: Particle distribution of as-received 60Al-40V master alloy powder 49
Figure 4.3: Particle size distribution of vanadium elementary powder 49
Figure 4.4: Particle size distribution of aluminium elementary powder 49
Figure 4.5: Particle size distribution of the pre-alloyed Ti-6Al-4V powder 50
Figure 4.6: Particle morphology of the as-received (a) pure Ti, (b) 60Al:40V master alloy and (c) pre-alloyed Ti-6Al-4V powders 50
Figure 4.7: EDS chemical analysis of the 60Al:40V master alloy powder 51
Figure 4.8: EDS analysis of the pre-alloyed Ti-6Al-4V powder 52

Figure 4.9: XRD pattern of as-received 60Al-40V master alloy powder 53
Figure 4.10: XRD pattern of as-received pre-alloyed Ti-6Al-4V powder..... 53
Figure 4.11: PSD curve of the blended elemental Ti-6Al-4V powder obtained by alloying additions in the form of elemental powders..... 55
Figure 4.12: EDS spectra of the blended elemental Ti-6A-4V powder obtained by alloying additions in the form of elemental powders..... 55
Figure 4.13: PSD curve of the blended elemental Ti-6Al-4V after attrition milling at 1350 rpm for 1 hour 56
Figure 4.14: PSD curve of the commercial grade titanium powder after attrition milling at 1350 rpm for 1 hour..... 56
Figure 4.15: SEM backscattered images of cross-sectioned (a) as-received pure Ti powder particles (b) pure titanium powder particles after 1 h of milling at a fixed speed of 1350 rpm (c) manually mixed Ti-6Al-4V alloy powder particles and (d) manually mixed Ti-6Al-4V alloy powder particles after 1 hour of milling at a fixed speed of 1350 rpm..... 57
Figure 4.16: EDS microanalysis of the Ti-6Al-4V powder produced using the attritor mill at fixed speed of 1350 rpm for 1 hour 57
Figure 4.17: XRD pattern of the attrition milled blended elemental Ti-6Al-4V powder 58
Figure 4.18: Compaction curve of unalloyed titanium powder 60
Figure 4.19: Compaction curve of the blended Ti-6Al-4V powder..... 61
Figure 4.20: Effect of sintering temperature on the linear shrinkage of a titanium pellet..... 62
Figure 4.21: Variation of the density of titanium compacts with spark plasma sintering temperature 63
Figure 4.22: Optical micrographs of pressed titanium pellets after sintering at (a) 600°C and (b) 750°C for 10 minutes in the SPS furnace..... 63
Figure 4.23: Optical micrographs of pressed titanium compacts after sintering at (a) 800°C and (b) 1000°C (c) 1200°C and (d) 1250°C for 10 minutes in the SPS furnace 64
Figure 4.24: SEM microstructure of the Ti-6Al-4V alloy obtained by cooling from a sintering temperature of (a) 1000°C at low magnification, (b) 1000°C at high magnification, (c) 1100°C at low magnification and (d) 1100°C at high magnification 65

Figure 4.25: SEM microstructures of the Ti-6Al-4V alloy obtained by cooling from a sintering temperature of (a) 1200°C at low magnification (b) 1200°C at high magnification, (c) 1250°C at low magnification and (d) 1250°C at high magnification 66
Figure 4.26: EDS spectra of the Ti-6Al-4V alloy obtained by cooling from temperatures in the range of 1000 °C and 1100 °C in the SPS furnace.....67
Figure 4.27: Phase composition of the Ti-6Al-4V alloy obtained by cooling from 1000°C at a rate of 250°C/min in the SPS furnace under vacuum 67
Figure 4.28: Phase composition of the Ti-6Al-4V alloy obtained by cooling from 1100°C at a rate of 250°C/min in the SPS furnace under vacuum 68
Figure 4.29: Phase composition of the Ti-6Al-4V alloy obtained by cooling from 1200°C at a rate of 250°C/min in the SPS furnace under vacuum 68
Figure 4.30: Phase composition of the Ti-6Al-4V alloy obtained by cooling from 1250°C at a rate of 250°C/min in the SPS furnace under vacuum 69
Figure 4.31: Effect of sintering temperature on the sintered density of blended elemental Ti-6Al-4V compacts.....69
Figure 4.32: Microstructure of the titanium rods produced by cold isostatic pressing at 700 MPa followed by conventional sintering at 1350 °C for 1 hour.....71
Figure 4.33: Optical microscopic structure of a cold isostatically pressed and sintered Ti-6Al-4V rod at (a) low magnification and (b) higher magnification.....73
Figure 4. 34: EDS spot analyses of (a) grains, (b) grain boundaries and (c) overall cross-section of Ti-6Al-4V alloy rods produced by the CIP and pressureless sinter method.....74
Figure 4.35: Outer appearance of the Ti-6Al-4V tensile sample fabricated by the rapid manufacturing route.....74
Figure 4.36: SEM microstructure of the Ti-6Al-4V tensile specimens fabricated by the rapid manufacturing method.....75
Figure 4. 37: EDS spot analysis of Ti-6Al-4V specimen produced directly from pre-alloyed powder using rapid manufacturing.....76
Figure 4.38: Titanium tensile specimen obtained by casting in a centrifugal field 76
Figure 4.39: Optical micrographs of the titanium tensile specimen obtained by centrifugal casting.....77
Figure 4.40: Optical microscopic structure of CP-Ti obtained by conventional casting in a vacuum chamber furnace at (a) low magnification and (b) higher magnification 77

Figure 4.41: Microstructure of the Ti-6Al-4V tensile specimen produced by (a) centrifugal casting, (b) vacuum casting and (c) EDS spot analysis of vacuum cast Ti-6Al-4V alloy 79
Figure 4.42: Microstructure of a pressed and sintered titanium rod in the HIP'ed condition 79
Figure 4.43: Microstructure of the pressed and sintered Ti-6Al-4V alloy in the HIP'ed condition 80
Figure 4.44: Microstructure of vacuum cast titanium in the HIP'ed condition 80
Figure 4.45: Microstructure of cast Ti-6Al-4V alloy in the HIP'ed condition 81
Figure 4.46: Exterior appearance of the titanium specimen after annealing and tensile testing, showing a slight discoloration 82
Figure 4.47: Microstructure of the rapidly manufactured pre-alloyed Ti-6Al-4V (a) in the as-fabricated condition, (b) after annealing at 750°C for 2 hours and (c) 850°C for 2 hour followed by furnace cooling 82
Figure 4.48: Effect of annealing on the mean strength and ductility of cast plus HIP'ed unalloyed titanium 85
Figure 4.49: Tensile stress-strain curve of test specimens machined from the top section of the vacuum cast unalloyed titanium ingot 85
Figure 4.50: Tensile stress-strain curve of test specimens machined from the bottom section of the vacuum cast unalloyed titanium ingot 86
Figure 4.51: Exterior appearance of the gage length of a fractured unalloyed vacuum cast titanium tensile specimen 86
Figure 4.52: Tensile stress-strain curve of the pressed and sintered titanium test specimen CP-Ti2 88
Figure 4.53: Tensile stress-strain curve of the pressed and sintered titanium test specimen CP-Ti7 88
Figure 4.54: Tensile stress-strain curve of the pressed and sintered titanium test specimen CP-Ti9 89
Figure 4.55: Tensile stress-strain curves of the HIP'ed and annealed vacuum cast Ti-6Al-4V alloy 90
Figure 4.56: Tensile stress-strain curve of the of the HIP'ed and annealed sinteredTi6Al-4V alloy 92
Figure 4.57: Pre-alloyed Ti-6Al-4V specimen showing a significant reduction in area and a cup and cone ductile fracture 93

Figure 4.58: Effect of annealing temperature on the mean strength and ductility of the rapidly manufactured Ti-6Al-4V alloy 94
Figure 4.59: Tensile stress-strain curves of the laser formed Ti-6Al-4V specimens... 95

LIST OF TABLES

Table 2.1: Typical stress relief treatments for α+β titanium alloys [2000Don].....16
Table 2.2: Effect of various heat treatments on the microstructure of α+β titanium alloys [2000Don] 17
Table 2.3: Qualitative correlation between important mechanical properties and microstructural features for fully lamellar structures of α+β titanium alloys [2003Lut] 23
Table 2.4: Effect of microstructure on tensile properties of Ti-64 at room temperature and at 600°C [1998Lut] 24
Table 2.5: Qualitative correlation between mechanical properties and important microstructural features for bi-modal structures of α+β titanium alloys [2003Lut] 26
Table 2.6: Qualitative correlation between mechanical properties and important microstructural features for fully equiaxed structures of α+β titanium alloys [2003Lut] 26
Table 4.1: Oxygen content of raw powders as determined by Leco.....54
Table 4.2: Oxygen analysis of attrition milled powders as determined by Leco.....59
Table 4.3: Comparison between oxygen content of as-received Ti and Ti-64 mix prepared by Turbula mixing.....59
Table 4.4: Density of CP-Ti rods obtained by cold isostatic pressing at 700 MPa 70
Table 4.5: Density of P/M Ti rods after sintering at 1350°C for 1 hour.....71
Table 4.6: Densities of Ti-6Al-4V rods obtained by cold isostatic pressing at 700 MPa 72
Table 4.7: Densities pressed Ti-6Al-4V rods after sintering at 1350°C for 1 hour.....72
Table 4.8: Density of the laser fabricated Ti-6Al-4V tensile specimens.....75
Table 4.9: Gas analysis of vacuum cast titanium.....78
Table 4.10: Tensile properties of vacuum cast unalloyed titanium 84
Table 4.11: Tensile properties of unalloyed titanium produced by CIP and sintering 87
Table 4.12: Tensile properties of vacuum cast blended Ti-6Al-4V alloy.....90
Table 4.13: Tensile properties of the sintered, HIP'ed and annealed Ti6Al-4V tensile specimens.....91

Table 4.14: Tensile properties of the pre-alloyed Ti-6Al-4V alloy produced by rapid manufacturing 93

CHAPTER 1: INTRODUCTION

Titanium is the fourth most abundant metal after aluminium, iron and magnesium and accounts for 0.6% of the metals in the earth's crust [2003Lut]. The most common mineral sources for this material are ilmenite ($FeTiO_3$) and rutile (TiO_2), the latter being the most titanium rich mineral containing approximately 95% TiO_2, while ilmenite contains between 40 and 65% TiO_2 [2011Zha]. Although it has long been known that titanium has an attractive combination of mechanical properties compared to other common structural materials, the high cost associated with the extraction of the metal from the mineral sources, and the cost of processing the raw titanium metal powder into usable products hinders its application in many industries [1996All, 2004Don, 2009Soe, 2011Oos]. In the past years, the cost of extracting titanium was estimated to be 20 times that of steel on a 1:1 weight basis, and approximately 11 times when the density of titanium is taken into account [2001Ger]. However, a recent patent by Pretorius [2006Pre] offers prospects for reducing the cost of titanium metal powder production by using a much simpler and cheaper process compared to the most widely used chemical reduction process. Further progress is the ability of the recently developed rapid prototyping (RP) or rapid manufacturing (RM) technology to rapidly build metal components of complex shape and accurate dimensions directly from metal powder. This technology promises a higher reduction in production costs and delivery time for the manufacturing industry compared to traditional metal forming operations such as casting.

It has been reported that the production of titanium based materials by the traditional casting method requires the use of special refractory materials for the lining of melting crucibles to prevent chemical attack by the titanium melt [2000Yas]. Additionally, the melting of titanium powder requires strict control of the atmosphere in the furnace to prevent oxygen contamination [2006Jov]. Therefore this may impose additional costs due to the need for specialised equipment. Furthermore, titanium components produced through conventional casting have been observed to have a poor density due to shrinkage porosity resulting from the inadequate filling ability of the melt in the mould during casting [2008Sui]. These challenges, with others, have

served as the motivation for most researchers over the past years to investigate alternative metallurgical processes and technologies for producing titanium components directly from powder without melting.

The ability of the powder metallurgy (PM) methods to produce net-shape components directly from powders while simultaneously reducing material input and fabrication costs makes it an attractive alternative for the production of titanium parts [1981Smu]. The two classical PM methods for producing useful titanium alloys, such as Ti-6Al-4V, are the pre-alloyed and blended elemental approach [1996Fuj, 2012Bol1]. A typical pre-alloyed method begins with the melting of a pre-alloyed bar or billet into a homogeneous liquid metal which is subsequently poured and atomized by a high pressure inert gas to form a metal powder usually consisting of spherical particles. In contrast, the blended elemental route involves the mixing of pure titanium powder with alloying additions either in the form of a master alloy or elemental powders. The blended powder is then cold pressed and sintered to produce a homogeneous alloy [2011Gos]. While some researchers [1996Fuj, 2011Gos] are confident that titanium alloys with a relative density over 99.5% can be produced using the blended elemental method, others [2012Bol1] argue that the presence of chlorides in the titanium sponge can hinder the closure of residual porosity during sintering.

Gas atomized titanium powders are known to contain less of the chlorides compared to the titanium sponge usually produced through the Kroll process. However, this powder consists of spherical particles which are difficult to consolidate at room temperature and it is therefore seldom used in the conventional cold pressing and sintering method. Nevertheless, the good flowability characteristics of these powders can be taken advantage of in the recently developed additive or rapid manufacturing method. Rapid manufacturing begins with generating a computer aided design (CAD) model of the object to be built. The model is thereafter mathematically sliced into thin layers and the powder is successively sintered and melted by a high powered laser or electron beam, one layer at a time, until a three dimensional component is built [2009Wil, 2012Gu]. Although there are many additive manufacturing processes, several authors [2007Kru, 2010Fac, 2012Gu] regard direct metal laser sintering (DMLS) and selective laser melting (SLM) as the most versatile due to their capability to process a wide range of metals, ceramics, alloys and metal matrix

composites (MMCs). Gu et al. [2012Gu] mention that a relative density of approximately 99.5% can be achieved in SLM-processed pure metals. The main features of the SLM process include the possibility of processing pure metals such as Ti, Al and Cu which cannot be processed by DMLS method to date [2012Gu].

The aim of this research is to investigate the link between microstructure, tensile properties and processing of solid Ti and Ti-6Al-4V materials from powder. The main objective is to demonstrate the production of solid titanium and Ti-6Al-4V alloy materials from cheap powders using advanced and conventional technologies, and compare their properties to identify the best approach. Advanced technologies investigated include spark plasma sintering (SPS), cold isostatic press (CIP) and sinter, hot isostatic pressing (HIP), rapid manufacturing and centrifugal casting. The three former technologies are considered as powder metallurgy methods in this work, and vacuum casting is identified as the conventional method for shaping of titanium materials. Although the properties of interest are primarily the density, microstructure and tensile properties, others such as oxygen pick-up, phase and chemical composition are also considered for academic interest.

In order to fulfil the above mentioned aim and objective, this work is approached as follows. An extensive literature review on the classification and properties of titanium alloys, production of titanium metal powders, advanced and conventional technologies for producing solid titanium materials, effect of heat treatment and thermomechanical processing on the microstructure and tensile properties and the effect of oxygen content and aging on the tensile properties of titanium and Ti-6Al-4V material is presented in Chapter 2. The raw materials, equipment, consumables and experimental procedures followed are highlighted in Chapter 2. The results obtained from experimental work are presented in Chapter 4 and critically analysed in Chapter 5. Finally, the best approach is identified in the conclusion section under Chapter 6 and the necessary recommendations are made.

CHAPTER 2: LITERATURE REVIEW

The aim of this chapter is to show, by referring to literature, that titanium powder metallurgy and laser sintering technologies are ideal replacements of conventional methods. The conventional methods referred to here are casting and thermomechanical processing. The objective is to identify the challenges and achievements associated with processing of titanium materials, as reported in publications accessible during this time. To begin with, the properties of pure titanium and the criteria used to categorize titanium alloys are highlighted. The extraction of titanium powder from mineral sources and subsequent processing into functional components are critically reviewed in order to identify the key factors driving the cost of titanium products. The processing steps associated with the most popular conventional and advanced technologies are discussed in detail, and the quality of the resultant materials is evaluated with reference to critical properties such as density, microstructure and mechanical properties. Finally, the effect of post-processing operations such as heat-treatment and aging, and interstitial oxygen on the mechanical properties is reviewed.

2.1 Classification and properties of titanium alloys

Commercial purity titanium (CP-Ti) exhibits a hexagonal close packed (hcp) structure of the α-phase and transforms to the β phase with a body centred cubic (bcc) crystal structure upon heating above the β transus temperature [2000Don]. The β transus temperature is dependent on the purity of the titanium powder, ranging from 910±15°C for commercially purity Ti with 0.25 wt. % O_2 to 945±15°C for Ti with 0.40 wt. % O_2 [1990ASM]. The addition of specific alloying elements in sufficient proportions makes it possible to stabilize either the α phase or the β phase or to promote the co-existence of both phases at room temperature. Therefore the alloying additions are usually classified as either α stabilizers or β stabilizers, depending on their effect on the α and β phases. Alloying elements which increase the temperature range over which the α phase is stable are called α-stabilizers, and typical examples include aluminium, oxygen and nitrogen. The elements which decrease the β transus temperature are called β-stabilizers [2000Don]. The most common β-stabilizers

include vanadium, molybdenum and iron [2012Wan]. Therefore due to this, it is common practice to classify titanium alloys into α, α+β and β alloys [2000Don].

The α-alloys are exclusively composed of α stabilizing elements and/or neutral elements; and their examples include all commercial grades of pure titanium [2003Ley, 2012Wan]. Due to the single phase nature of α-alloys, they cannot be heat treated to manipulate their microstructure and mechanical properties [2000Don]. If minor fractions of β stabilizing elements are added to these alloys, they are referred to as near-α alloys. The combination of excellent creep properties and high strength of α-alloys makes these alloys suitable for high temperature applications.

The α+β titanium alloys are classified as alloys which permit complete transformation of the α phase to β-phase on heating above the β transus and transform to α-phase plus retained and/or transformed β-phase on cooling to lower temperatures [2000Don]. These alloys are known to contain β volume fractions ranging from 5 to 40% [2003Ley]. The Ti-6Al-4V alloy is by far the most widely used α+β titanium alloy, and accounts for approximately 50% of commercial titanium alloys [2000Don, 2003Ley]. The ability of this alloy to permit the co-existence of α and β phases at room temperature makes it possible to obtain a wide range of microstructures and combinations of mechanical properties by heat treatment [2000Don, 2005Zhe, 2012Wan]. The preferential use of Ti-6Al-4V alloy in several industries is mainly due to a combination of corrosion resistance, moderate ductility and high strength-to-weight ratio. The α+β alloys are characterized by good fabricability as well as high room temperature strength and moderate elevated temperature strength.

Finally, the β-alloys are composed of extremely high concentrations of β stabilizing elements and they are extremely formable. The microstructure of these alloys consists mainly of the β phase. However, it should be noted that these alloys are prone to ductile-brittle transformation and they are therefore not suitable for cryogenic applications [2005Zhe]. The β-alloys are also characterized by their high specific weight, modest weldability, poor oxidation resistance, and complex microstructure, all of which limit their use in most industrial applications. Although titanium alloys are attractive for a range of engineering applications, their relatively high cost has

limited their use in special applications, such as in the aerospace and military industries [2012Bol].

2.2 Production of pure titanium and titanium alloy powders

The most widely used commercial processes for manufacturing titanium powders include chemical reduction, hydrogen-dehydrogenation, gas atomization, plasma rotating electrode and plasma (PREP). Of these processes, chemical reduction is the primary method for producing pure titanium powder. The chemical reduction route generally begins with the chlorination of natural or synthetic rutile (TiO_2) in a fluidized bed reactor at 1000°C to produce a chloride salt ($TiCl_4$) according to Equation 1 [2001Ger].

$TiO_2 + 2Cl_2 + C \rightarrow TiCl_4 + CO_2$ **Equation 1**

The $TiCl_4$ is then reduced with either magnesium (Kroll process) or sodium (Hunter Process) in an inert atmosphere to form titanium metal powder. The Kroll process, introduced by William J. Kroll in the 1930s, involves the reduction of $TiCl_4$ at temperatures in the range of 800 – 900°C according to Equation 2 [2001Ger].

$TiCl_4 + 2Mg \rightarrow Ti + 2MgCl_2$ **Equation 2**

Due to the fact that magnesium is fed in excess of 15 to 30%, the retort usually contains unreacted magnesium together with $MgCl_2$ and titanium at the end of the process. The separation of titanium from magnesium and $MgCl_2$ is achieved by vacuum distillation. Vacuum distillation is achieved by heating up the retort under vacuum, thereby causing the removal of volatile magnesium and $MgCl_2$ while leaving behind porous titanium also referred to as titanium sponge. Although the Kroll process is perceived as relatively expensive and inefficient due to a series of batch steps which are labour intensive, it is still by far the most widely used commercial method for producing titanium powder. The disadvantage of this process is that the production of the powder is time consuming and labour intensive.

The Hunter process is very similar to the Kroll process, except for the use of sodium as a substitute for magnesium. Due to the fact that the Hunter process is more expensive, it is only used to produce high purity titanium for special applications [2001Ger]. The high costs associated with the extraction of titanium and production of titanium products using conventional metal forming processes has generated interest among researchers to investigate and develop alternative materials processing methods.

2.3 Titanium powder metallurgy

The emphasis of powder metallurgy (PM) is usually on the shaping of near-net-shape metallic components directly from powdered materials in the solid state [1983Ram]. The preferential use of powder metallurgy is mainly due to its ability to produce complex components, such as tungsten filament and porous self-lubricating bearings, which are otherwise difficult or impossible to make through conventional metal shaping operations.

A traditional powder metallurgy process usually involves the blending of the metal powders with other constituents, such as a binder material, followed by compaction in the die at room temperature to form a component of a desired size and shape [1983Ram]. The green compact is then sintered at elevated temperatures, usually below the melting point of the major constituent, to achieve full density. Alternatively, the compaction and sintering steps can be combined into a single step in hot isostatic pressing (HIP).

The high cost of good quality titanium powder and the inability to achieve full density without including a secondary densification step, such as HIP, undermines the benefits of powder metallurgy [2010Ger]. However, the blended elemental (BE) approach offers prospects for eliminating the need for secondary densification. The BE method involves blending of the titanium powder with alloying additions, followed by the cold compaction of the mixture in a die to form a green compact. Finally, the heterogeneous powder compact is sintered to form a homogeneous alloy. Smugeresky and Dawson [1981Smu] and Fujita et al. [1996Fuj] investigated the sintering behaviour of blended elemental Ti-6Al-4V alloy, and it was found that fully

dense compacts could be produced by sintering at 1260°C for 4 hours under a vacuum pressure of approximately 10^{-3} Pa. Welsch et al. [1983Wel] investigated the deformation behaviour of blended elemental Ti-6Al-4V compacts sintered to 99% of the theoretical density, and the alloy was found to have a good yield strength and ultimate tensile strength as well as good ductility. However, it should be noted that the density obtained after sintering is also dependent on the composition of starting powders. For example, the use of titanium-hydride metal powder results in high densification rates during sintering and highly dense sintered compacts compared to pure Ti metal powder [2010Rob]. The cold compaction pressure also has an effect on the level of densification achieved after sintering. Froes and Williams [1986Fro] demonstrated that a fully dense sintered PM titanium component can be produced if the green density is in the range of 85-90%.

2.3.1 Compaction of titanium powders

The conventional powder compaction process involves loading the powder into the die with the shape and size of the desired part and compressed under a uniaxial load. The main objective for pressing is usually to form a compact with sufficient strength for safe handling in downstream processes. Powder compaction generally occurs in three stages, which involve particle rearrangement, particle deformation and particle impingement [2012Chen, 2010Ger]. Although die pressing is widely used in powder metallurgy, it has limitations due to the possible variation of the green density at different parts of the pressed component as a result of inter-particle and particle-die wall friction. The effect of friction is usually overcome by light application of a suitable lubricant on the wall of the die or by mixing the lubricant into the powder. Ederer [1999Ede] studied the effect of zinc stearate on the compaction and sintering characteristics of a Ti-6Al-4V hydride-dehydride (HDH) powder; it was found that mixing 0.5 wt. % of this lubricant with the powder increased the green density and sintered density by at least 4% and 2 to 6 % respectively compared to when no lubricant was used. The low melting point of zinc stearate (120−130°C) made it possible to burn off most of the lubricant prior to sintering, while its low density of 1.095 g/cm^3 ensured minimal contamination of the sintered part. It should be noted that, for thick or large compacts, the force required to eject the pressed compact

rapidly increases after a few runs, resulting in a compact eventually seizing inside the die when no lubricant is used [1999Ede]. The limitations of die pressing makes cold isostatic pressing (CIP) an attractive technique for compaction of large components.

The CIP method involves loading the powder in an enclosed rubber membrane, and a hydrostatic fluid pressure is applied at ambient temperature. This technique is most suitable for production of semi-fabricated products such as bars and cylinders. Although it is possible to apply pressures as high as 1400 MPa during cold isostatic pressing, pressures in the range of 350−700 MPa are typical in commercial operations [2010Ger]. Under such commercial operations, the resultant compacts are not fully dense and therefore require further densification by either sintering or HIP or both.

2.3.2 Sintering of titanium powders

The sintering behaviour of powders is usually investigated by dilatometric studies. For titanium powders, this technique involves pressing the powder in a cylindrical die to form pellets which are subsequently heated at a constant rate to temperatures in the range of 700−1250°C in a dilatometer. Each pellet is then isothermally held for approximately 1 hour at that specific temperature followed by slow cooling [2006Dab]. The change in the height of the compact is recorded throughout the sintering cycle in order to study the rate of linear shrinkage and variation of density with sintering temperature. A commercial sintering process usually involves heating powder compacts at temperatures below the melting temperature of the major constituent. The objective of the sintering is usually to promote densification and simultaneous formation of a chemically homogeneous material due to mutual diffusion [2002Iva].

The particle size is among other factors which determine the sintering behaviour of powders. Sintering temperatures in the range of $0.5-0.8T_m$ are typical for conventional titanium powders, while the sintering of titanium nano-powders initiates in the range of $0.2-0.3T_m$ where T_m is the melting temperature [2006Dab]. By definition, nano-powders are particulate materials with a particle size in a nanometric range (<100 nm) and they are known to contain a high density of defects which are

expected to act as an additional driving force during sintering [2001Dab, 2006Dab]. Although several mechanical milling methods can be used to produce nano-powders, attrition milling is by far the most preferred due to its ability to produce large quantities of material in the solid state at room temperature by using simple equipment [2001Dab]. Dabhade et al. [2001Dab] demonstrated that a titanium powder with an average particle size of 35 nm can be produced by attrition milling of conventional titanium powder at 450 rpm for 30 hours. It is common practice to mill titanium powders under an inert gas atmosphere. The protective gas serves to limit or eliminate the contamination of the powder by oxygen due to the constant exposure of fresh metal to normal atmosphere during subsequent milling [2001Dab]. However, contamination may also come from the erosion of the milling media over time. Attrition milling has also been widely used for solid state alloying (mechanical alloying) of metal powders, such as the Ti-6Al-4V alloy. During mechanical alloying, elemental powders are mixed in desired proportions and fed into the mill containing suitable grinding media. The mixture is then milled for a given period of time under a protective atmosphere until the elemental composition of every particle almost matches that of the starting powder mixture [2012Mah].

It should be noted that for PM titanium products to have mechanical properties suitable for a practical application, a relative density not less than 98% must be obtained after sintering [2002Iva]. However, Ivasishin et al. [2002Iva] mention that the relative density of PM α+β titanium alloys produced by conventional cold pressing and sintering hardly exceeds 95%, while Froes and Williams [1986Fro] demonstrated that a fully dense sintered Ti-6Al-4V alloy can be obtained if the relative green density of a cold compacted blended elemental powder is in the range of 85−90%. Furthermore, Robertson et al. [2009Rob] proved that green densities over 95% of the theoretical could be obtained when hydrogenated Ti powders are used as a substitute for pure titanium powders. This is mainly due to the fact that titanium hydride powders are brittle and fracture to form finer particles during compaction, resulting in smaller pores which may be easily closed during sintering [2009Rob].

Regardless of the realization that full density can be obtained after the sintering of compacts based on TiH_2 powder, the Ti-6Al-4V alloy is known to suffer from additional porosity due to phase and structural transformations [2002Iva]. Ivasishin et

al. [2002Iva] investigated the synthesis of the Ti-6Al-4V alloy by using the blended elemental method and recommended that additional porosity can be avoided by using a master alloy with a high melting point compared to elementary aluminium powder, or by activating the powders through preliminary mechanical working in order to promote the reaction of titanium with aluminium below the melting point of aluminium. This serves to avoid the violent reaction of molten elemental aluminium with titanium to form secondary brittle phases such as titanium aluminide [2002Iva].

Among other difficulties associated with thermal processing of titanium-based materials is the rapid oxidation of titanium at temperatures over 600°C [2003Chan]. Therefore PM titanium alloys are usually sintered under vacuum or inert gas atmosphere. Industrial argon gas is normally used in cases where an inert gas atmosphere is desired. It is also possible to upgrade the purity of the Ar gas by passing it through an oxygen getter furnace or oxygen trap prior to introducing it into the sintering furnace [2006Pan]. Gas purification is achieved by the absorption of oxygen from the stream of Ar gas by a material which has a high affinity for oxygen at near-ambient temperatures such as activated copper oxide. Another challenge with processing of titanium is that the more thermal processing steps are involved, the higher is the risk of oxygen contamination. Titanium is also known to suffer from grain growth when the heat treatment temperature and the heat treatment time are increased, and this may have a negative effect on a range of properties including mechanical strength, toughness and hardness [1995Gil]. These challenges make spark plasma sintering (SPS) an attractive technique over conventional sintering due to the application of high heating and cooling rates and short sintering times under vacuum. This method also allows for simultaneous pressing of the powder during sintering thus resulting in denser sintered materials compared to conventional sintering [2006Han].

2.3.3 Hot isostatic pressing of titanium and α+β titanium alloys

Hot isostatic pressing (HIP) is a PM method used for the secondary densification of cold compacted and sintered metallic or ceramic materials by the application of a hydrostatic gas pressure at temperatures below the melting point of the major constituent. For titanium alloys, a pressure of about 105 MPa is normally applied for 2−4 hours while simultaneously heating the compact at temperatures in the range of

845−955°C [2008Lap]. Delo and Piehler [1999Del] studied the HIP of blended elemental Ti-6Al-4V powder and found that relative densities in the range of 98−100% can be obtained if the powder is heated at temperatures in excess of 800°C, while simultaneously applying compressive pressures in the range of 10−60 MPa for 1 hour [2000Lap].

2.4 Casting of titanium

Casting is another conventional metal shaping process used for manufacturing titanium products, and it offers a significant reduction of material losses and production costs over forging and machining [2007Ber]. However, the high affinity of titanium for oxygen at slightly elevated temperatures makes it difficult to produce high quality castings [2006Jov]. In order to avoid oxygen contamination, melting and pouring of titanium and titanium alloys is usually performed under vacuum. The moulds used in conventional casting of titanium may include graphite and ceramic moulds. These moulds are usually coated with a chemically stable material or compounds which are slightly reactive with the melt in order to decrease the probability of melt-mould interaction [2006Jov]. Additionally, the poor flowability of the melt makes the casting prone to generating porosity during solidification. In order to improve the filling and feeding of the melt during pouring of the melt into the mould, it is recommended that titanium melts be poured in a centrifugal field [2007Sui].

Investment casting has been used for centuries to produce materials with excellent dimensional accuracy, surface finish and complex shapes, and it is the most fully developed net-shape technology [2012Sar, 2009Jov]. This process involves forming the desired shape, usually out of wax, which is then placed inside a cylinder. Plaster is poured inside the cylinder and allowed to harden around the wax pattern. The investment is then heated in a kiln to burn off the wax, and the molten metal is poured into the cavity left by the wax. When solidification is complete, the plaster is chipped off to reveal the as-cast metal [2012Sar]. The process has been investigated by several researchers [2002Kim, 2004Hun, 2012Sar] over the past years for net-shape processing of titanium and titanium alloy products.

2.5 Rapid manufacturing

The additive or layered manufacturing method is a cost effective method by which complex titanium components can be rapidly built one layer at a time directly from metal powders using a high powdered laser or electron beam under vacuum. The most popular layered manufacturing techniques include photo-polymerisation (Stereo lithography (SLA) and its derivatives), ink-jet printing (IJP), 3D printing (3DP), fused deposition modelling (FDM), selective laser sintering or melting (SLS/SLM), electron beam melting (EBM) and to a lesser extent, laminated object manufacturing (LOM) and laser cladding (LC) [2007Kru]. Kruth et al. [2007Kru] categorises these processes into two classes, namely rapid prototyping (RP) and rapid manufacturing (RM). While RP is only used to produce test parts which are used in the product development stage, RM is mostly used for the fabrication of usable parts [2007Kru]. The SLS and SLM methods are the most versatile among other rapid manufacturing methods. These processes are capable of processing a variety of metals, polymers, ceramics and a wide range of composites [2007Kru]. Just like most layered manufacturing processes, SLS/SLM mainly begins with generating a computer aided design of part to be fabricated. The design is thereafter mathematically sliced into thin layers followed by intermittent addition of the metallic powder which is continuously scanned by a laser or electron beam one layer at a time until a three dimensional part is built [1991Kru].

2.6 Heat treatment

2.6.1 Heat treatment of pure titanium

Heat treatment is a fundamental metallurgical process which involves controlled heating and cooling of metals and alloys to alter their physical and mechanical properties without changing the shape of the material. All commercial grades of unalloyed titanium are classified as α-alloys, and one feature of these alloys is that they cannot be heat treated to manipulate their microstructure and to obtain high strength [2000Don]. Therefore pure titanium is usually heat treated at temperatures in the range of 480−595°C for the relief of undesirable residual stresses due to thermomechanical processing, cold forming, machining, welding and unequal cooling

[2000Don]. All grades of titanium can also be annealed at temperatures in the range of 650−760°C followed by air cooling.

Donatchie [2000Don] recommends that any heat treatment at temperatures above approximately 427°C must be performed under a protective atmosphere that prevents the pickup of oxygen and formation of the alpha case. Dobeson et al. [2011Dob] investigated the effect of oxygen contamination on the tensile properties of commercial wrought ASTM grade 2 titanium containing 0.15 wt. % O. Samples were annealed at temperatures below and above the β-transus temperature, 900°C and 950−1050 ºC respectively. Microstructural examinations showed that the cross-section of cylindrical samples heat treated in air consisted of three concentric regions. The first region was a layer rich in oxygen, also referred to as the alpha case, formed on the outer surface of the rod, followed by an inner second region of stabilized α which was formed by the diffusion of oxygen deep into the sample. The innermost region of the samples which were heat treated below the beta transus consisted of equiaxed α grains, while the samples which were heat treated above the β-transus temperature (T_β) underwent a phase transformation to form colonies of aligned α laths inside prior β grains upon cooling.

Furthermore, a small variation in hardness values was observed for samples treated at temperatures below the β-transus as the cross-section was traversed from the outer surface towards the centre. This phenomenon was attributed to the fact that no appreciable change in microstructure took place when cooling from heat treatment temperatures below T_β. By contrast, samples cooled from temperatures above T_β exhibited higher hardness values. The increase in hardness was mainly attributed to a combination of phase transformation, from equiaxed α grains to aligned α laths, and bulk oxygen contamination. It was also concluded that the level of oxidation is a function of temperature, with samples heat treated at 1050ºC showing the higher hardness at the centre of the tensile specimens due to high oxygen diffusion. A significant decrease in ductility was observed with increasing α-case thickness for samples treated above the T_β, while no major decrease in ductility was observed in the samples heat treated below the T_β, even for samples with a thick α-case.

2.6.2 Heat treatment of α+β titanium alloys

Significant research work [2003Fil, 2006Bož, 2006Jov, 2009Zha, 2012Vra, 2013Red] has been performed over the past years on manipulating the microstructure and improving the mechanical properties of the α+β alloys by heat treatment. Jovanovic´ et al. [2006Jov] studied the effect of heat treating investment cast Ti–6Al–4V alloy by X-ray diffraction analysis, light microscopy, metallography, hardness and room temperature tensile tests. It was found that the volume fraction of martensite decreases as annealing temperature decreases. Furthermore, it was found that hardness and tensile strength increased with increasing annealing temperature and cooling rate. Additionally, this heat treatment schedule resulted in lower elongation values. Filip et al. [2003Fil] investigated the effect of microstructure on the mechanical properties of two-phase titanium alloys after different heat treatment schedules. It was observed that the thickness and length of the α phase decreased with increasing cooling rate and content of the β-stabilizing elements. It was also seen that the tensile elongation approaches a maximum value at intermediate cooling rates. Božić et al. [2006Bož] investigated the effect of various hot-pressing conditions on the microstructure, tensile properties and impact toughness of Ti-6Al-4V alloy, and it was found that heating the alloy at 950°C resulted in a fully lamellar microstructure characterized by a high tensile strength, high impact toughness and a high crack initiation and propagation resistance. Increasing the exposure time and applied pressure during hot pressing considerably refined the colony size and thickness of the α lamellae.

Although a variety of heat treatment processes for commercial titanium alloys such as Ti-6Al-4V are known, a typical heat treatment process involves solution treatment and aging. Solution treatment involves heating the alloy to a temperature either slightly below or above the β transus temperature, usually at 955−970°C to obtain a combination of high strength and moderate ductility. Heating the α+β titanium alloy to the solution treatment temperature produces a large fraction of the β phase which subsequently transforms to β-Ti plus martensite and sometimes retained α upon quenching [1991ASM, 2000Don]. The isothermal holding time is determined by the thickness of the work piece. The rule is to heat the component at that specific temperature for 20 to 30 minutes for every 25 mm of thickness [2000Don]. The alloy is finally aged at temperatures in the range of 425−650°C resulting in the

decomposition of the unstable β phase and martensite, if present [2000Don]. Lütjering and Williams [2003Lut] recommend the annealing of martensite at temperatures in the range of 700−850°C to form a fine lamellar α+β microstructure. Another important heat treatment process for the α+β titanium alloys is stress relief annealing. Typical stress relieving treatments for various α+β titanium alloys are shown in Table 2.1.

Table 2.1: Typical stress relief treatments for α+β titanium alloys [2000Don]

Alloy	Temperature		Time, h
	°C	°F	
α-β titanium alloys			
Ti-6Al-4V	480–650	900–1200	1–4
Ti-6Al-7Nb (IMI 367)	500–600	930–1110	1–4
Ti-6Al-6V-2Sn (Cu + Fe)	480–650	900–1200	1–4
Ti-3Al-2.5V	540–650	1000–1200	¼–2
Ti-6Al-2Sn-4Zr-6Mo	595–705	1100–1300	¼–4
Ti-4Al-4Mo-2Sn-0.5Si (IMI 550)	600–700	1110–1290	2–4
Ti-4Al-4Mo-4Sn-0.5Si (IMI 551)	600–700	1110–1290	2–4
Ti-5Al-2Sn-4Mo-2Zr-4Cr (Ti-17)	480–650	900–1200	1–4
Ti-7Al-4Mo	480–705	900–1300	1–8
Ti-6Al-2Sn-2Zr-2Mo-2Cr-0.25Si	480–650	900–1200	1–4
Ti-8Mn	480–595	900–1100	¼–2

Although the cooling rate from the stress relief temperature is not a critical parameter for titanium alloys, quenching in water or oil to accelerate cooling is not recommended because of the possibility of inducing residual stresses as a result of unequal cooling. Therefore furnace and air cooling is most suitable [2000Don]. The microstructures obtained by various heat treatment processes are provided in Table 2.2.

Table 2.2: Effect of various heat treatments on the microstructure of α+β titanium alloys [2000Don]

Heat treatment designation	Heat treatment cycle	Microstructure
Duplex anneal	Solution treat at 50–75 °C (90–135 °F) below T_β(a), air cool and age for 2–8 h at 540–675 °C (1000–1250 °F)	Primary α, plus Widmanstätten α – β regions
Solution treat and age	Solution treat at ~40 °C (70 °F) below T_β, water quench(b) and age for 2–8 h at 535–675 °C (995–1250 °F)	Primary α, plus tempered α′ or a β – α mixture
Beta anneal	Solution treat at ~15 °C (30 °F) above T_β, air cool and stabilize at 650–760 °C (1200–1400 °F) for 2 h	Widmanstätten α – β colony microstructure
Beta quench	Solution treat at ~15 °C (30 °F) above T_β, water quench and temper at 650–760 °C (1200–1400 °F) for 2 h	Tempered α′
Recrystallization anneal	925 °C (1700 °F) for 4 h, cool at 50 °C/h (90 °F/h) to 760 °C (1400 °F), air cool	Equiaxed α with β at grain–boundary triple points
Mill anneal	α – β hot work plus anneal at 705 °C (1300 °F) for 30 min to several hours and air cool	Incompletely recrystallized α with a small volume fraction of small β particles

(a) T_β is the β transus temperature for the particular alloy in question. (b) In more heavily β-stabilized alloys such as Ti-6Al-2Sn-4Zr-6Mo or Ti-6Al-6V-2Sn, solution treatment is followed by air cooling. Subsequent aging causes precipitation of α phase to form an α – β mixture.

The mechanical properties of α+β titanium alloys are dependent on the amounts and distribution of α and β phases. The amounts of the α and β phases change in the α+β phase field with decreasing temperature for the α+β alloys [2012Wan]. As shown in Figure 2.1, slowly heating Ti-6Al alloy containing 4 wt. % V to temperatures high up in the α+β phase field increases the amount of the β phase at the expense of the primary α phase. Furthermore, the β phase formed as the temperature is increased further within the α+β phase field becomes less rich in vanadium, the β stabilizing element.

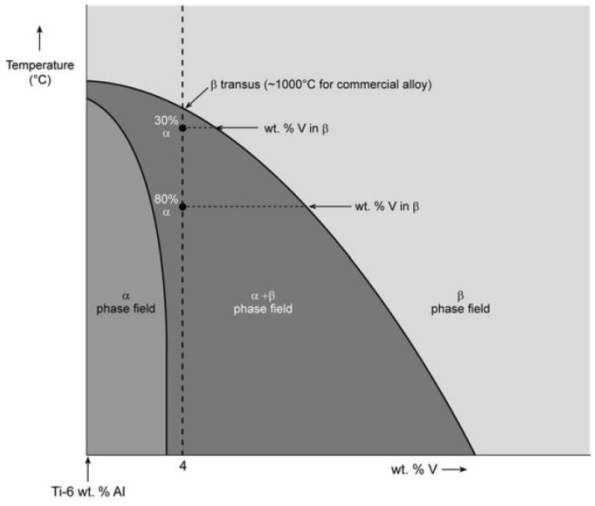

Figure 2.1: Pseudo-Binary phase diagram of Ti-6Al-4V alloy [2012Wan]

2.7 Thermomechanical processing of the α+β titanium alloys

Three main types of microstructures can be obtained in α+β alloys: fully lamellar microstructures, fully equiaxed structures, and bi-modal (duplex) microstructures. These structures can be obtained through a series of conventional thermomechanical processing steps which include deformation, recrystallization, annealing and aging, or a combination of the two later processes [2003Lut]. A critical parameter during thermomechanical processing is usually the β- transus temperature. The β transus separates the β phase field from the α+β phase field in the pseudo-binary phase diagram of the Ti-6Al-4V alloy. The properties of α+β titanium alloys are primarily dependent on the size of the α and β phases and the type of microstructure.

2.7.1 Processing route for fully lamellar microstructures

A lamellar microstructure is classified as one which consists of alternating plates of the α and β phases. The two phases are often clearly distinguished under a scanning electron microscope (SEM) in backscatter electron mode, with the α phase normally identified as light plates and the β phase appearing as a dark thin layer between α plates. The lamellar grains are separated by a network of the α phase, also referred to as grain boundary α (GB-α) as shown in Figure 2.2. Lamellar microstructures are normally obtained by cooling the alloy from heat treatment temperatures above the β transus temperature. The heat treatment temperature is usually kept within 30−50°C above the β transus [2003Lut].

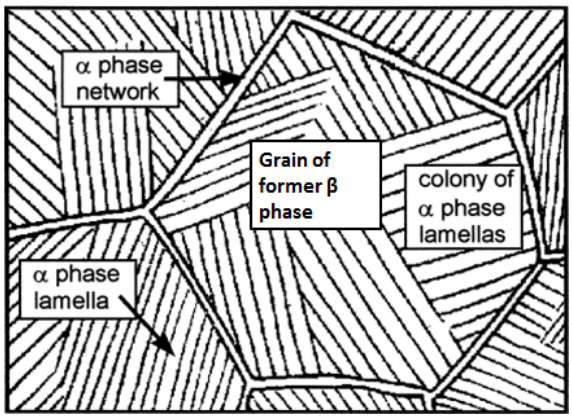

Figure 2.2: Diagram of a fully lamellar microstructure of α+ β titanium alloy [2001Chr]

The morphology of a lamellar microstructure is dependent on the cooling rate, ranging from colonized plate-like α at a low cooling rate, a basket-weave morphology at a medium cooling rate, Widmanstätten at a high cooling rate, to martensite when quenched in water [2002Din]. According to Lamirand et al. [2006Lam], a cooling rate below 10°C/ min is usually classified as a low cooling rate, while a medium cooling rate is within the range of 10−50°C/min and a high cooling rate is above 50°C/min. Additionally, Lutjering and Williams [2003Lut] estimate water quenching or rapid cooling at 8000°C/min.

Žitňanský and Čaplovič [2004Žit] and Leyens and Peters [2003Ley] mention that the transformation of the β phase to α phase begins by the formation of the α nuclei at grain boundaries which subsequently grow as lamellas into the prior β grains. It should be noted that the α phase produced by transformation of the β phase has a different structure compared to the α phase which may have been present before heat treatment. The α phase formed from the β transformation normally exhibits a serrated, acicular, plate-like, Widmanstätten, or ά (martensite) structure. Therefore the term transformed β is used to describe these various α structures including any beta phase that may be retained after cooling to room temperature [1990ASM].

Although the width of individual α plates and the size of colonies of α lamellae in fully lamellar microstructures both decrease with increasing cooling rate, the change in the size of each feature occurs during different ranges of the cooling rate [2003Lut]. The width of α plates decreases drastically from about 5 μm in a slowly cooled material to about 0.5 μm for a high cooling rate. A further increase in cooling rate leads to an additional size reduction down to about 0.2μm (which is the average width of martensite plates) with a fair amount of thicker martensite present in the microstructure [2003Lut]. On the contrary, the α colony size only exhibits a moderate decrease from approximately 300 μm to about 100 μm for a high cooling rate [2003Lut]. Rapid cooling by water quenching leads to a transformation of the β phase to a very fine martensitic microstructure. Therefore cooling rates of approximately 8000°C/min may lead to a drastic decrease in the colony size down to the width of individual martensite plates [2003Lut]. It should be noted that the formation of a

network of the α phase (GB α phase) cannot be avoided even for very fast cooling rates, but its thickness generally decreasesαα with increasing cooling rate.

Annealing temperature is a critical parameter during the final steps in thermomechanical processing of Ti-6Al-4V titanium alloy. This is because the selected temperature will determine whether age hardening of Ti-6Al-4V by Ti_3Al will occur or not [2003Lut]. For example, at 500°C a relatively brittle Ti_3Al phase will precipitate while a final heat treatment at temperature of approximately 600°C will only result in stress relief.

2.7.2 Processing route for bi-modal microstructures

A bi-modal microstructure consists partly of the primary α phase (α_p) in a lamellar α+β matrix [2003Ley] as shown in Figure 2.3. According to literature [1974Avn], primary α in physical metallurgy usually refers to the first solid to form during slow cooling of the alloy from the liquid phase field.

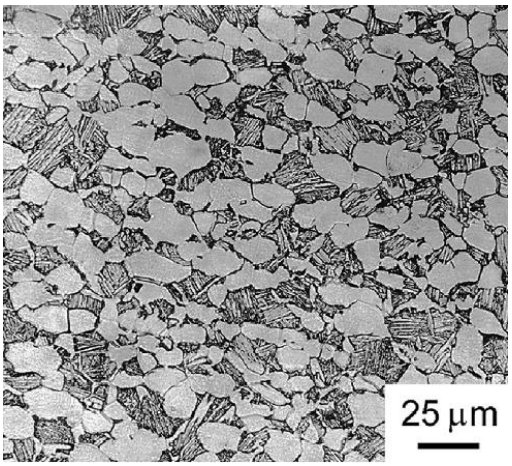

Figure 2.3: Bi-modal microstructure of the Ti-6Al-4V alloy [2002Nal]

Bi-modal microstructures are normally produced through a series of processes which include homogenization in the β phase field, deformation in the (α+β) phase field, recrystallization in the (α+β) phase field, and finally aging and/or stress relieving heat treatment [2003Lut]. The cooling rate from the β phase field is the most critical parameter during homogenization as it determines the width of the resultant α

lamellae. The lamellar structure obtained after homogenization is then subjected to plastic deformation high enough to introduce sufficient stored energy to ensure complete recrystallization of the α and β phases during the recrystallization step. The recrystallization annealing temperature determines the volume fraction of the recrystallized equiaxed α_p phase located at the triple points of recrystallized β grains [2003Lut]. The annealing time is not very critical during the recrystallization step as long as enough time is allowed for the generation of isolated equiaxed α_p grains.

The most important microstructural feature of the bi-modal structure is the β grain size [2003Lut]. While the cooling rate from the recrystallization temperature affects the width of the individual α lamellae in bi-modal microstructures, the α colony size and thickness of continuous GB-α layers are determined mainly by the β grain size [2003Lut]. Cooling rates in the range of 30−600°C/min result in α colony size about equal to the β grain size and slower cooling rates increase both the size and volume fraction of α_p.

2.7.3 Processing of fully equiaxed microstructures

Equiaxed microstructures are obtained through the recrystallization process. The material is sufficiently cold worked prior to heat treatment. Subsequent solution heat treatment is then performed at temperatures in the α+β phase field thereby forming a less strained recrystallized equiaxed microstructure. An example of an equiaxed microstructure of Ti-6Al-4V alloy is shown in Figure 2.4.

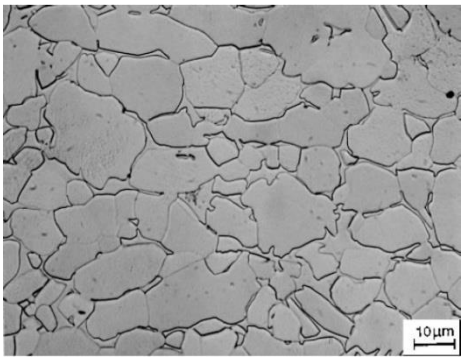

Figure 2.4: Fully equiaxed microstructure of the Ti-6Al-4V alloy [2002Bie]

In the case of Ti-6Al-4V, it is possible to obtain a fully equiaxed microstructure with α grain sizes of about 2 μm by using recrystallization temperatures between 800 and 850°C. It is also possible to change fully equiaxed microstructures to bimodal microstructures. This is achieved by solution heat treatment just below the β transus to obtain the desired α_p volume fraction followed by cooling with a sufficiently high rate to form α lamellae within the β grains. The three microstructures discussed exhibit different mechanical properties, as explained in the next section.

2.8 Microstructure and mechanical properties of a+ß titanium alloys

2.8.1 Effect of lamellar microstructures on the mechanical properties

The most important microstructural feature which greatly affects the mechanical properties of lamellar microstructures is the α colony size [2003Lut]. The colony size is controlled by the cooling rate from the β heat treatment temperature. Increasing the cooling rate up to 1000°C/min increases the yield stress by 50−100 MPa, and a large increase is observed as the colony structure is transformed to martensite [2003Lut]. The increasing cooling rate is usually accompanied by an initial increase in ductility which ultimately reaches a maximum value then declines as the fracture mode changes from a ductile transcrystalline dimple type of fracture at low cooling rates, to ductile intercrystalline dimple fracture along the continuous GB α layers [2003Lut]. Decreasing the β grain size is also beneficial in increasing ductility of lamellar microstructures. This effect was demonstrated by Lütjering et al. [2003Lut] for Ti-6Al-4V alloy by decreasing the β grain size from 600 μm to 100 μm by rapid heating.

Similar to yield stress, low and medium cooling rates result in a moderate increase of high cycle fatigue (HCF) strength, and rapid cooling results in a much higher increase [2003Lut]. It is noteworthy that the HCF strength and yield stress also depend on the details of the final annealing/aging treatment. For example, water quenching of Ti-6Al-4V from 800°C followed by aging at 500°C for 24 hours increases the HCF strength from 350 MPa for an alloy in a stress relieved condition (1hour at 650°C) to about 500 MPa. This heat treatment is also accompanied by an increase in yield stress from 830 MPa to 930 MPa. In microstructures composed of more individual α plates,

typical for faster cooling rates, the fatigue cracks usually nucleate at the longest and widest plate.

Low cycle fatigue, defined as the resistance to crack nucleation and propagation of micro-cracks, is generally improved with increasing cooling rate from the β phase field [2003Lut]. Micro-cracks propagate faster in coarse lamellar microstructures compared to fine lamellar microstructures. In coarse lamellar microstructures, colony boundaries and β grain boundaries act as strong barriers because the micro-cracks have to change direction when they encounter these boundaries. In fine lamellar structures, micro-cracks generally initiate at the coarsest plate and propagate initially along the interface and eventually propagate through the matrix [2003Lut]. This behaviour is influenced by the presence of individual martensite plates in fine lamellar microstructures which impede the propagation of micro-cracks. Fracture toughness of α+β titanium alloys usually increases with increasing α colony size [2003Lut]. A fracture toughness value of 75 MPa $m^{1/2}$ is typical of a slowly cooled coarse lamellar structure while 50 MPa $m^{1/2}$ corresponds to a rapidly cooled fine lamellar structure. Table 2.3 summarizes the influence of the microstructural features on the mechanical properties of fully lamellar microstructures.

Table 2.3: Qualitative correlation between important mechanical properties and microstructural features for fully lamellar structures of α+β titanium alloys [2003Lut]

					Macrocracks		
Microstructural feature	**$\sigma_{0.2}$**	**ε_f**	**HCF**	**Microcracks Ki_{th}**	**ΔK_{th} R=0.7**	**K_{Ic}**	**ΔK_{th} R=0.1**
Small α Colonies, α Lamellae	+	+	+	+	-	-	-

The notation (+) indicates an increase while (-) indicates a decrease. The mechanical properties are compared to those of fully lamellar microstructures containing course α lamellae.

2.8.2 Effect of bi-modal microstructures on the mechanical properties

Among other parameters which greatly affect the mechanical properties of bimodal microstructures are the β grain size and the alloying element partitioning effect [2003Lut]. A small β grain size in bi-modal microstructures leads to a small α colony size. In commercially processed bi-modal microstructures, the β grain size is usually in the range of about 30−70 μm. For cooling rates in the range of 30−600°C/min, the α colony size is about the same size as the β grains and consequently smaller than colonies in fully lamellar microstructures. Therefore if the α colony size was the only parameter which governs the mechanical properties of bi-modal microstructures, then these structures would be expected to exhibit a higher yield stress, higher HCF strength, higher ductility, a slower crack propagation rate of micro-cracks compared to a fully lamellar microstructure for the same cooling rate, while the fracture toughness and resistance to macrocracks propagation would be better for a fully lamellar microstructure [1998Lut]. However, the mechanical properties of bi-modal structures cannot be considered based on the β grain size alone, but the alloying element partitioning effect also needs to be considered.

The alloying element partitioning effect generally increases with increasing α_p volume fraction. The yield stress usually has a maximum value between 10 and 20 vol. % α_p. For small volume fractions of α_p, the effect of the α colony size effect dominates, whereas the alloy element partitioning effect dominates at large volume fractions of α_p (Table 2.4).

Table 2.4: Effect of microstructure on tensile properties of Ti-64 at room temperature and at 600°C [1998Lut]

Microstructure	Test Temp.	$\sigma_{0.2}$ (MPa)	UTS (MPa)	σ_F (MPa)	El. (%)	RA (%)
Lamellar	RT	925	1015	1145	5.2	12
Bi-modal (20% α_p)	RT	995	1100	1350	12.9	20
Bi-modal (30% α_p)	RT	955	1060	1365	12.6	26
Lamellar	600°C	515	640	800	10.5	26
Bi-modal (10% α_p)	600°C	570	695	885	9.9	30
Bi-modal (40% α_p)	600°C	565	670	910	14.4	36

As seen in Table 2.4, a slight decrease in the yield stress is observed at elevated temperatures in the high α_p volume fraction regime. Increasing the α_p volume fraction decreases the resistance to crack nucleation (HCF strength). This is because the alloy partitioning effect results in lamellar grains which are softer than α_p thereby leading to fatigue crack nucleation in lamellar grains of the bi-modal microstructures [2003Lut]. However, at elevated temperatures, the HCF strength is equal to or higher for bi-modal microstructures as compared to fully lamellar microstructures. This observation may be an indication that the alloy partitioning effect is less critical at high temperatures.

It should be noted that the influence of the alloy partitioning effect on crack nucleation behaviour is pronounced for aged microstructures, and much smaller for unaged microstructures for which their final heat treatment is only a stress relieving treatment [2003Lut]. Alloy element partitioning effect is also dependent on the alloy chemistry. For example, the effect is large for IMI 834 and smaller for Ti-6Al-4V alloy. The influence of alloy partitioning effect on the HCF strength can be eliminated by introducing an intermediate annealing treatment step between the bi-modal recrystallization treatment and the final aging treatment. This treatment will promote the diffusion of α stabilizing elements, such as aluminium and oxygen, into the α lamellae regions of the bi-modal microstructures thereby increasing the strength of the lamellar α regions. For example, annealing at 830°C for 2h increases the HCF strength of bi-modal microstructures to the level of fully lamellar microstructures or even above [2003Lut].

The presence of smaller α colony size in bi-modal structures improves the resistance to microcrack propagation, and the crack propagation rate is slower compared to fully lamellar microstructures [2003Lut]. Additionally, the resistance to macrocrack propagation is higher for lamellar structures due to a rougher crack front profile of the lamellar structures as compared to bi-modal structures. Due to the differences in crack front profiles, the fracture toughness of a bi-modal microstructure of Ti-6Al-4V alloy is usually around 55 MPa $m^{1/2}$, which is slightly higher than the fracture toughness of the fine lamellar microstructure (50 MPa $m^{1/2}$) but much lower than the toughness of the coarse lamellar microstructure (75 MPa $m^{1/2}$) [2003Lut]. Table 2.5 shows a

summary of the influence of the most important microstructural feature for bi-modal microstructures on the mechanical properties of α+β titanium alloys.

Table 2.5: Qualitative correlation between mechanical properties and important microstructural features for bi-modal structures of α+β titanium alloys [2003Lut]

					Macrocracks		
Microstructural feature	**$\sigma_{0.2}$**	**ε_f**	**HCF**	**Microcracks ΔK_{th}**	**ΔK_{th} R=0.7**	**K_{Ic}**	**ΔK_{th} R=0.1**
Bi-modal structure	+	+	-	+	-	-	-

2.8.3 Effect of fully equiaxed microstructures on the mechanical properties

The most important microstructural feature which affects the mechanical properties of fully equiaxed microstructures is the α grain size [2003Lut]. The effect of the α grain size in these structures is qualitatively similar to that of the α colony size in fully lamellar microstructures. Table 2.6 provides a summary of the influence of the most important microstructural features for fully equiaxed microstructural features on the mechanical properties of α+β titanium alloys. The properties are compared to those of fully equiaxed structures containing larger α grain size.

Table 2.6: Qualitative correlation between mechanical properties and important microstructural features for fully equiaxed structures of α+β titanium alloys [2003Lut]

					Macrocracks		
Microstructural feature	**$\sigma_{0.2}$**	**ε_f**	**HCF**	**Microcracks ΔK_{th}**	**ΔK_{th} R=0.7**	**K_{Ic}**	**ΔK_{th} R=0.1**
Small α grain size	+	+	+	+	-	-	-

As indicated in Table 2.6, a high yield strength and high HCF strength can be achieved for small α grain sizes in fully equiaxed microstructures, and their tensile ductility are generally very high as compared to bi-modal microstructures [2003Lut]. For example, the reduction in area (RA) values increases from 40% for the 12 μm grain size to about 50% for the 2 μm grain size. However the evaluation of the HCF

strength of a fully equiaxed microstructure can best be evaluated against that of a bi-modal microstructure if the volume fraction of $\alpha_p$in a bi-modal microstructure is about 60 vol. % [2003Lut]. In this α_p volume fraction regime, the α_p grains start to interconnect and are no longer separated by lamellar grains. The resultant structure is then called an equiaxed microstructure. This equiaxed microstructure has a lower HCF strength as compared the original bi-modal microstructure, thereby resulting in crack nucleation sites to shift from the lamellar regions to interconnect α grains in the equiaxed microstructure. Additionally, the HCF strength of a fully equiaxed structure can be evaluated relative to that of a fully lamellar microstructure if the thickness of the α plates in the lamellar structure is equal to the α grain size in the equiaxed structure. If this condition is met, then the HCF strength values of fully equiaxed microstructures are generally higher than the HCF strength values of fully lamellar microstructures.

2.9 Effect of aging and oxygen content on the mechanical properties

It must be noted that the α phase in titanium alloys can be age hardened by Ti_3Al (α_2) precipitates if the Ti-xAl-4V alloy contains approximately 6 wt. % of aluminium [2003Lut]. The formation of α_2 precipitates is dependent on the final annealing treatment temperature. For example, final annealing treatment of Ti-6Al-4V alloy at temperatures in the range of 550−600°C results in a formation of α_2 precipitates, while annealing at higher temperatures in the range of 600−700°C will only lead to stress relieving [2003Lut]. It should also be noted that the heat treatment temperature range at which α_2 precipitates form is dependent on the content of aluminium and oxygen in the alloy.

Lütjering [2003Lut] compared the mechanical response of a coarse lamellar microstructure of Ti-6Al-4V in the aged condition (1h 800°C/WQ, 24h 500°C) to that in a stress relieved condition (1h 650°C), where WQ stands for water quenching. The results showed that the HCF strength increased from 350 MPa for the stress relieved condition to about 500 MPa for the aged condition. Aging also resulted in an increase of the yield strength value from 830 to 930 MPa, while the tensile ductility dropped from 21% for the stress relieved condition to about 14% for the aged condition. A

similar effect was also observed for varying oxygen content of the Ti-6Al-4V alloy. The effect of oxygen content was evaluated by comparing the extra low interstitial (ELI) grade alloy containing 0.08% oxygen to the normal grade alloy containing 0.19% oxygen. It was discovered that, for a fine lamellar microstructure, the HCF strength increases from about 480 MPa for the ELI grade to about 580 MPa for the regular grade material [2003Lut]. This effect was also accompanied by an increase in yield strength value from 910 MPa to 990 MPa and a decline in RA value from 27% to 23%.

Macrocracks are generally observed to propagate at a faster rate for α titanium alloys in the aged condition (500°C for 10 hours.) as compared to the unaged condition [2003Lut]. For α+β titanium alloys, increasing aging and/ oxygen content will result in larger microcrack propagation rates for coarse microstructures compared to fine microstructures. Unlike the HCF strength, the LCF strength is generally higher for the low oxygen material. The fracture toughness of α+β titanium alloys decreases with aging and increasing oxygen content.

CHAPTER 3: EXPERIMENTAL PROCEDURE

A detailed description of the raw materials, equipment, consumables and experimental methods used in this research are presented in this chapter. Firstly, in the first section (3.1 Raw materials), the analyses of the as-received powders are provided to enable comparison to the analyses of processed materials. It is also noteworthy that the analysis of the as-received titanium powder is provided to identify its commercial grade (based on oxygen content), which is very crucial for titanium alloys for critical applications. In the second section (3.2 Equipment and consumables), the brand name, model number and capabilities of processing and characterization technologies used in this work are highlighted, finishing off with a brief description of consumables used during metallographic specimen preparation. Lastly, a detailed description of the procedure and parameters used during laboratory experiments is given in the last section of this chapter.

3.1 Raw materials

The starting materials used in this work include powders of commercial purity titanium (purity 99.5%), aluminium (purity 99.5%), vanadium (purity 99.5%), 60Al:40V (wt. %) master alloy and the supposedly pre-alloyed Ti-6Al-4V (wt. %) powder. The unalloyed titanium powder (-45 µm) was supplied by Industrial Analytical (South Africa) and was of a chemical composition shown Table 3.1.

Table 3.1: Composition of as-received CP-Ti powder (Supplier's specification)

Element	Ti	Fe	O	C	N	H
Content (wt. %)	Balance	0.110	0.377	0.020	0.018	0.022

The 60Al:V40 master alloy powder (-45 µm) was supplied by TLS Technik GmbH & Co. (Germany). The chemical composition of this powder as per supplier's specification is shown in Table 3.2.

Table 3.2: Composition of the 60Al:40V master alloy (Supplier's specification)

Element	Al	V	Cr	Fe	Mo	Ni
Content (wt. %)	Balance	39.45	0.01	1.10	0.01	0.01

The pre-alloyed Ti-6Al-4V powder was received from the Centre for Rapid Prototyping and Manufacturing (South Africa). The chemical composition of the starting powder was not provided by the supplier, however the oxygen content was determined to be 0.13% by the Leco TCH 600 gas fusion technique. The composition of the vanadium elemental powder (-45 µm), also supplied by Industrial Analytical, is shown in Table 3.3.

Table 3.3: Composition of vanadium powder (Supplier's specification)

Element	V	Fe	Al	C	O	N	H	Cr	Si
Content (wt. %)	Balance	0.04	0.01	0.04	0.4	0.04	0.01	0.03	0.01

Spherical titanium powder (-45 µm) containing 0.18% O was also sourced from TLS Technik GmbH & Co but could not be used in this work due to poor densification during die pressing. It should be noted that elemental Al and V powders were used to prepare the blended Ti-6Al-4V powder for the powder compactability and SPS experiments research due to the difficulty in finding a cheaper supplier for the 60Al-40V master alloy powder in the early stages of this research. The master alloy was used for the remainder of the work, except for rapid manufacturing. The only facility for rapid manufacturing accessible during this time could only build specimens from their own pre-alloyed Ti-6Al-4V powder and not from other powders, including pure titanium and blended Ti-6Al-4V alloy, due to concerns of contamination.

3.2 Equipment and consumables

The brand name, model number and capabilities of the equipment used during milling, blending, cold compaction, sintering, casting hot isostatic pressing, heat treatment of titanium and Ti-6Al-4V alloy are highlighted first in this section. However, in some cases (HIP and CIP) the model numbers and features of the equipment used by other facilities are not given due to confidentiality issues. Therefore only the brand name could be supplied in this case. The name and

composition of consumables used during wet grinding, polishing and etching of metallographic specimens are also given at the end of the chapter.

3.2.1Milling and blending of raw powders

A Dispermat attritor mill (2000 rpm maximum speed) was used to attempt the production of nano-sized pure titanium powder and homogeneous Ti-6Al-4V alloy powder from micron-sized elemental powders. The attritor mill was fitted with a 250 ml polyamide mill vial, and WC balls with a diameter of 3 mm were used as the milling media. The mill vial was placed inside a hollow steel water jacket fitted with water inlet and outlet pipes to constantly circulate cold water around the vessel during mechanical milling to keep the contents of the mill at room temperature. Hexane was used as the dispersant and the mill vessel was sealed with a lid fitted with an o-ring. A WAB TURBULA® SYSTEM SCHATZ mixer (97 rpm maximum speed) was used for the dry mixing of the commercial grade titanium powder with the 60Al-40V master alloy powder to produce a Ti-6Al-4V powder mix.

3.2.2Powder compaction

The blended elemental Ti-6Al-4V powder and the as-received commercial grade titanium powders were cold compacted in cylindrical hardened steel dies. The dies consisted of a hardened steel bushing which was press fit into a steel restraint cylinder. The bushing was drilled at the centre and fine polished to obtain smooth cylindrical cavities of a diameter 19.9 and 24 mm for two separate dies. A hardened steel rod was also purchased and machined to make a short plug for the bottom of the die and a pressing plunger for the top section of the die. A manually controlled Amlser hydraulic press capable of delivering a maximum compressive load of 2000 kN was used to press all compacts, and a digital linear displacement transducer was used to measure the displacement of the plunger during preliminary compaction experiments.

Medium and large size cylindrical green compacts of pure titanium and blended elemental Ti-6Al-4V powder were also produced using an EPSI cold isostatic press at the Fraunhofer Institute for Ceramic Technologies and Systems (IKTS) in Germany. The press used was capable of reaching a maximum hydrostatic pressure of 4000 bar..

3.2.3Sintering

The pressure-aided sintering of the previously compacted pellets of pure titanium and the Ti-6Al-4V powder mix was performed in a HP-DS (FCT Systeme, Germany) spark plasma sintering (SPS) furnace shown in Figure 3.1. The SPS furnace is technically comparable to the conventional hot press in terms of the sintering method used. The furnace is provisioned with mechanisms for simultaneous sintering and compaction of the powder under vacuum. The sintering of the loose or compacted powder is achieved by the application of a pulsed voltage and resistance heating of the graphite mould containing the sample.



Figure 3.1: Spark plasma sintering (SPS) furnace

Graphite dies with an inner diameter of 20 mm were used in this work. The inner wall of the dies was lined with hexagonal boron nitride (HBN) to prevent the interaction of the graphite with compacts during sintering. The minimal uniaxial pressure which can be applied on the sample during sintering is 10 MPa. The SPS furnace is also capable

of sintering under vacuum and recording the linear height displacement of the compact as a function of temperature and time.

The horizontal tube furnace, Elite TSH17/75/150, was used for the pressureless or conventional sintering experiments. This furnace was fitted with a 1500 mm long mullite ceramic work tube with an outside diameter of 75 mm and an inside diameter 65 mm. After the specimen is placed in a ceramic boat and loaded into the work tube, each end of the tube can be tightly sealed with water cooled steel flanges fitted with high temperature Viton O-rings. The furnace has a control panel to program the desired thermal profile. The sintering of the sample is achieved by resistance heating of the mullite tube by the heating elements positioned in the ceramic lining. The maximum operating temperature of this furnace was 1700°C. The furnace was fitted with two activated copper oxygen traps in series at a later stage in this work in order to decrease the oxygen and moisture content of the argon baseline 5.0 gas prior to being fed into the work tube.

3.2.4Casting

Two types of furnaces were used for the casting of commercial purity titanium and Ti-6Al-4V green compacts. The first furnace was a Manfredi M10H3 centrifugal casting furnace. This furnace was equipped with a rotary pump to evacuate the casting chamber and also fitted with a gas inlet line to backfill the chamber with argon gas. It was also equipped with a pyrometer positioned directly above the melting crucible to measure the temperature during melting and solidification. The pyrometer was only capable of measuring temperatures above 700°C. A ZrO_2 based crucibles were used for the melting of compacted powders by induction melting. The melt was cast into a copper mould with a cavity shaped like a dumbbell shaped tensile test specimen. The second furnace was a Leybolt Heraeus ISPIII/Ds three chamber vacuum furnace shown in Figure 3.2. This furnace was capable of reaching a vacuum pressure of approximately $1x10^{-5}$ mbar and a temperature as high as 1850°C. A ZrO_2 based crucible and copper mould were also used for casting.



Figure 3.2: Leybolt Heraeus ISPIII/Ds three chamber vacuum furnace

3.2.5Hot Isostatic Pressing

All sintered and as-cast specimens were shipped to the HIP facility abroad. A small scale AVURE hot isostatic press was used to further consolidate the sintered and cast rods prior to machining of tensile specimens. The model number and detailed features of the HIP machine were classified information, and could not be revealed by the service provider. However, the parameters used are provided in the experimental procedures section.

3.2.6Heat treatment

The annealing heat treatment of the unalloyed titanium and Ti-6Al-4V alloy samples was performed in both the Elite TSH17/75/150 horizontal tube furnace and the vacuum furnace.

3.2.7Characterization techniques

All microscopic examinations were performed using a Phillips (XL30 Series) scanning electron microscope (SEM) fitted with an electron dispersive spectrometer (EDS). The Axiotech optical microscope fitted with a high magnification Zeiss

AxioCam camera was also used for microstructural examinations. The phase composition and oxygen content of as-received and fabricated samples were determined using a Bruker D2 Phaser X-ray diffractometer fitted with a CoK_{α} radiation source and a Leco TCH 600 gas fusion analyser respectively. Finally, the particle size distribution of the as-received and milled powders was determined using a Malvern Mastersizer 2000. The particle size analyser was fitted with an ultrasonic probe to prevent the agglomeration of the powder after pouring it in de-ionized water.

3.2.8Metallographic specimen preparation

The sintered and cast samples were sectioned with a Struers diamond cut-off wheel for cutting of ceramics and minerals with a Vickers hardness greater than 800HV. The cut-off wheel was fitted on the Struers Secotom-10 cutting machine. A cutting speed of 1350 rpm and a feeding rate in the range of 0.005−0.015 mm/min were used. The sectioned metallic specimens were hot mounted on a Struers PolyFast thermosetting resin using a Struers CitoPress-10 mounting machine. The cold mounting of powdered materials was performed under vacuum using a Struers EpoFix slow curing transparent resin.

Hot mounted specimens were ground and polished using a Leco Spectrum Systems 2000 automatic polishing machine. The SiC papers (grit numbers P320−P4000), 0.04 μm colloidal silica suspension (OP-S) and Krolls reagent consisting of 3ml HF (40% conc.) and 5ml HNO_3 (65% conc.) in 100 ml H_2O were used for the wet grinding, polishing and chemical etching of mounted sections respectively. The grinding of mounted powdered materials was performed on SiC powder of grit numbers ranging from P800 to P4000 to avoid complete erosion of the sample, and no etching was done after polishing with OP-S since the aim was to study the particle morphology and not the microstructure.

3.3 Experimental procedures

This section gives a detailed description of the steps involved and parameters used in milling, blending, cold compaction and sintering, hot isostatic pressing, casting, rapid manufacturing and the fabrication of tensile specimens from solid Ti and Ti-6Al-4V alloy materials, heat treatment, tension testing experiments and metallographic specimen preparation. The aim of sintering, casting and rapid manufacturing is to attempt the production of solid titanium and Ti-6Al-4V alloys from pure Ti powder and Ti-6Al-4V powders, respectively. The solid materials are produced in the form of buttons in cases where only the density, microstructure, chemistry and phase composition are of primary interest, while cylindrical rods from which dumb-bell shaped tensile specimens can be machined are produced in cases where the tensile properties are investigated. The only exception is rapid manufacturing, where the tensile specimens are produced directly from powder.

3.3.1Milling of titanium and Ti-6Al-4V powder mix

The elemental Al and V powders were mixed with commercial grade titanium powder in appropriate proportions to make 50 g of Ti-6Al-4V alloy powder with a composition of approximately 6 wt. % Al, 4 wt. % V and the balance Ti. It is noteworthy that elemental powders were used at this point due to the difficulty in finding a supplier for an affordable 60Al-40V master alloy powder in the early stages of this research. High speed attrition milling of the commercial titanium powder and the Ti-6Al-4V powder mix was then attempted in order to decrease the particle size down to nanometric range (<100 nm), and to achieve homogeneous mixing and distribution of the alloying elements in the Ti-6Al-4V powder mix. The decrease in the particle size was necessary to decrease the sintering onset temperature and increase the densification rate and sintered density of the compacted powders. The powders were milled in 20 mL of hexane using approximately 500 g of WC balls with a diameter of 3 mm as the milling media. Attrition milling was performed for 1 hour at a speed of 1350 rpm. After milling, hexane was drained and the powder was dried for 30 minutes in the oven at 60°C under normal atmosphere. The dry powder was then passed through a -45 µm sieve to break up any agglomerates, and the particle size distribution was measured using a Mastersizer 2000 particle size analyser.

Finally, the milled powders were characterized for phase composition, oxygen content and particle morphology using the XRD, Leco and SEM.

3.3.2Blending of titanium powder with a 60Al:40V master alloy powder

Following the success in finding a supplier for cheaper high quality 6Al-40V master alloy powder, the Ti-6Al-4V powder was prepared by dry mixing of pure 90 wt.% Ti powder and 10 wt.% of the master alloy in a Turbula® mixer. The main objective was to compare the efficiency of dry mixing, on the basis of oxygen contamination, to high energy milling. The 60Al:40V master alloy powder (10 wt.%) was mixed manually with commercial grade titanium powder (90 wt.%) to make a 50 g of the Ti-6Al-4V powder mixture. The mixture was then sealed in a 500 ml plastic sample holder containing two WC balls with a diameter of 10 mm in order to facilitate the blending. The blending was performed for 1 hour using a rotational speed of 67 rpm. The blended powder was then analysed for oxygen content.

3.3.3Compaction of powders

The as-received commercial titanium powder and the Ti-6Al-4V powder mix, obtained by alloying additions in the form of Al and V elemental powders, were first tested for compactability prior to cold pressing and sintering experiments. The reason for using elemental Al and V powders for alloying at this point was due to the difficulties in sourcing the 60Al-40V master alloy powder in the early stages of this work. The main objective for compactability tests was to trend the densification of powders as a function of applied uniaxial load. The resultant compactability curve could then be used to estimate the load required to obtain a green compact of a specific density for subsequent sintering and casting experiments.

For the compactability test, 9 g of powder was weighed and poured into a cylindrical die with a diameter of 24 mm. After loading the powder, pressure was gently applied by hand on the plunger to compact the loose powder slightly. The die containing the powder was then placed between two rams of an Amsler hydraulic press, and the pressure was slowly increased intermittently at intervals of 5 kN and the

corresponding displacement of the plunger was measured using a portable linear displacement transducer until a maximum die pressure of 619 MPa was reached.

It should be noted that the height of the plunger protruding from the die was measured prior to adding the powder and after the light compaction of the powder by hand. The initial height of the powder in the die could then be calculated by subtracting the height of the plunger after loading the powder from the height of the plunger prior loading the powder. This also made it possible to calculate the height of the compact at any given pressure during die pressing by subtracting the displacement of the plunger from the initial height of the powder. Lastly, it should be noted that the diameter of the compact remained constant throughout the compaction experiment due to restrain by the die wall. Therefore the change in volume of the compact at any given applied pressure could be calculated from the diameter of the die cavity and corresponding height of the compact. At the end of the compaction test, the compact was removed from the die and weighed and the mass was used together with the changes in volume to calculate the density at any given pressure. The green density obtained at the end of the compaction experiment was calculated from the geometry and mass of the pressed compact. The green density was then plotted against the applied uniaxial pressure to generate a compaction curve.

3.3.4Cold isostatic pressing

The main objective during cold compaction of powders was to produce disc and large cylindrically shaped compacts with a sufficient strength for safe handling in succeeding densification experiments. The disc shaped specimens are mainly fabricated for density and microstructural examination purposes, while the cylinders are fabricated to enable easy fabrication of dumb-bell shaped tensile specimens after sintering.

The cold compaction of titanium and the blended elemental Ti-6Al-4V alloy powder was also performed using an EPSI cold isostatic press at the Fraunhofer Institute for Ceramic Technologies and Systems (Germany). It should be noted that the master alloy powder was used as alloying additions at this point onwards, unless otherwise

stated, due to the success in finding a supplier a later stage of this research. To prepare a single rod for sintering experiments, 50 g of powder was encapsulated in a rubber membrane and then pressed by applying a hydrostatic fluid pressure of 700 MPa to produce a rod with a diameter and length of approximately 16 mm and 63 mm respectively (Figure 3.3). A total of 10 rods were prepared from pure Ti powder and the blended Ti-6Al-4V powder prepared using the Turbula® mixer.

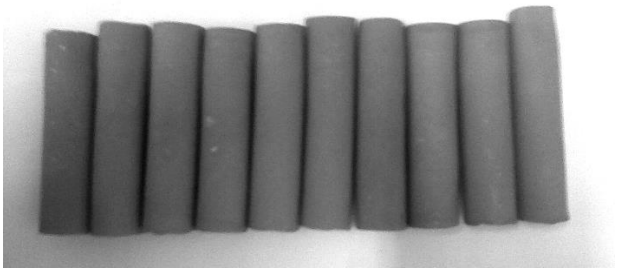

Figure 3.3: Titanium rods produced by cold isostatic pressing at a pressure of 700 MPa

Two large cylindrical green compacts of the commercial purity titanium powder and blended elemental Ti-6Al-4V powder were also produced using the EPSI cold isostatic press. These compacts were to be used for vacuum casting experiments in the Leybolt Heraeus ISPIII/Ds three chamber furnace. For a single compact, 2 kg of powder was encapsulated in a rubber membrane and cold compacted under a hydrostatic pressure of 400 MPa to produce a billet with a diameter and height of approximately 86 mm and 207 mm respectively as shown in Figure 3.5. The dimensions of the billet were restricted by the geometry of the ZrO_2 crucible to be used during melting.

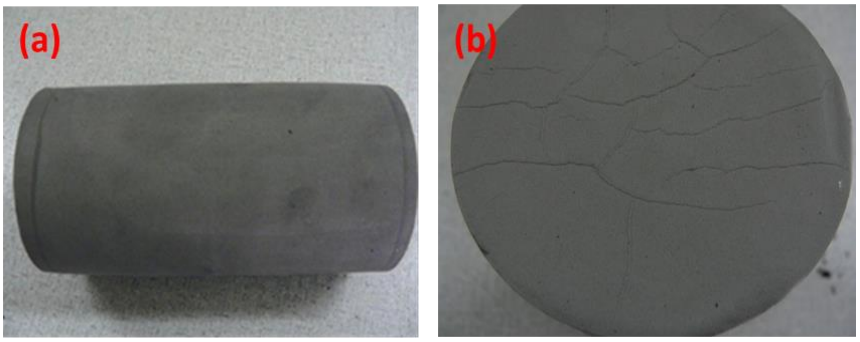

Figure 3.4: A 2 kg titanium billet formed by cold isostatic pressing at a pressure of 400 MPa.

3.3.5 Sintering of titanium powder and Ti-6Al-4V powder mixture

The spark plasma sintering (SPS) and pressureless sintering (tube furnace) technologies were investigated in this research. The main objectives for spark plasma sintering were to trend the density of pure titanium and blended elemental Ti-6Al-4V and study the microstructural evolution as a function of sintering temperature at a fixed isothermal holding time. In contrast, the objectives for pressureless sintering were simply to produce semi-finished rods from which tensile specimens can be machined and compare their microstructure, density and chemistry to materials obtained by the SPS method.

Due to the large number of samples required for the SPS method in this research and difficulties in sourcing the 60Al-40V master alloy powder in the early stages of this work, Al nd V elemental powders were used to prepare the blended elemental Ti-6Al-4V powder for spark plasma sintering experiments. To prepare green compacts for spark plasma sintering, commercial grade titanium powder and the Ti-6Al-4V powder blend obtained by alloying additions in the form of elemental Al and V powders were cold uniaxially pressed in a hardened steel die with a diameter of 19.9 mm. The density of the resultant disc shaped compacts was 71 % to the theoretical. The uniaxial pressure required to obtain this level of density was estimated as 300 MPa from the compactability curves discussed earlier under heading 3.3.3 (Cold compaction of powders). The die pressed disc was then loaded in the graphite die with an inside diameter of approximately 20 mm and fitted in the SPS machine. The die was lined with a thin foil of hexagonal boron nitride (HBN) to prevent the diffusion of the carbon from the die into titanium during sintering at elevated temperatures. For titanium compacts, SPS was performed at temperatures in the range of 600−1250°C for 10 minutes under vacuum, while temperatures in the range of 1000−1250°C were used for discs based on the blended Ti-6Al-4V powder. Spark plasma sintering was achieved by a pulsed voltage and resistance heating of the graphite die. A minimal compaction pressure of 10 MPa was applied by the ram on the top surface of the compacts to record the displacement of the height during the sintering cycle. A heating and cooling rate of 250°C/min was maintained for all sintering experiments. Sintered compacts were characterized for density using the Archimedes water

immersion method and then sectioned to study the microstructure and phase composition.

For conventional sintering, each of the cold isostatically pressed (CIP'ed) cylindrical rods was placed between ceramic boats containing sacrificial titanium powder in the tightly sealed mullite work tube. The horizontal tube furnace was fitted with two oxygen traps in series through which a stream of Argon Baseline 5.0 gas was passed prior to introducing it into the work tube. The oxygen traps consisted of activated copper oxide to remove most of the oxygen and moisture from the argon gas. The sacrificial titanium powder was used to absorb any residual oxygen from the argon gas entering the work tube. The work tube was then heated at a rate of 5°C/min to a sintering temperature of 1350°C. The rods were isothermally held at this temperature for 1 hour followed by furnace cooling at a rate of 5°C/min. The density of the each sintered rods was calculated from the geometry and mass, and the underlying microstructure was studied by optical and electron microscopy.

3.3.6Hot isostatic pressing

The cylindrical Ti and Ti-6Al-4V materials produced by sintering and casting technologies were shipped to a hot isostatic pressing (HIP'ing) facility abroad (Belgium) for further densification following a radiographic examination for internal porosity. HIP'ing was performed at gas pressure of approximately 1000 ± 50 bar while simultaneously heating at 915°C ± 10 for 120 ± 15 min followed by slow cooling.

3.3.7Fabrication of tensile specimens from sintered materials

The sintered plus hot isostatically pressed (HIP'ed) titanium rods were thereafter machined into small size dumbbell shaped tensile test specimens in accord with the ASTM E8 standard. The diameter and gage length of tensile specimens were approximately 5 mm and 28 mm respectively. Figure 3.4 shows a typical tensile specimen machined from the sintered titanium rod.



Figure 3.5: Exterior appearance of the tensile specimens machined from pressureless sintered titanium rod

3.3.8Fabrication of tensile specimens from cast materials

To prepare for centrifugal casting, 25 g of commercial grade titanium powder and Ti-6Al-4V powder mix obtained by alloying additions in the form of a 60Al:40V master alloy powder were cold uniaxially pressed in a die at 300 MPa. The resultant green compacts had a diameter and height of approximately 24 and 15 mm. Each compact was then loaded in the yttria lined ZrO_2 crucible and placed inside the copper heating coil fitted in the melting chamber of the Manfredi M10H3 centrifugal casting furnace. The furnace was then evacuated to approximately -90 kPa using a rotary pump and back-filled with argon gas, repeating this cycle 5 times. The green compact was then melted in a ZrO_2 based crucible under an argon atmosphere. When the temperature of the melt reached 1850°C, the melt was poured into the copper mould fixed adjacent to the melting crucible under a centrifugal force. The cavity of the copper mould was shaped like a round dumbbell-type tensile specimen with dimensions conforming to the ASTM E8 standard. The resultant tensile specimens had a diameter and gage length of approximately 5 mm and 28 mm respectively. The melt took approximately 15 minutes to cool from 1850°C to room temperature. The as-cast tensile specimens were then sectioned for oxygen analysis and metallographic examination.

A Leybolt Heraeus ISPIII/Ds three chamber vacuum furnace was used for vacuum casting. A 2 kg billet, previously shown in Figure 3.5, was placed in a ZrO_2 based crucible and melted at approximately 1800°C under a vacuum pressure of $1x10^{-3}$ mbar. The melt was subsequently poured in a copper mould and allowed to solidify

under vacuum to form an ingot shown in Figure 3.6. The ingot had a diameter and length of approximately 50 mm and 180 mm respectively. The ingot was then sectioned in half and labelled as bottom and top section as indicated in Figure 3.6.



Figure 3.6: Cylindrical ingot obtained by vacuum casting of the cold isostatically pressed CP-Ti billet

Six cylinders of a diameter and length of approximately 13 and 75 mm, respectively, were cut out from the bottom and top sections using wire cutting as shown in Figure 3.7. The cylinders labelled ON in Figure 3.7 (b) represent samples based on the bottom section of the ingot, while those labelled BO (Figure 3.7 (a)) are from the top section which is a fraction of the last melt to solidify After radiographic examination, the cylinders were HIP'ed at a temperature of 915℃ ±10 for 120 min ± 15 under a hydrostatic argon gas pressure of approximately 100 MPa to eliminate residual porosity prior to the machining of tensile specimens.

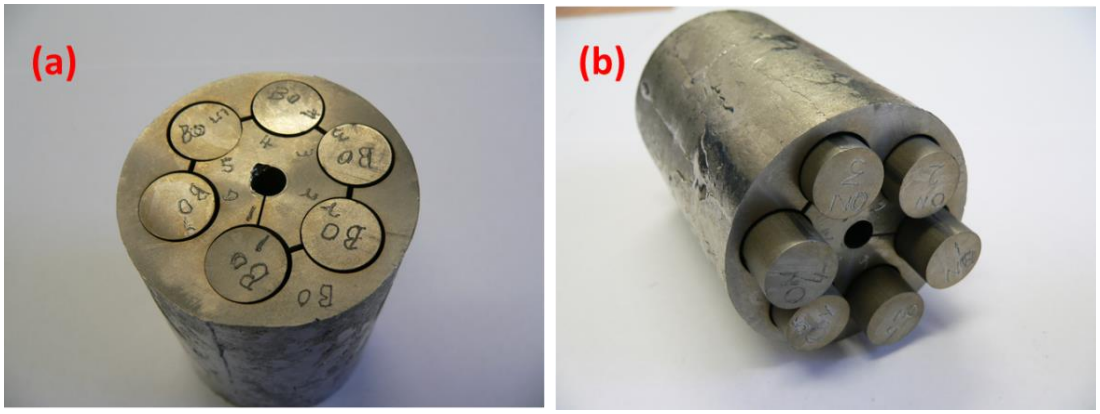

Figure 3.7: Cylinders cut out from the (a) top section and (b) bottom section of the titanium ingot obtained by conventional casting under vacuum

The rods were then machined using a computer numerically controlled (CNC) machine to make tensile dumbbell shaped tensile specimens shown in Figure 3.8. The reduced section and gage length of the tensile specimens were 7 mm and 35 mm, respectively.



Figure 3.8: Cast titanium tensile specimen

3.3.9Fabrication of tensile specimens using rapid manufacturing

Eleven dumbbell shaped tensile specimens were fabricated using the layered or rapid manufacturing technology directly from the supposedly pre-alloyed Ti-6Al-4V powder. It is noteworthy that the rapid manufacturing research facilities accessible during this time could only use their own pre-alloyed Ti-6Al-4V as the starting material to limit contamination. Therefore the tensile specimens could not be produced from the blended elemental Ti-6Al-4V and pure Ti powders prepared used for other experiments in this research. Nevertheless, layered manufacturing is a computer controlled process which involves scanning a focused laser or electron beam to selectively melt or sinter atomised powder one layer at a time until a three

dimensional component is built. The process is able to fabricate layers of thickness ranging from 30 to100 µm, depending on the specifications of the powder and system used. The as-fabricated specimens had a reduced section and gage length of 6 mm and 30 mm respectively. The as-fabricated specimens were analysed for density, oxygen content, microstructural features and phase composition. The reduced sections of the fabricated specimens were fine ground with abrasive paper to obtain a smooth surface prior to tensile testing. The final diameter of the tensile specimens after grinding was approximately 5.6 mm. The as-fabricated specimens were analysed for density and microstructure prior to heat treatment and tension testing. Figure 3.9 shows the exterior appearance of the fine polished layer manufactured Ti-6Al-4V tensile specimens



Figure 3.9: Exterior appearance of the fine polished Ti-6Al-4V specimen produced by rapid manufacturing

3.3.10 Heat treatment

The annealing of pressureless sintered and vacuum cast titanium tensile specimens was performed at a temperature of 750°C for 2 hours in a vacuum furnace followed by furnace cooling. However, it should be noted that only half of the specimens from the top and bottom sections of the vacuum cast titanium were annealed, while the other half was left in the HIP condition.

The annealing of the pressureless sintered and vacuum cast Ti-6Al-4V tensile specimens was performed at a temperature of 850°C for 4 hours in a vacuum furnace followed by furnace cooling. The Ti-6Al-4V tensile specimens produced by rapid manufacturing were annealed at temperatures of 750 and 850°C for 2 hours in a

horizontal tube furnace followed by furnace cooling. It should be noted that a set of three specimens was annealed at each of the temperatures, while the remaining four specimens were left in the as-built condition. The samples were then analysed for any changes in the microstructure by optical microscopy.

3.3.11 Tension testing

The annealed pressureless sintered and vacuum cast titanium tensile specimens were tested at a strain rate of 1 mm/min on the Instron 1242 tensile tester at room temperature. An extensometer was used for accurate measurement of the percentage elongation up to approximately 1 mm of extension and the tensile tester measured the remainder of the strain. The initial and final diameters of the specimens were measured and the reduction in area was calculated. The pre-alloyed Ti-6Al-4V alloy specimens obtained by layered manufacturing were tested using the same procedure, but using an MTS Criterion Model 45 tensile tester. The gage length of the laser fabricated specimens was not long enough to allow the use of an extensometer, so the elongation was only measured by the tensile tester.

3.3.12 Metallography

For metallographic examination, the specimens were cut to a thickness of approximately 2.5 mm using a diamond cut-off wheel. The surface to be examined was placed facing down on the stage of the compression mounting machine and was lowered down into the heating chamber. Approximately 20 ml of the Struers PolyFast thermosetting resin was poured to cover the sample and the chamber was sealed. Compression mounting was performed by applying a pressure of 250 bar while simultaneously heating the resin at a temperature of 180°C for 3 minutes followed by water cooling for 1.5 minutes. The mounted metallographic samples had a diameter of 30 mm, while the thickness was dependent on the amount of resin used. The samples were then wet ground on SiC abrasive papers (grit numbers P400−P4000) and polished to a 0.04 µm finish with colloidal silica (OP-S) suspension. The specimens were washed in the ultrasonic bath after each grinding step and with acetone after polishing with OP-S. The polished specimens were thereafter chemically etched for

approximately 3 seconds in diluted Krolls reagent followed by immediate rinsing under running water to stop the corrosive action of the etchant. The etched specimens were characterized for microstructure using the optical microscope as a result of thermal treatment.

The commercial grade titanium powder was poured in a cylindrical rubber mould and a clear epoxy resin was poured over the powder and allowed to cure under vacuum for 24 hours. The mounted powder was thereafter ground on SiC papers (grit numbers P800−P4000) and polished to a 0.04 μm finish with OP-S suspension. The polished powder samples were thereafter examined for particle morphology using the SEM. By contrast, the 60Al:40V master alloy and the supposedly pre-alloyed Ti-6Al-4V powders were analysed for particle morphology in their loose form. The supposedly prealloyed powders were further analysed for elemental composition using the EDS to confirm that they were indeed alloyed.

It should be noted that for both metallic and powder specimens, fine polishing was performed by pouring small amounts of the OP-S suspension intermittently on a MD-Chem synthetic leather plate. Grinding and polishing speeds of 150 rpm were used and the grinding direction was clockwise while the polishing direction was counter-clockwise. A force of 10 N was applied at the centre of the specimens during grinding and polishing in order to ensure consistency in the quality of sample preparation. Wet grinding was performed for approximately 3 minutes on each SiC paper while polishing was performed for approximately 5 minutes.

CHAPTER 4: RESULTS

The results obtained by characterization of starting powders and materials obtained from experimental work are presented and analysed concisely in this chapter. The particle size, morphology, chemistry, phase composition and oxygen content of the starting powders are presented in the beginning of the chapter, and compared to the particle size, oxygen content and chemistry of mechanically milled titanium and blended Ti-6Al-4V powders later on in this chapter. The densities, microstructural features and tensile properties materials produced by the cold press and sinter, rapid manufacturing, casting, HIP and heat treatment techniques are then presented and compared.

4.1 Characterization of as-received powders

The respective particle size distributions of the as-received powders are shown in Figures 4.1 to 4.5.

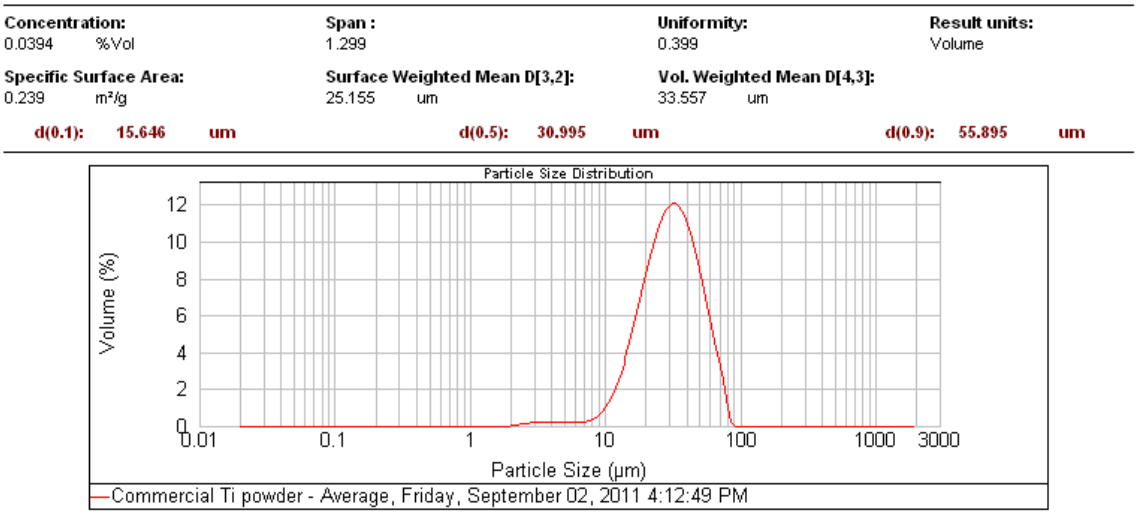

Figure 4.1: Particle size distribution of as-received commercial grade titanium powder

Concentration:	Span :	Uniformity:	Result units:
0.0177 %Vol	1.493	0.458	Volume
Specific Surface Area:	**Surface Weighted Mean D[3,2]:**	**Vol. Weighted Mean D[4,3]:**	
0.537 m²/g	11.179 um	16.158 um	
d(0.1): 5.970 um	**d(0.5):** 14.917 um	**d(0.9):** 28.239 um	

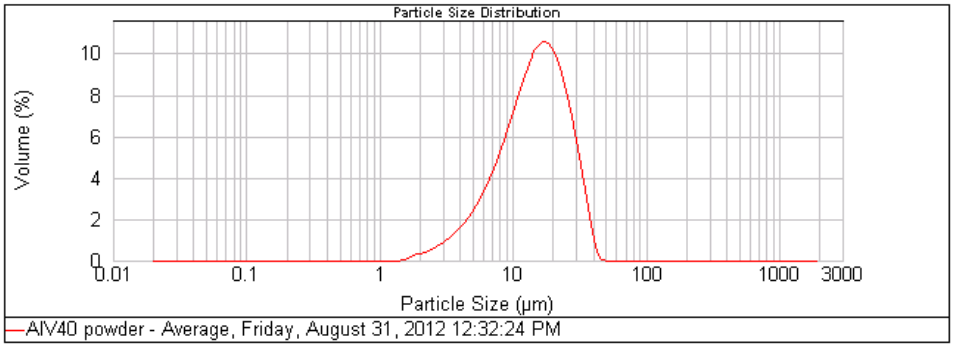

Figure 4.2: Particle distribution of as-received 60Al-40V master alloy powder

Concentration:	Span :	Uniformity:	Result units:
0.0234 %Vol	1.735	0.537	Volume
Specific Surface Area:	**Surface Weighted Mean D[3,2]:**	**Vol. Weighted Mean D[4,3]:**	
0.526 m²/g	11.414 um	16.615 um	
d(0.1): 6.056 um	**d(0.5):** 14.212 um	**d(0.9):** 30.712 um	

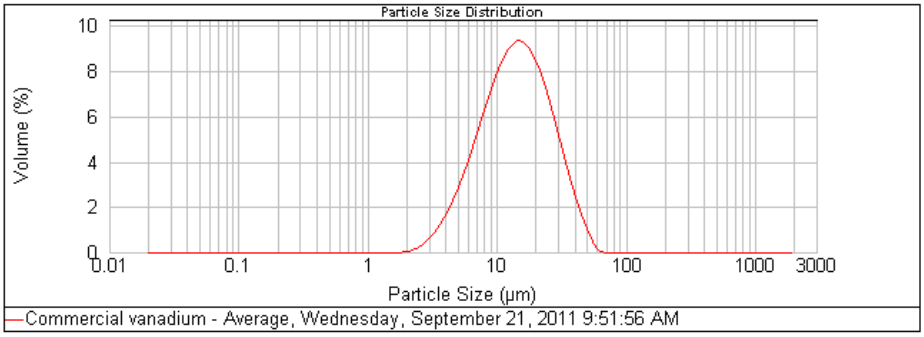

Figure 4.3: Particle size distribution of vanadium elementary powder

Concentration:	Span :	Uniformity:	Result units:
0.0175 %Vol	1.478	0.458	Volume
Specific Surface Area:	**Surface Weighted Mean D[3,2]:**	**Vol. Weighted Mean D[4,3]:**	
0.662 m²/g	9.060 um	11.998 um	
d(0.1): 5.132 um	**d(0.5):** 10.609 um	**d(0.9):** 20.811 um	

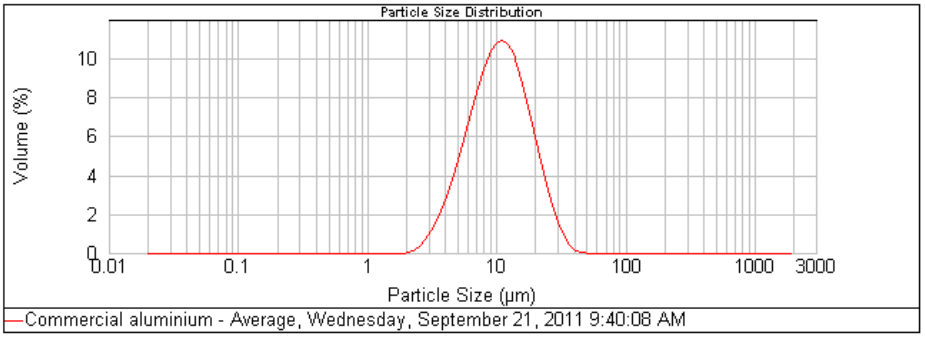

Figure 4.4: Particle size distribution of aluminium elementary powder

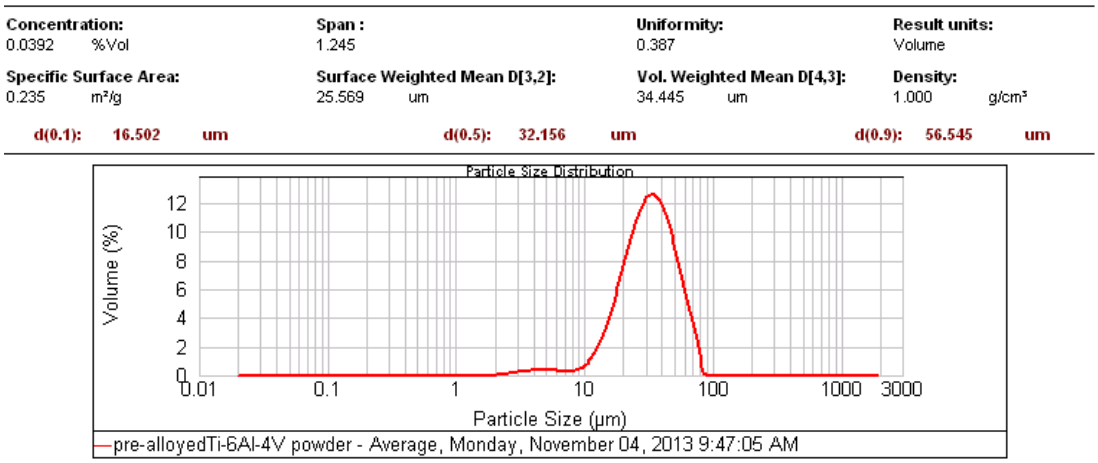

Figure 4.5: Particle size distribution of the pre-alloyed Ti-6Al-4V powder

The PSD analysis in Figure 4.1 shows that the d_{50} particle size of the commercial grade powder was approximately 31 µm, and 90% of the particles in this powder had a particle size (d_{90}) less than 57 µm. Figures 4.2 to 4.5 show that the d_{50} particle size of the 60Al:40V master alloy, vanadium, aluminium and pre-alloyed Ti-6Al-4V powders was approximately 15, 14, 11 and 32 µm respectively. The SEM micrographs of the most important powders (commercial titanium, 60Al:40V and pre-alloyed Ti-6Al-4V) are shown in Figure 4.6. It can be seen that the titanium powder mainly consisted of irregular-blocky particles, while the 60Al-40V powder (Figure 4.6(b)) and pre-alloyed Ti-6Al-4V powder (Figure 4.6(c)) mainly consisted of spherical particles.

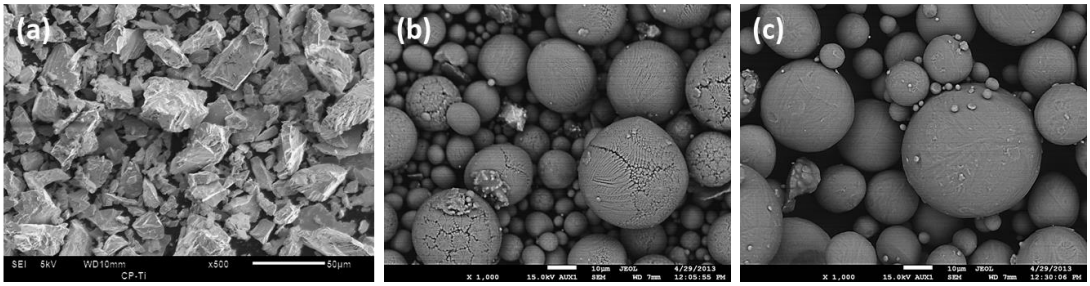

Figure 4.6: Particle morphology of the as-received (a) pure Ti, (b) 60Al:40V master alloy and (c) pre-alloyed Ti-6Al-4V powders

Figure 4.7 shows the EDS analyses obtained by scanning various free-standing particles and the bulk 60Al:40V powder. The EDS spectra indicate that individual powder particles mainly consisted of both Al and V elements. The average proportions of these elements in the bulk powder were 56±0.4 and 43.7±0.5 wt. %, respectively, as determined by EDS. The chemical composition of Al and V in the master alloy powder are within the society of automotive engineers (SAE) AMS4911 standard for Ti-6Al-4V alloy for aerospace applications (5.5-6.5 wt.% Al and 3.5-4.5 wt.%V).

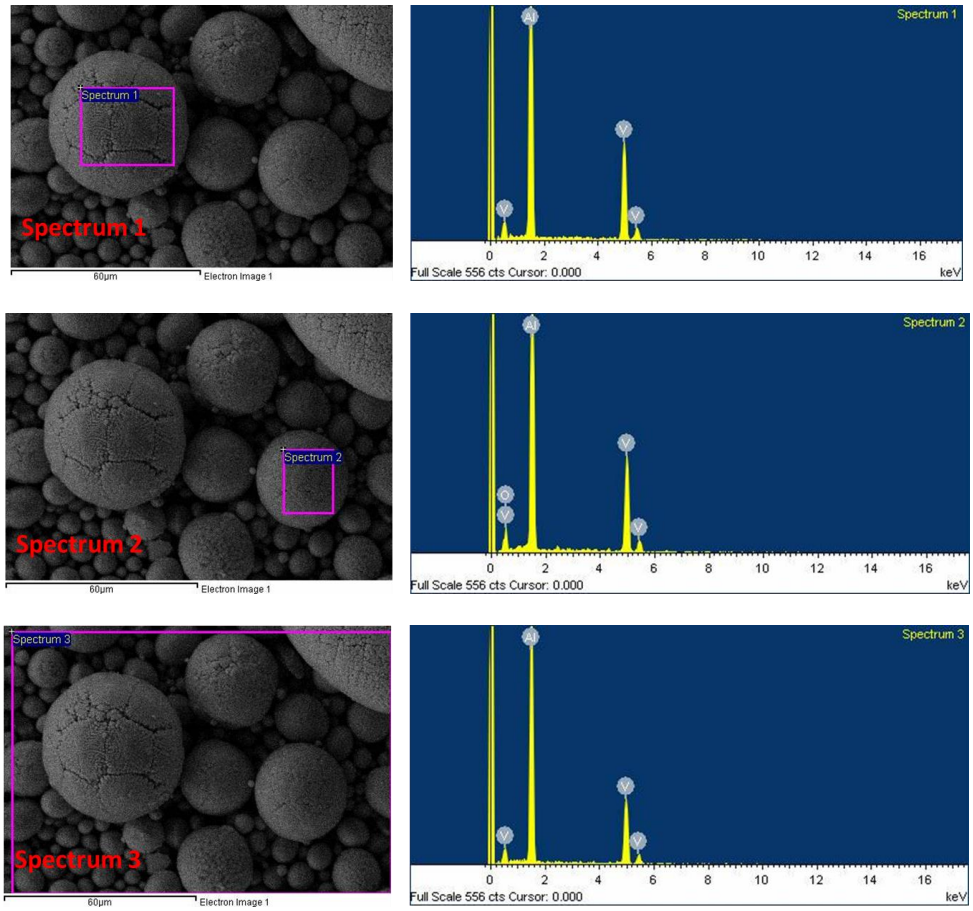

Figure 4.7: EDS chemical analysis of the 60Al:40V master alloy powder

The EDS spectra in Figure 4.8 show that individual particles and the bulk pre-alloyed Ti-6Al-4V powder mainly consisted of all the mandatory elements (Ti, Al, and V), and the average chemical composition of the bulk powder was 5.8 ±0.1wt.% Al, 4.2±0.3 wt.% V and 90±0.6 wt.% Ti, as determined by EDS. Similarly, the composition of alloying elements is within the SAE AMS4911 standard.

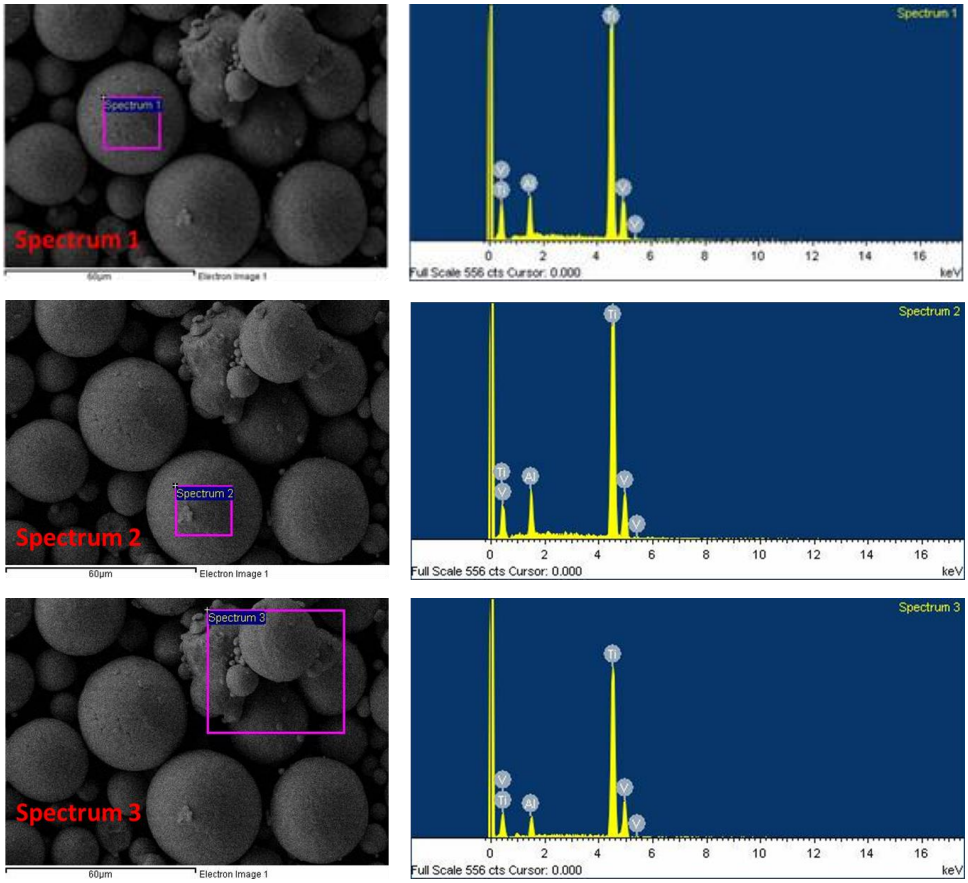

Figure 4.8: EDS analysis of the pre-alloyed Ti-6Al-4V powder

The two alloy powders were further characterized for phase composition and their respective XRD patterns are shown in Figure 4.9 and Figure 4.10. The pattern in Figure 4.9 shows that the as-received 60Al:40V master alloy powder mainly consisted of the V_5Al_8 and Al_3V intermetallics, while Figure 4.10 shows α-Ti as the predominant phase in the pre-alloyed Ti-6Al-4V alloy powder. However, it is noteworthy that the most intense peak has shifted to a higher angle compared to the standard diffraction pattern of α-Ti.

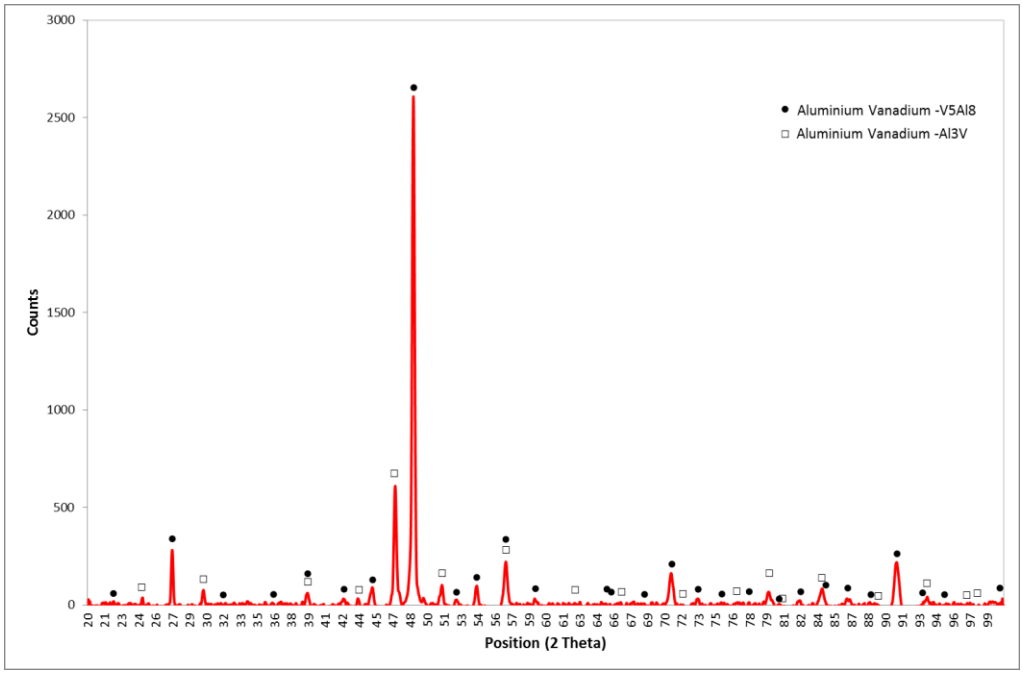

Figure 4.9: XRD pattern of as-received 60Al-40V master alloy powder

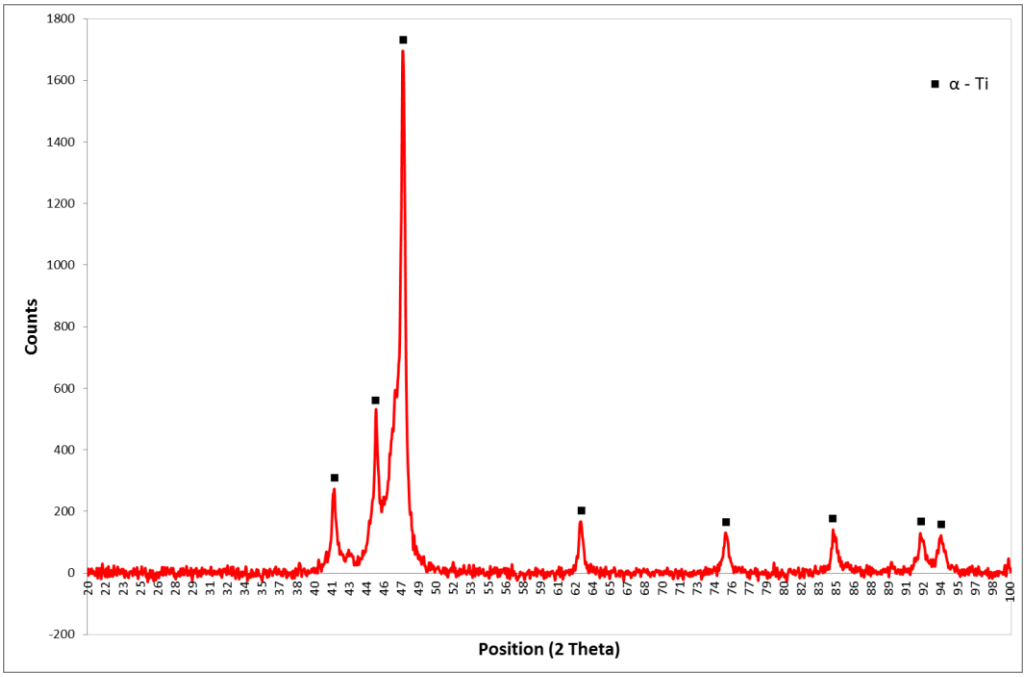

Figure 4.10: XRD pattern of as-received pre-alloyed Ti-6Al-4V powder

Since oxygen is usually a major concern during the processing of titanium products, the oxygen content of the as-received commercial grade titanium, 60Al:40V and pre-alloyed Ti-6Al-4V powders was determined by the gas fusion technique (Leco TCH 600) prior to commencing with the experiments. The Leco analyses in Table 4.1 show

that the oxygen content of the commercial grade titanium was approximately 0.08% higher than the manufacturer's specifications (0.377%). Secondly, it is evident that the oxygen content of the 60Al:40V master alloy powder was below the 0.2% limit for the commercial Ti-6Al-4V alloy. Finally, the analyses reveal that the oxygen content of the pre-alloyed Ti-6Al-4V powder was within the specification of the Ti-6Al-4V ELI (extra low interstitial) alloy.

Table 4.1: Oxygen content of raw powders as determined by Leco

Specimen label	***Supplier***	***O (wt. %)***
CP-Ti	Industrial Analytical	0.46
60Al-40V	TLS Technik GmbH & Co.	0.020
Ti-6A-4V	CRPM	0.13

4.2 Milling of pure Ti and blended elemental Ti-6Al-4V powders

The particle size distribution, microstructure, chemistry and oxygen analyses of pure titanium and blended Ti-6Al-4V powder prepared using the high energy attritor mill are presented and compared to the starting powders in this section. The oxygen analysis of the blended Ti-6Al-4V powder prepared using the Turbula mixer are also presented and compared to that of mechanically milled powder.

Figure 4.11 shows the particle size distribution curve of the Ti-6Al-4V powder prepared by manual mixing of commercial Grade 4 titanium powder with Al and V elemental powders in proportions of 6 and 4 wt.%, respectively. The PSD analysis shows that the as-mixed powder consisted of micron-sized particles of average size 22 μm, while the EDS analyses (Figure 4.12) reveal that only the Ti and Al elements could be detected in the Ti-6Al-4V mix, indicative of inhomogeneity.

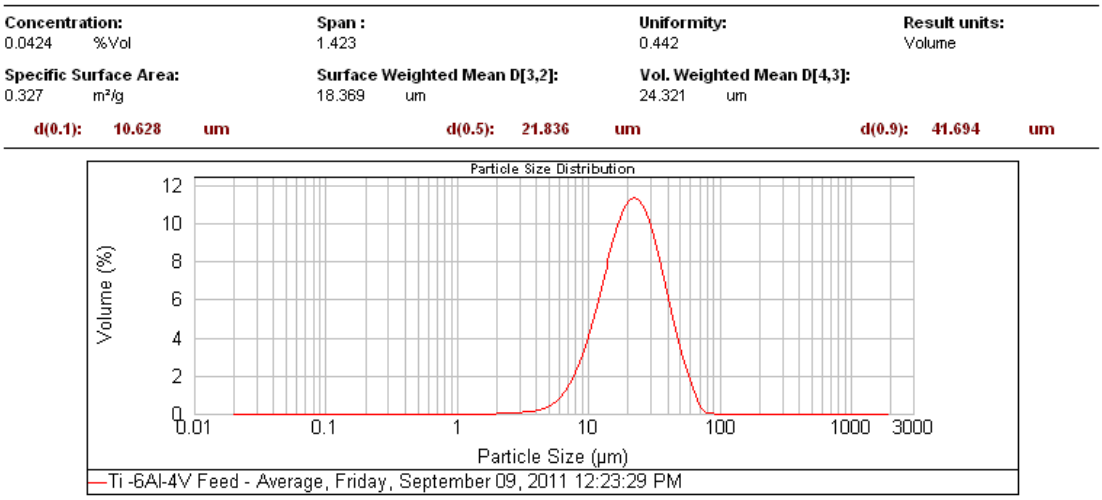

Figure 4.11: PSD curve of the blended elemental Ti-6Al-4V powder obtained by alloying additions in the form of elemental powders

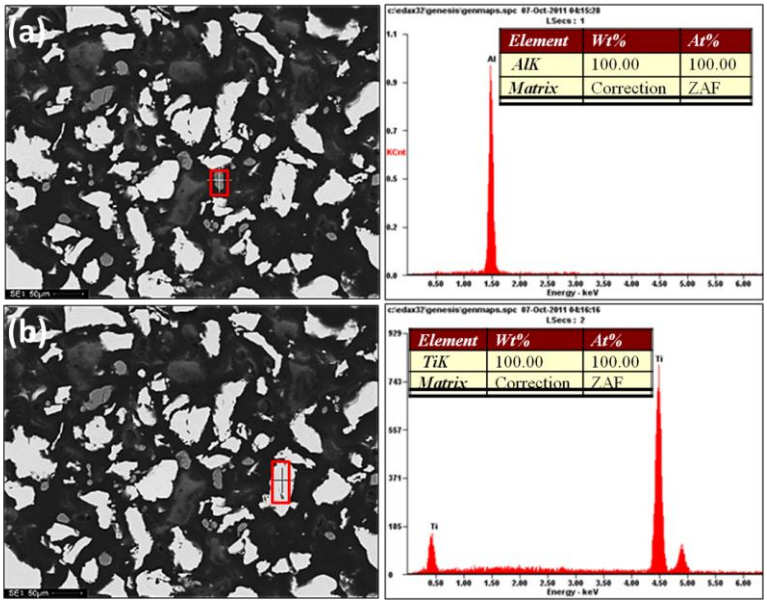

Figure 4.12: EDS spectra of the blended elemental Ti-6A-4V powder obtained by alloying additions in the form of elemental powders

The manually mixed Ti-6Al-4V powder and as-received commercial grade titanium powder were then processed in the high energy attritor mill and subsequently characterized for particle size distribution. Comparing the particle size analysis in Figure 4.13 to Figure 4.13, it is evident that the d_{50} particle size of the Ti-6Al-4V powder increased by approximately 3 µm after milling for 1 hour at a fixed speed of 1350. Similarly, the particle size analysis in Figure 4.14 and Figure 4.1 confirm that

the average particle size of the titanium powder increased by 3 µm after milling at 1350 rpm for 1 hour.

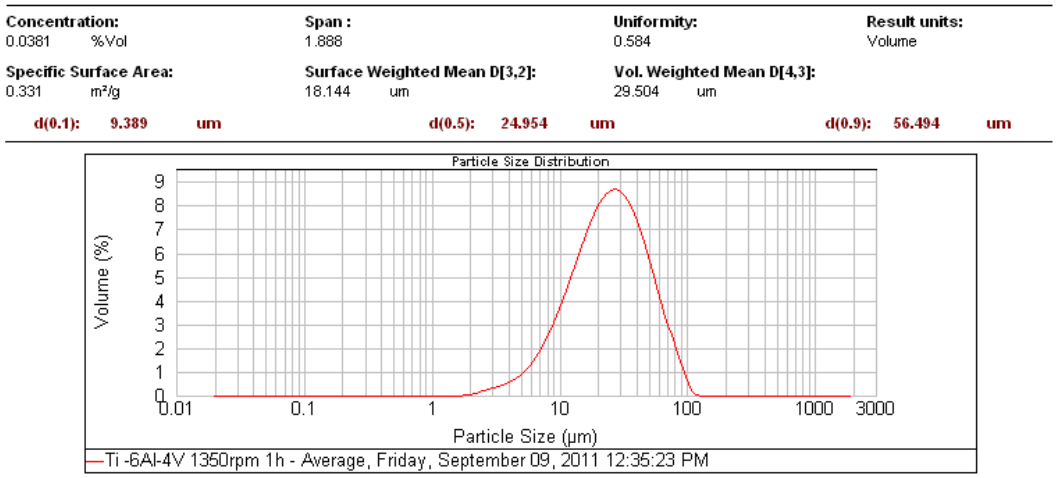

Figure 4.13: PSD curve of the blended elemental Ti-6Al-4V after attrition milling at 1350 rpm for 1 hour

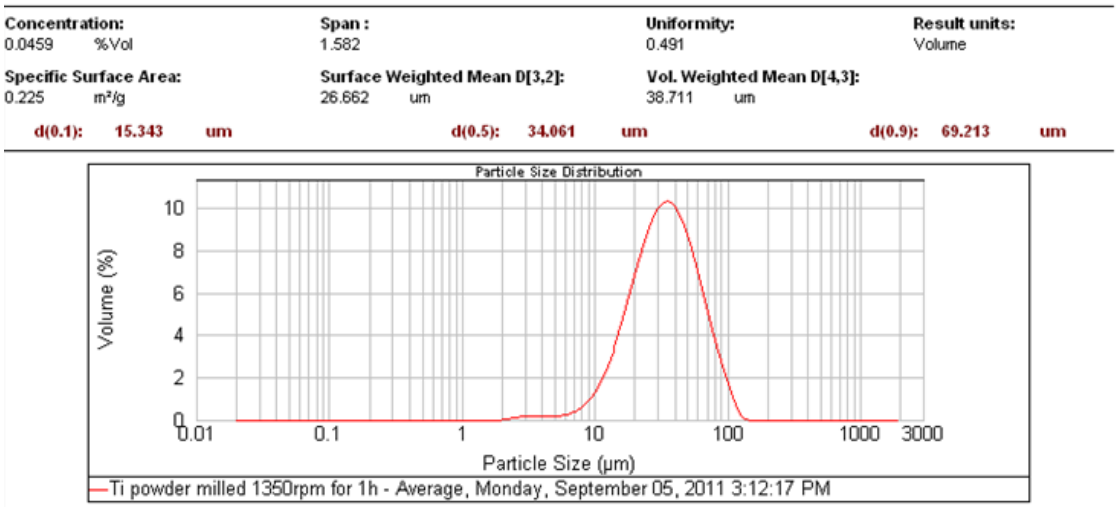

Figure 4.14: PSD curve of the commercial grade titanium powder after attrition milling at 1350 rpm for 1 hour

Figure 4.15 shows the backscattered SEM images of cross-sectioned titanium and mixed Ti-6Al-4V powder particles before and after processing in the attritor mill for 1 hour at a fixed impeller speed of 1350 rpm. By comparing the milled powders (Figures 4.15(b) and 4.15(d)) to the starting powders (Figures 4.15(a) and 4.15(c)), it is evident that the particles changed from irregular to a plate-like shape after high

speed attrition milling. Figure 4.15 (b) also shows evidence of particle aggregates and presence of cracks in some titanium particles after milling.

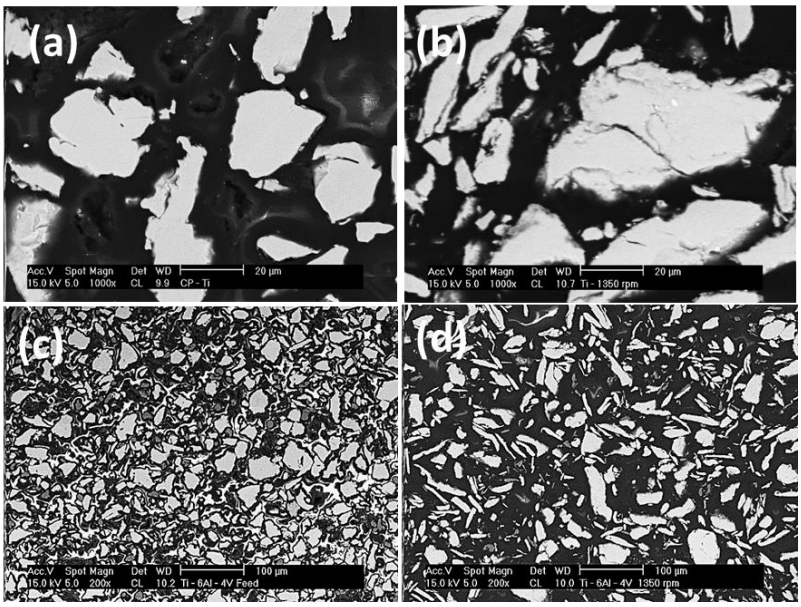

Figure 4.15: SEM backscattered images of cross-sectioned (a) as-received pure Ti powder particles (b) pure titanium powder particles after 1 h of milling at a fixed speed of 1350 rpm (c) manually mixed Ti-6Al-4V alloy powder particles and (d) manually mixed Ti-6Al-4V alloy powder particles after 1 hour of milling at a fixed speed of 1350 rpm

The EDS microanalysis of the Ti-6Al-4V powder produced using the attritor mill is shown in Figure 4.16. Similar to milled titanium powder, the highlighted particle in the complementary SEM micrograph shows evidence of particle agglomeration. The EDS spectra reveals that the highlighted particle consisted of all the elements initially added when preparing the Ti-6Al-4V power mixture.

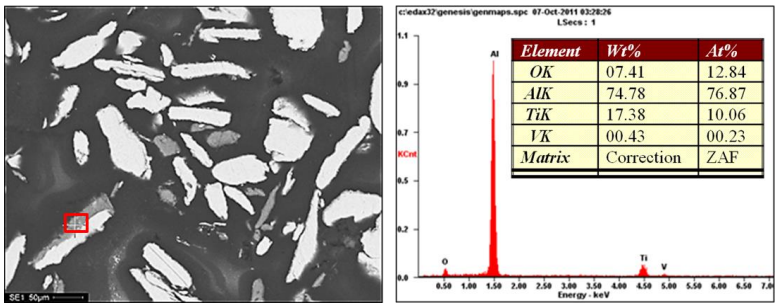

Figure 4.16: EDS microanalysis of the Ti-6Al-4V powder produced using the attritor mill at fixed speed of 1350 rpm for 1 hour

The milled Ti-6Al-4V powder mixture was then characterized for phase composition to check for contamination by the milling media and evidence of mechanical alloying, if any, in the bulk powder. The XRD pattern in Figure 4.17 shows that the milled Ti-6Al-4V blended powder only consisted of Ti, Al and V in elemental form. No noticeable shift in the peak position can be observed in diffraction pattern to suggest alloying. However, the peaks appear to be slightly broadened.

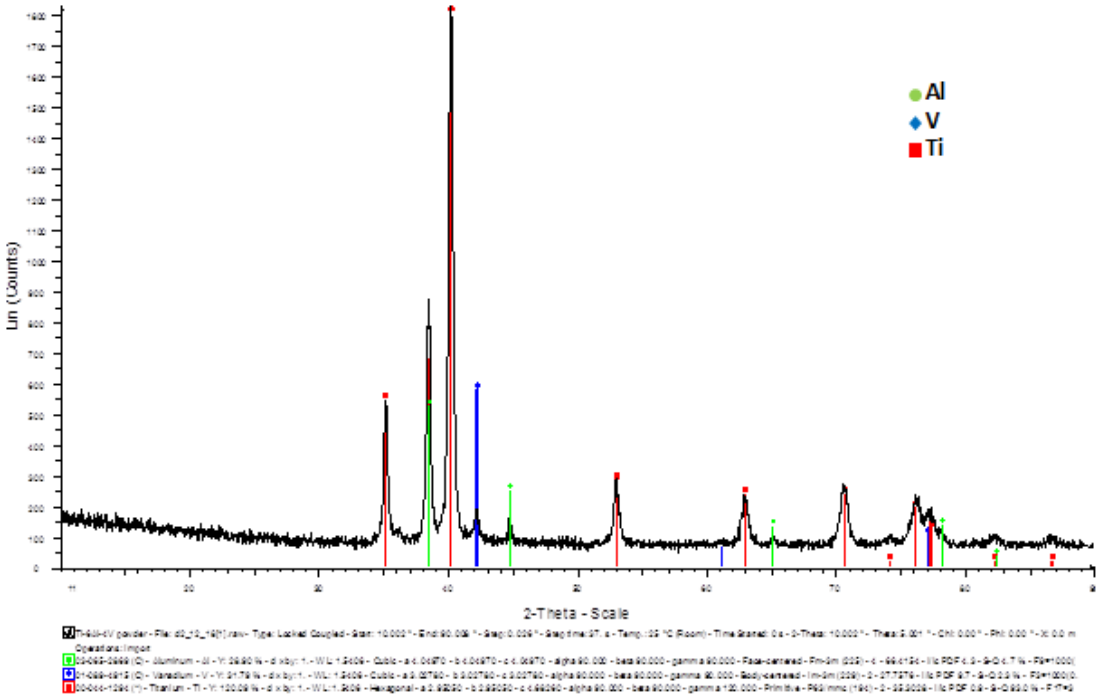

Figure 4.17: XRD pattern of the attrition milled blended elemental Ti-6Al-4V powder

The oxygen analyses of the milled and starting powders are compared in Table 4.2. It is shown that high energy milling under normal atmosphere almost doubled the oxygen content titanium powder, while that of the Ti-6Al-4V powder increased by 0.30 wt. %.

Table 4.2: Oxygen analysis of attrition milled powders as determined by Leco

Specimen label	*Sample description*	*% O*
Ti-M1	As-received Ti powder	0.45
BE-Ti-64	Initial Ti-6Al-4V powder mix	0.60
Ti-M2	Milled Ti powder	0.87
Ti-M3	Milled Ti-6Al-4V powder mix	0.9

As shown earlier, high energy mechanical milling under normal atmosphere barely satisfied the objectives stated earlier in chapter 3. Therefore an alternative powder blending technique had to be investigated. Due to the high oxygen content reflected in the analysis of the as –received aluminium powder, the master alloy was used as a substitute for Al and V elemental powders. The blending of Ti and 60Al-40V powders was then performed at a significantly low speed (67 rpm) for 1 hour under normal atmosphere using a Turbula mixer. The resultant powder blend was characterized for oxygen content, and the results are presented in Table 4.3. It is clear that the Turbula mixing approach did not result in any oxygen pick-up. Therefore, on the basis of oxygen contamination, the Turbula mixing approach is ideal for blending of powders compared to high energy mechanical milling, and was therefore used to prepare blended elemental Ti-6Al-4V powders throughout this research.

Table 4.3: Comparison between oxygen content of as-received Ti and Ti-64 mix prepared by Turbula mixing

Specimen label	*Sample Description*	*% O*
Ti-M1	As-received CP -Ti	0.45
Ti-64 MB	Blended Ti-6Al-4V powder	0.43

4.3 Pressing and sintering of titanium powder and Ti-6Al-4V powder

The microstructure and density of Ti and Ti-6Al-4V alloy materials produced by the SPS method are presented and briefly compared in the section. As mentioned in Chapter 3, the titanium powder and blended Ti-6Al-4V powders were tested for compactability prior to die pressing and CIP'ing. The compactability curve in Figure

4.18 illustrates the variation of the green density of titanium powder compacts with applied uniaxial pressure during die pressing. It is evident that the green density initially increased rapidly with increasing applied pressure up to approximately 66 MPa, and then increased gradually up to approximately 376 MPa and finally exhibits a linear trend until a maximum relative density of 88% (approximately 3.97 g/cm^3) could be obtained at a maximum die pressure of 619 MPa. These three regions are indicated as (a), (b) and (c) in Figure 4.18.

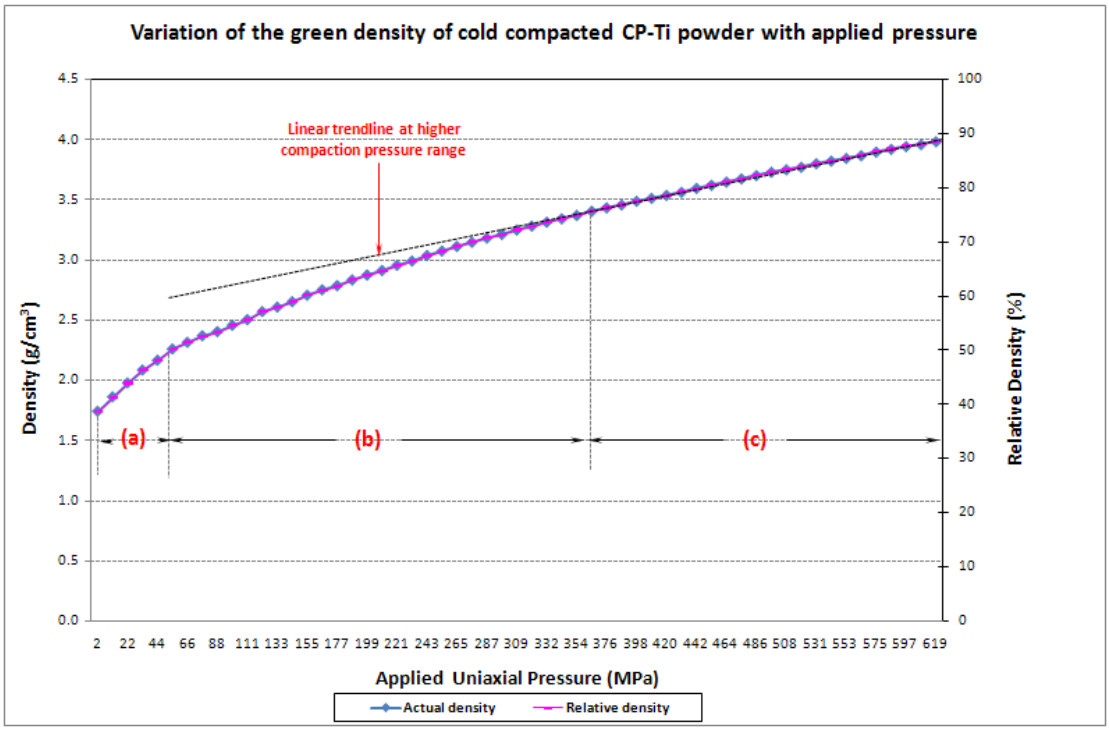

Figure 4.18: Compaction curve of unalloyed titanium powder

Similarly, the compactability of the blended elemental Ti-6Al-4V powder was investigated and the resultant curve is shown in Figure 4.19. The curve shows a trend similar to that of the unalloyed titanium powder. A relative density of 90% (approximately 3.98 g/cm^3) was obtained at a maximum die pressure of 619 MPa.

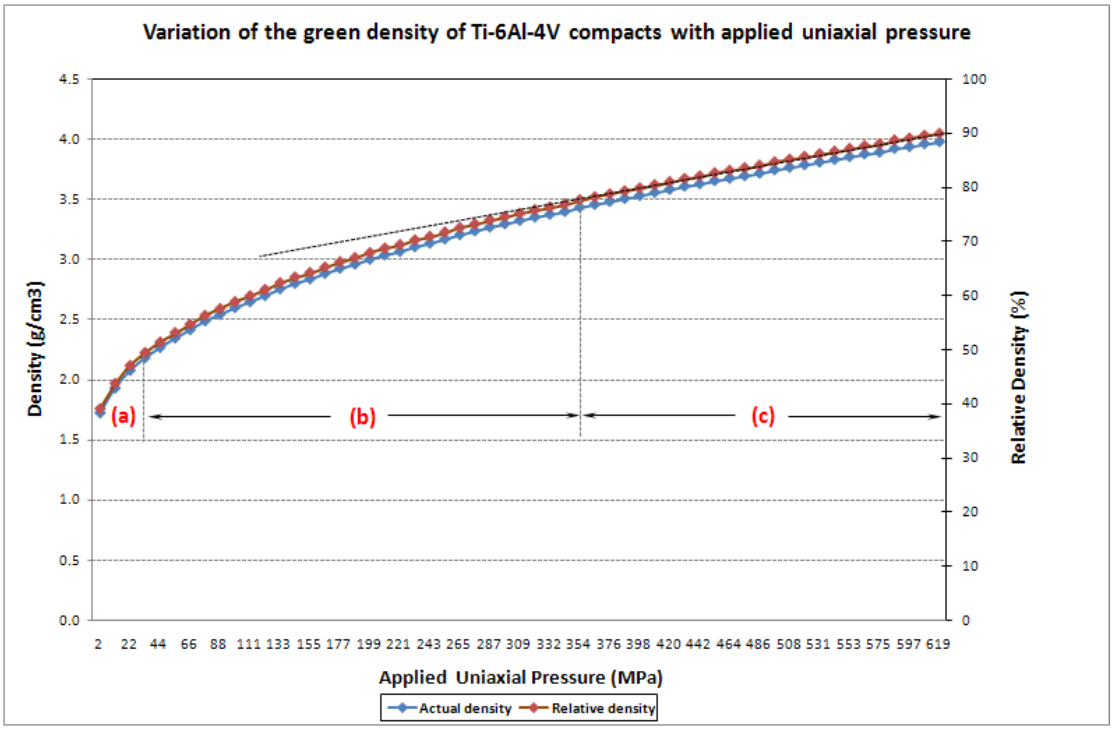

Figure 4.19: Compaction curve of the blended Ti-6Al-4V powder

The compactability curves were then used to determine the uniaxial pressure needed to produce cylindrical pellets with a relative density of 71% for spark plasma sintering experiments. Figure 4.20 illustrates the effect of sintering temperature on the linear (height) shrinkage of the pure titanium powder pellets during spark plasma sintering. The temperature profile of the sample which was sintered at 1250 °C is also included for discussion in Chapter 5. The shrinkage curves mainly consist of 4 regions (labelled (a) to (d)). A positive slope on the curve indicates linear shrinkage while a negative slope represents linear expansion. It can be clearly seen that the rate of linear shrinkage and total shrinkage generally increased with increasing sintering temperature.

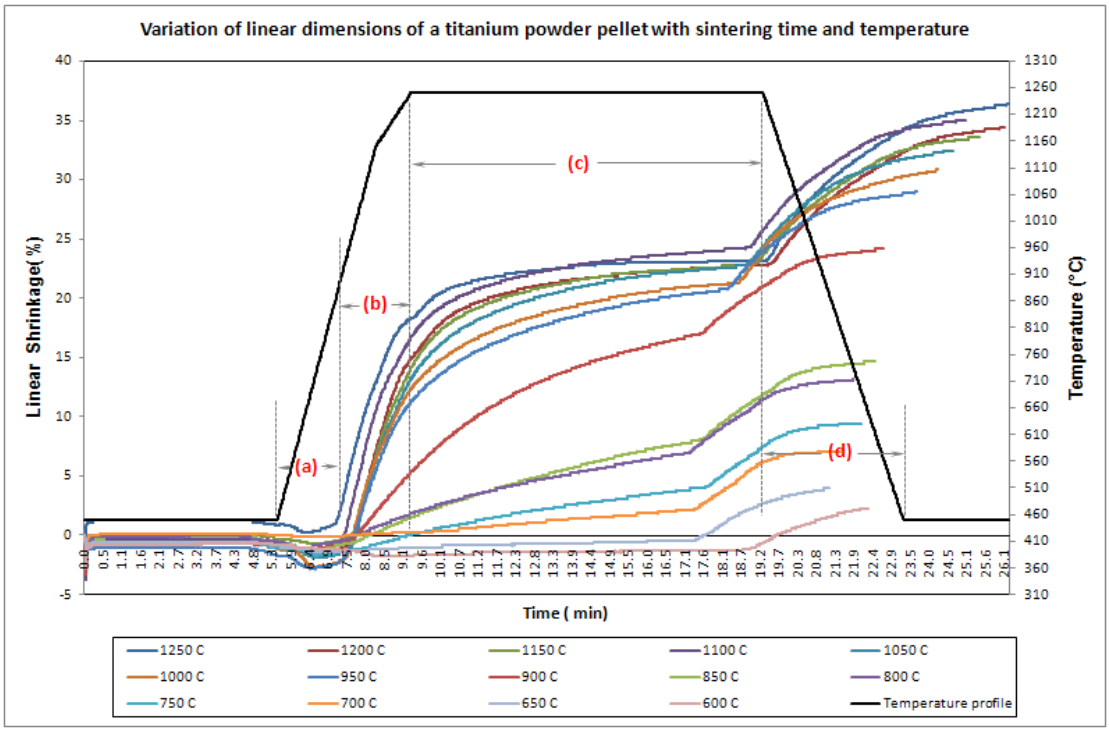

Figure 4.20: Effect of sintering temperature on the linear shrinkage of a titanium pellet

Figure 4.21 shows the variation of sintered density during spark plasma sintering of pure titanium pellets at temperatures in the range of 600−1250°C. It should be noted that an isothermal holding time was fixed at 10 minutes for all pellets and the lowest possible compressive pressure of 10MPa was used. It is observed that the density first three samples which were sintered at temperatures in the range 600−700°C remained constant at 72% of the theoretical density, and increased gradually with a further increase of the sintering temperature. A sintered density of 99% (4.46 g/cm^3) was obtained for samples sintered at the higher end of the temperature range (1200-1250).

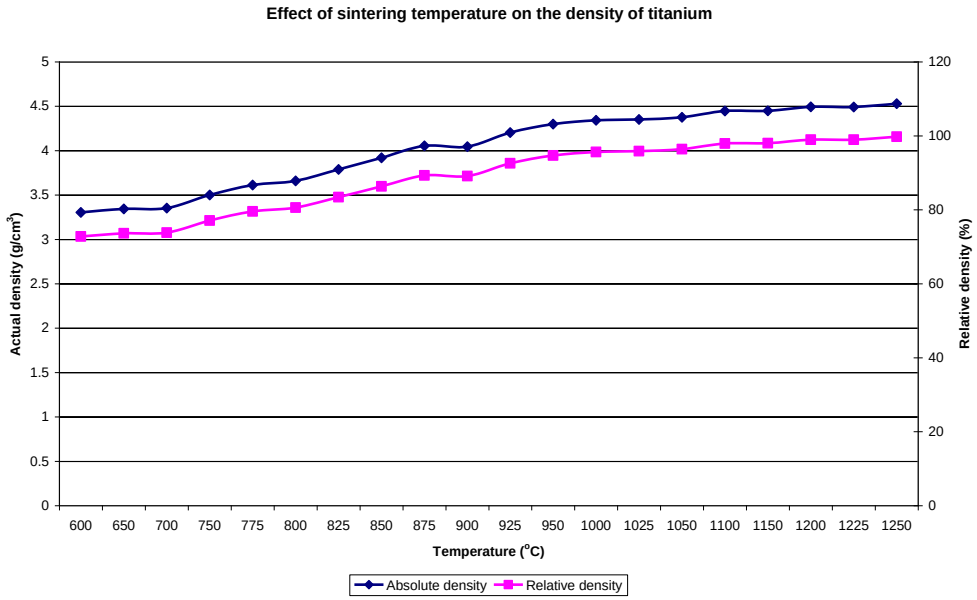

Figure 4.21: Variation of the density of titanium compacts with spark plasma sintering temperature

Figure 4.22 depicts the optical micrographs of cross-sectioned titanium powder pellets which were produced by the SPS method at temperatures of 600 and 750°C. The black phase represents residual porosity, while the grey phase is powder particle aggregates. From the optical micrographs, it can be seen that the sample which was sintered at 750°C (Figure 4.22(b)) had a smaller fraction of residual porosity compared to the sample produced at 600°C (Figure 4.22(a)). This is in agreement with the densification curve shown in Figure 4.21.

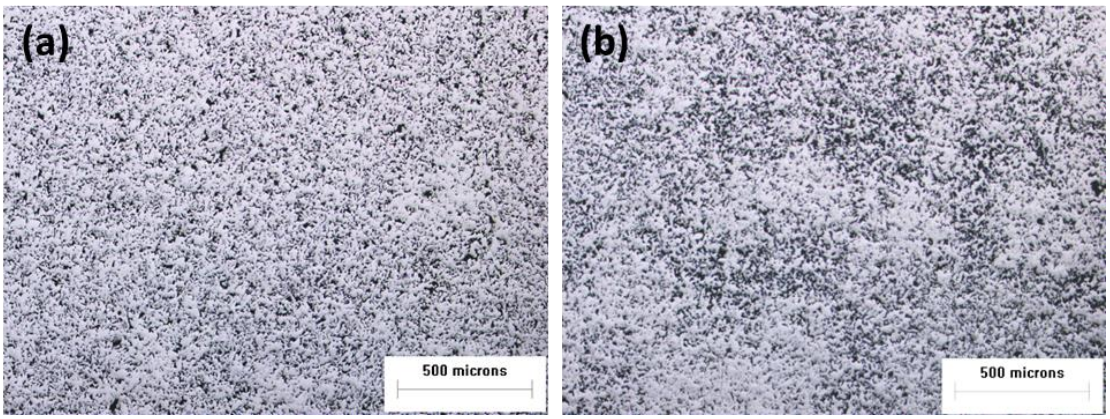

Figure 4.22: Optical micrographs of pressed titanium pellets after sintering at (a) 600°C and (b) 750°C for 10 minutes in the SPS furnace

The optical micrographs of cross-sectioned titanium powder pellets which were generated by the SPS method at temperatures in the range of 800−1250°C are shown in Figure 4.23. It is clear that the size and fraction of internal porosity decreased significantly with increasing sintering temperature, also in agreement with the densification curve shown in Figure 4.21. Figure 4.23(b) shows that microstructure began to develop at a temperature of 1000°C. This microstructure mainly consists of the α-Ti phase since this was unalloyed titanium. The morphology of the α-Ti phase appears to have a coarse plate-like appearance. The increment in sintering temperature to 1200 and 1250°C, Figures 4.23(c) and 4.23(d) respectively, resulted in distinct microstructures which appear to consist of thinner and longer plate-like α-Ti phase compared to the sample obtained at 1000°C. The α-Ti phase also appears to form colonies in other regions of the samples.

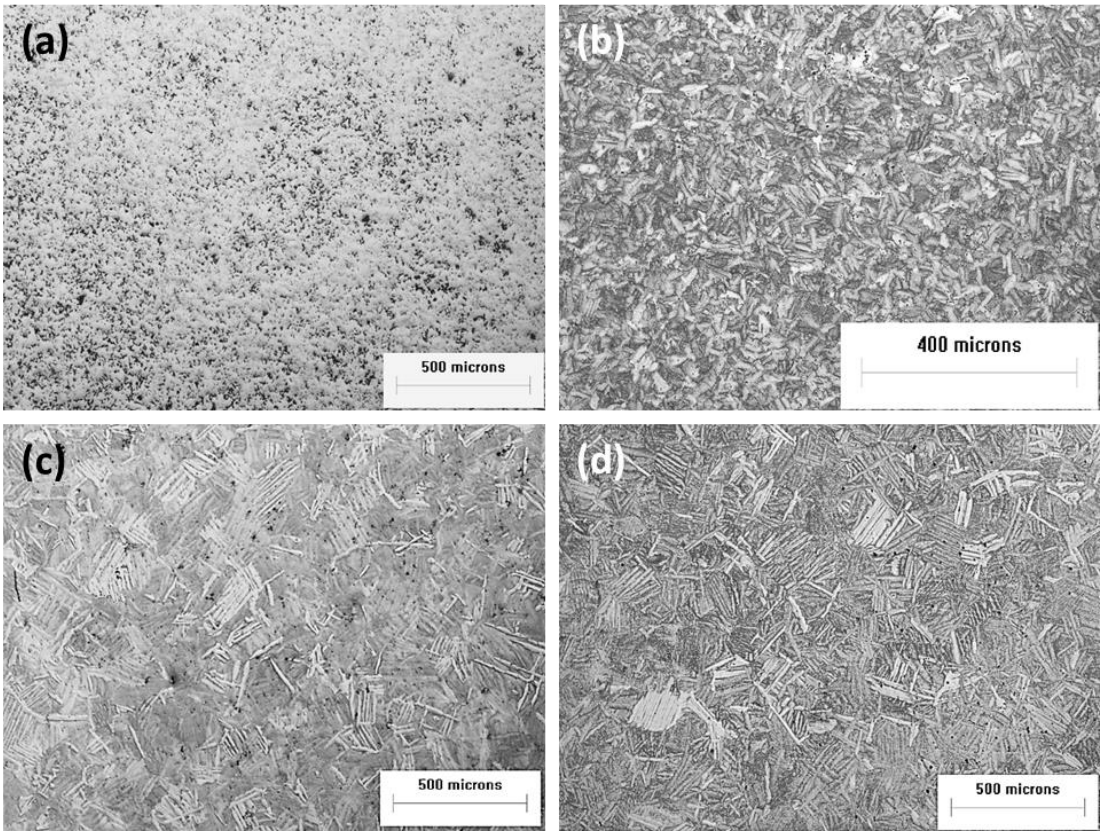

Figure 4.23: Optical micrographs of pressed titanium compacts after sintering at (a) 800°C and (b) 1000°C (c) 1200°C and (d) 1250°C for 10 minutes in the SPS furnace

Figure 4.24 shows the SEM micrographs of cross-sectioned Ti-6Al-4V pellet produced by the SPS method at a temperature of 1000°C. A large fraction of irregular

shaped and interconnected pores is clearly evident in Figure 4.24(a). Furthermore, the cross-section appears to consist of two randomly distributed phase regions of different morphologies (labelled 1 and 2) as shown at higher magnification in Figure 4.24(b). Region 2 appears to consist of two phases with a lamellar arrangement, while region 1 consists of a uniform phase. The increment of the spark plasma sintering temperature to 1100°C resulted in a significant decrease in the size and fraction of internal porosity as shown in Figure 4.24(c). The increment of sintering temperature was also accompanied by a change in the shape of internal porosity to a more rounded morphology, as seen in Figure 4.24(c). It can be seen in Figure 4.24(d) that the microstructure of this Ti-6Al-4V pellet still consisted of two distinct phase regions (1 and 2).

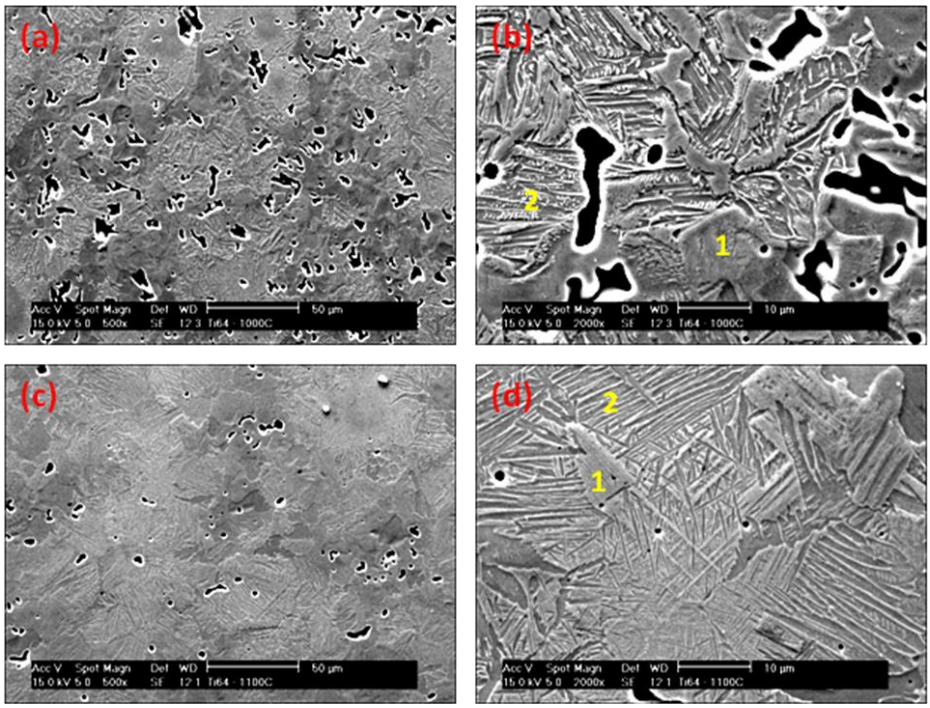

Figure 4.24: SEM microstructure of the Ti-6Al-4V alloy obtained by cooling from a sintering temperature of (a) 1000°C at low magnification, (b) 1000°C at high magnification, (c) 1100°C at low magnification and (d) 1100°C at high magnification

Figure 4.25 shows the SEM micrographs of cross-sectioned Ti-6Al-4V pellets produced by the SPS method at temperatures of 1200 and 1250°C. Figure 4.25(a) and Figure 4.25(c) show that both compacts exhibited distinct microstructural features compared to samples which were produced at lower sintering temperatures. The

microstructural features resemble those of a typical basket-weave microstructure of the Ti-6Al-4V alloy, although the microstructure generally looks inhomogeneous.

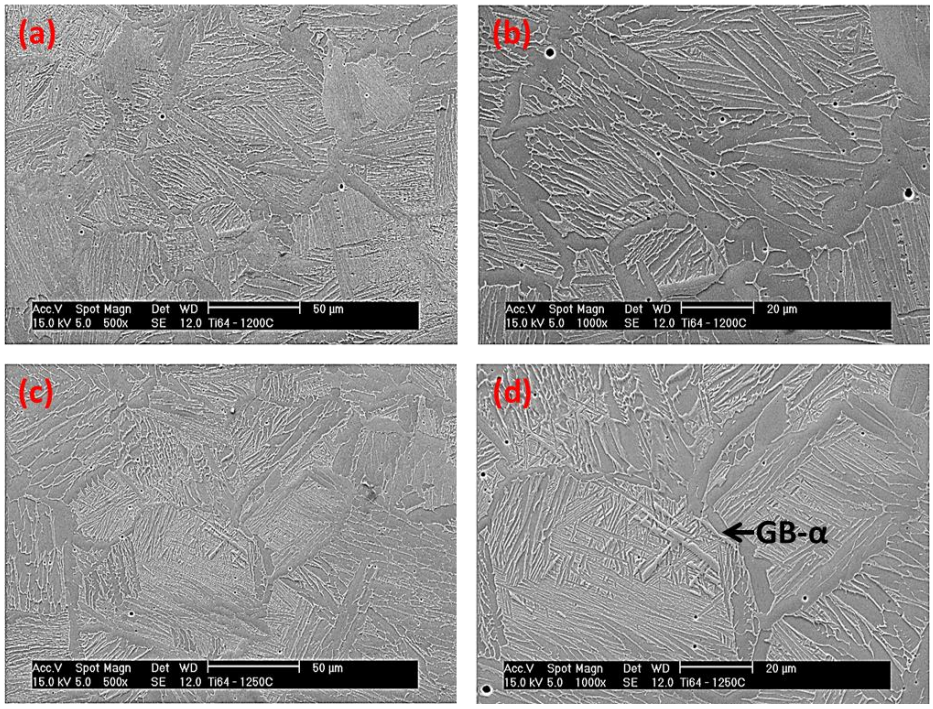

Figure 4.25: SEM microstructures of the Ti-6Al-4V alloy obtained by cooling from a sintering temperature of (a) 1200°C at low magnification (b) 1200°C at high magnification, (c) 1250°C at low magnification and (d) 1250°C at high magnification

The distribution of the alloying elements in some of the SPS produced Ti-6Al-4V alloy pellets was examined by EDS. The EDS spectra in Figure 4.26 show that the pellet produced at 1000°C one of the elements initially added when preparing the Ti-6Al-4V powder and impurities (Si and C), while the pellet produced at 1100°C contained all the constituents initially added when preparing the Ti-6Al-4V powder mixture and some carbon. Furthermore, the EDS spot analysis in Figure 4.26 (b) show that the composition of aluminium was below the SAE standard for aerospace specification (5.5-6.5 wt.%), while V was within the standard requirement .

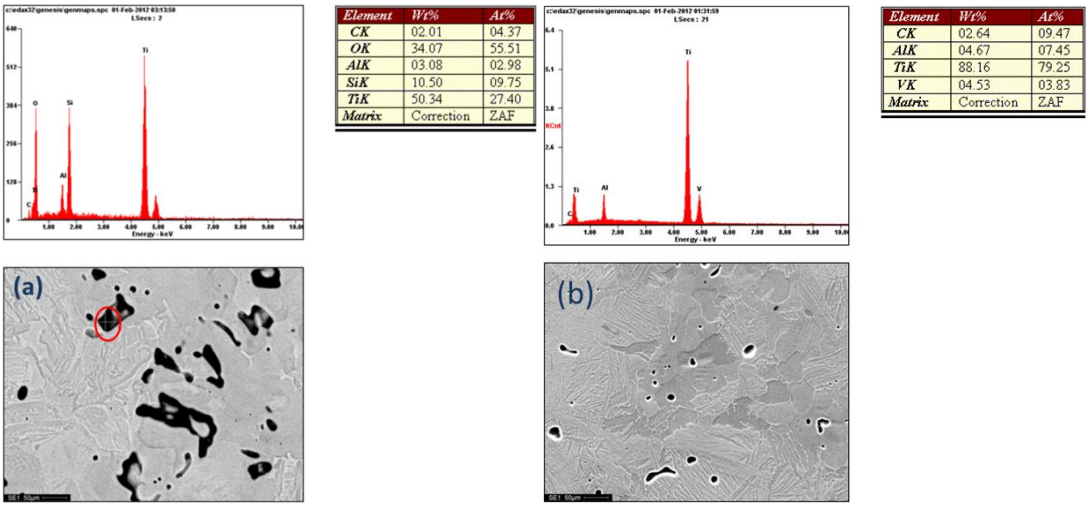

Element	Wt%	At%
CK	02.01	04.37
OK	34.07	55.51
AlK	03.08	02.98
SiK	10.50	09.75
TiK	50.34	27.40
Matrix	Correction	ZAF

Element	Wt%	At%
CK	02.64	09.47
AlK	04.67	07.45
TiK	88.16	79.25
VK	04.53	03.83
Matrix	Correction	ZAF

Figure 4.26: EDS spectra of the Ti-6Al-4V alloy obtained by cooling from temperatures in the range of 1000 °C and 1100 °C in the SPS furnace

The sintered compacts were further analysed for phase composition to determine if both α-Ti and β-Ti phases were retained after cooling at a rate of 250°C/min from spark plasma sintering temperatures in the range of 1000−1250°C. The respective XRD patterns are shown in Figures 4.27−4.30. The diffraction patterns show that the sintered Ti-6Al-4V pellets mainly consisted of the α-Ti phase. However, it is evident that the peaks between 2θ positions of approximately 38.5° and 40.2° appear to be broadened and combined.

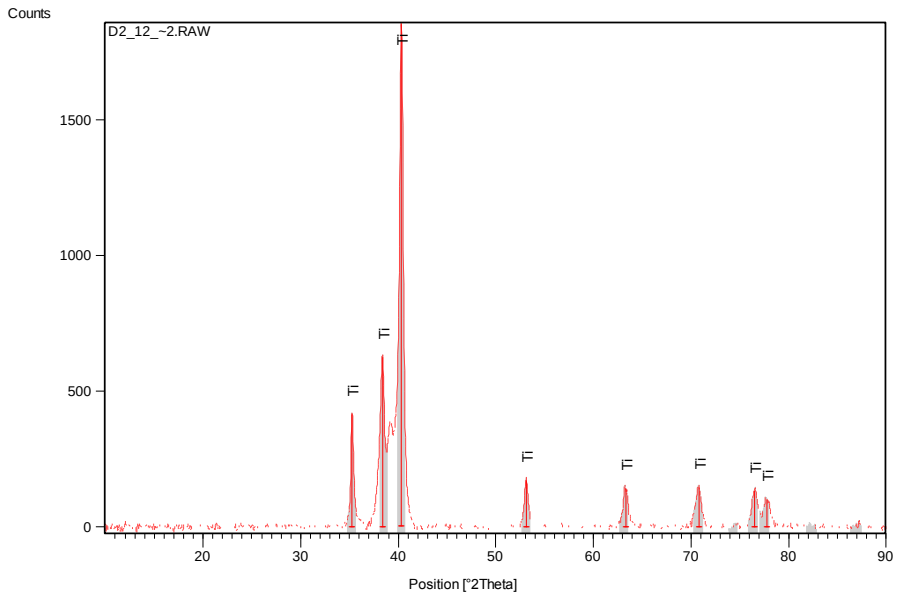

Figure 4.27: Phase composition of the Ti-6Al-4V alloy obtained by cooling from 1000°C at a rate of 250°C/min in the SPS furnace under vacuum

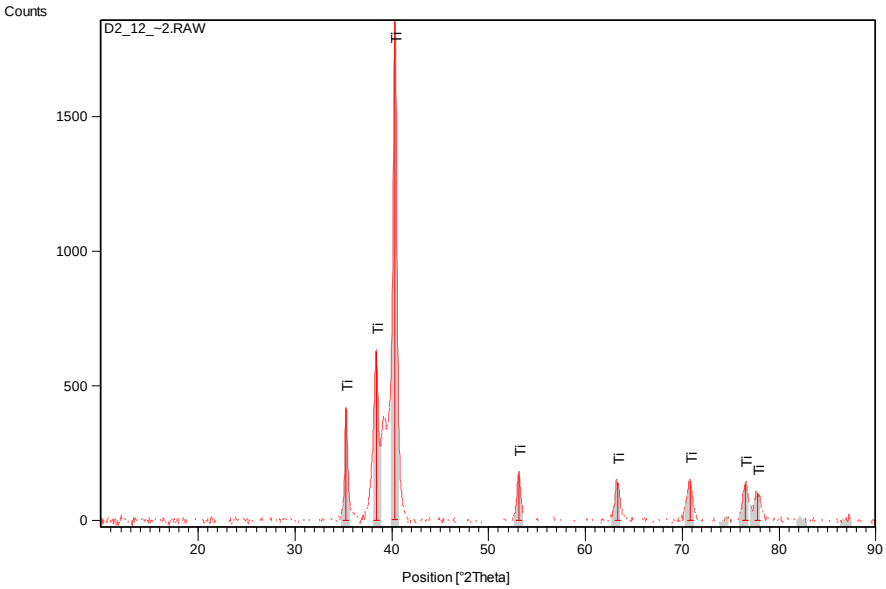

Figure 4.28: Phase composition of the Ti-6Al-4V alloy obtained by cooling from 1100°C at a rate of 250°C/min in the SPS furnace under vacuum

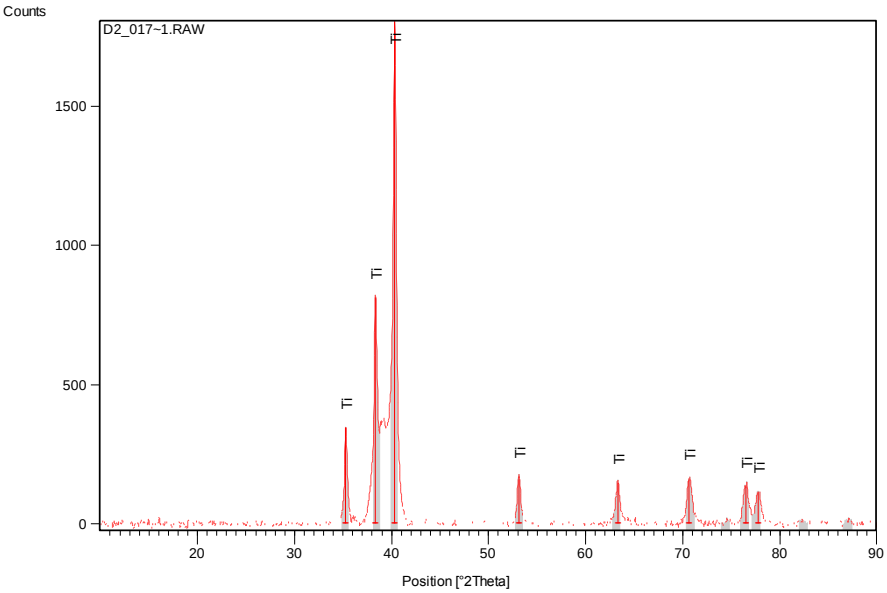

Figure 4.29: Phase composition of the Ti-6Al-4V alloy obtained by cooling from 1200°C at a rate of 250°C/min in the SPS furnace under vacuum

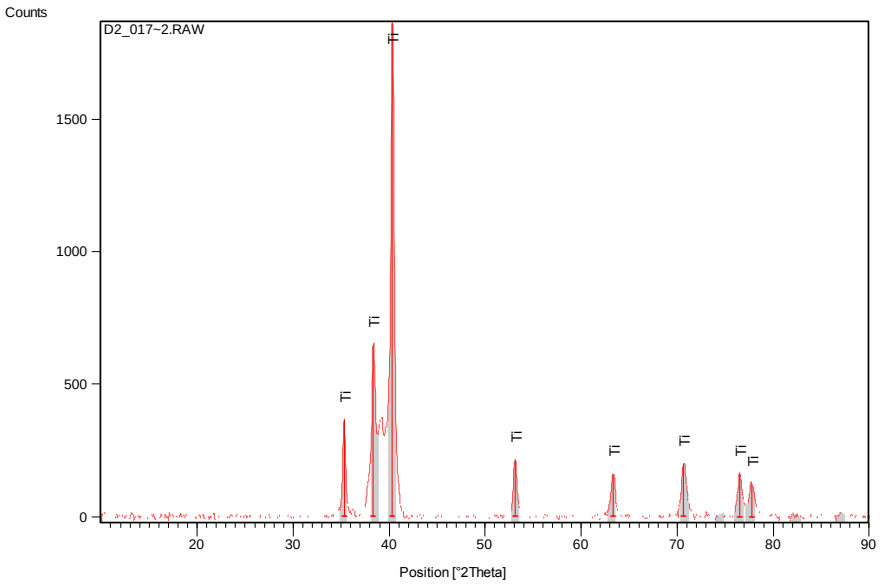

Figure 4.30: Phase composition of the Ti-6Al-4V alloy obtained by cooling from 1250°C at a rate of 250°C/min in the SPS furnace under vacuum

The Ti-6Al-4V pellets produced by the SPS method were also characterized for density, and the resultant densification curve is illustrated in Figure 4.31. It is shown that the density initially increased rapidly with increasing sintering temperature up to 1100°C, and thereafter increased gradually reaching a maximum density of 99.8% (4.42 g/cm^3) at 1200 °C, and remained constant at this value when the temperature was increased further to 1250°C.

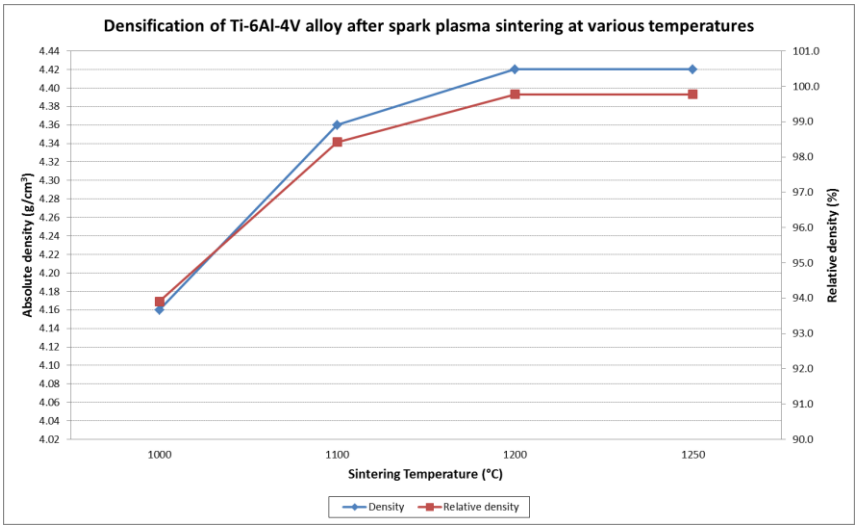

Figure 4.31: Effect of sintering temperature on the sintered density of blended elemental Ti-6Al-4V compacts

Due to the limitations of the dies to sustain higher loads and produce large green compacts, cold isostatic pressing was used as an alternative to produce cylindrical green compacts which were going to be cast or sintered and subsequently machined to make round tensile test specimens. Table 4.4 shows the densities of the cylindrical rods obtained by the cold pressing of the commercial unalloyed titanium powder at a pressure of 700 MPa. It can be seen that the average green density of the rods was 87±1.6% of the theoretical, which is comparable to the maximum density obtained at 619 MPa during compactability tests using die pressing.

Table 4.4: Density of CP-Ti rods obtained by cold isostatic pressing at 700 MPa

Specimen label	***Mass (g)***	***Diameter (mm)***	***Length (mm)***	***Green ρ (g/cm^3)***	***Relative ρ %***
CP-Ti1-CIP	49.13	16.21	60.00	3.97	88
CP-Ti2-CIP	49.73	15.90	66.20	3.78	84
CP-Ti3-CIP	49.95	16.20	63.14	3.84	85
CP-Ti4-CIP	49.76	16.40	60.60	3.89	86
CP-Ti5-CIP	50.20	16.41	60.80	3.90	87
CP-Ti6-CIP	50.31	15.70	65.20	3.99	89
CP-Ti7-CIP	49.62	16.21	61.20	3.93	87
CP-Ti8-CIP	49.81	15.94	62.94	3.97	88
CP-Ti9-CIP	49.65	15.70	66.70	3.85	85
Average					**87±1.6**

The titanium rods were then densified further by sintering in the tube furnace at a temperature of 1350°C for 1 hour under argon atmosphere, and the maximum densities achieved are presented in Table 4.5. It can be seen that the relative density increased to an average value of 95±0.96% after sintering, which is approximately 4% less than the density achieved at 1200-1250°C by the SPS method.

Table 4.5: Density of P/M Ti rods after sintering at 1350°C for 1 hour

Specimen label	*Mass (g)*	*Final diameter (mm)*	*Final length (mm)*	*Sintered ρ (g/cm^3)*	*Relative ρ %*
CP-Ti1-CIP	49.13	15.89	57.60	4.30	96
CP-Ti2-CIP	49.73	15.50	63.30	4.16	93
CP-Ti3-CIP	49.95	15.55	61.44	4.28	95
CP-Ti4-CIP	49.76	15.84	58.30	4.33	96
CP-Ti5-CIP	50.20	15.80	59.00	4.34	96
CP-Ti6-CIP	50.31	15.27	63.64	4.32	96
CP-Ti7-CIP	49.62	15.58	60.10	4.33	96
CP-Ti8-CIP	49.81	15.42	61.64	4.33	96
CP-Ti9-CIP	49.65	15.18	64.50	4.25	95
Average					**95±0.96**

The typical microstructure obtained on the cross-section of the cold pressed and pressureless sintered unalloyed titanium rods is shown in Figure 4.32. Similar to titanium materials obtained by the SPS method at 1200 and1250°C, the microstructure of pressureless sintered materials is observed to predominantly consist of plate-like α-Ti. However the size of the α-Ti plates is thicker compared to SPS produced. The width of the α-Ti plates can be estimated at 50 µm using the micron bar on the micrograph.



Figure 4.32: Microstructure of the titanium rods produced by cold isostatic pressing at 700 MPa followed by conventional sintering at 1350 °C for 1 hour

Similarly, the blended Ti-6Al-4V powder obtained by 60Al:40V master alloy addition was cold isostatically pressed at 700 MPa to make cylindrical rods which were subsequently sintered in the tube furnace. The densities achieved after cold isostatic pressing at 700 MPa and sintering at 1350°C are shown in Table 4.6 and Table 4.7

respectively. It can be seen that an average green density of 85±1.4% was obtained after cold pressing. The sintering of the rods at a temperature of 1350°C for 1 hour increased the relative density to an average value of 94±2.1%. Similar to the titanium rods, the sintered density of the Ti-6Al-4V rods is below that of the alloy produced by the SPS method at 1200-1250°C.

Table 4.6: Densities of Ti-6Al-4V rods obtained by cold isostatic pressing at 700 MPa

Specimen label	***Mass (g)***	***Diameter (mm)***	***Length (mm)***	***Green ρ (g/cm^3)***	***Relative ρ %***
CA1	49.67	16.20	61.60	3.91	87
CA2	50.36	15.90	66.14	3.83	85
CA3	50.35	16.00	63.50	3.94	88
CA4	50.14	16.40	62.22	3.81	85
CA5	50.07	16.10	63.20	3.89	86
CA6	49.98	15.80	65.30	3.90	87
CA7	50.18	16.20	65.20	3.73	83
CA8	49.22	16.16	62.60	3.83	85
CA9	50.22	16.33	62.50	3.84	85
CA10	50.32	17.60	56.00	3.69	82
Average					**85±1.4**

Table 4.7: Densities pressed Ti-6Al-4V rods after sintering at 1350°C for 1 hour

Specimen label	***Mass (g)***	***Final diameter (mm)***	***Final length (mm)***	***Sintered ρ (g/cm^3)***	***Relative ρ %***
CA1	49.67	15.87	59.1	4.25	94
CA2	50.36	15.6	63.9	4.12	92
CA3	50.35	15.57	61.3	4.32	96
CA4	50.14	16.0	61.0	4.09	91
CA5	50.07	15.5	61.1	4.34	97
CA6	49.98	15.4	63.7	4.21	94
CA7	50.18	15.7	62.9	4.14	92
CA8	49.22	15.5	59.9	4.35	97
CA9	50.22	15.7	60.0	4.31	96
CA10	50.32	16.9	53.3	4.23	94
Average					**94±2.1**

Figure 4.33 shows a typical microstructure obtained on the cross-section of cold isostaticaly pressed and pressureless sintered Ti-6Al-4V rods. The presence of

residual internal porosity (dark spots) can be seen in Figure 4.33(a), confirming incomplete densification suggested by density measurements presented in Table 4.6. In contrast to the Ti-6Al-4V alloy produced by the SPS method at 1200 and 1250°C, Figure 4.33(b) shows that the underlying microstructure mainly consisted of elongated α-Ti grains of the size ranging between approximately 10 and 50 µm. The microstructure appears to be homogeneous throughout the examined section, as opposed to the microstructures produced by the SPS method at 1200 and 1250°C. A thin layer of residual β-Ti phase can be clearly observed at grain boundaries as indicated in Figure 4.33(b). It can also be seen that the equiaxed α-grains appear to exhibit different shades, possibly due to different degrees of etching. The oxygen content of the as-sintered alloy was determined as 0.82 wt.% by the Leco gas fusion technique.

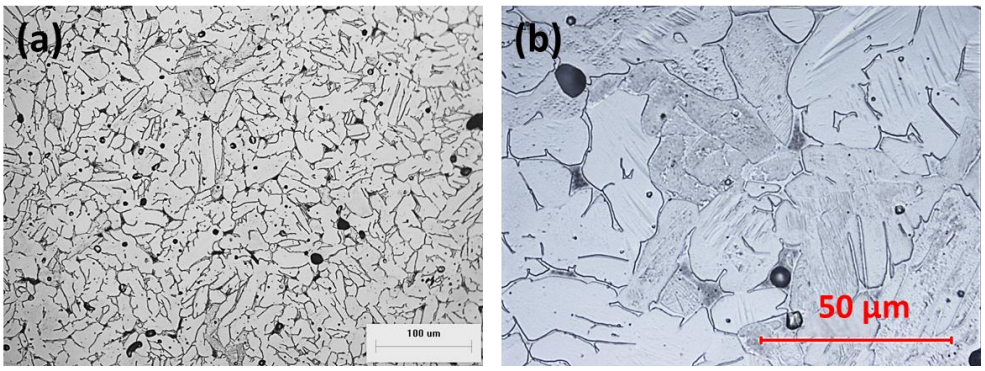

Figure 4.33: Optical microscopic structure of a cold isostatically pressed and sintered Ti-6Al-4V rod at (a) low magnification and (b) higher magnification

The EDS spot analyses of the grains, grain boundaries and overall cross-section of the Ti-6Al-4V alloy rods produced by the CIP and pressureless sinter method are shown in Figure 4.33. It is evident that the grains are reach in Al, confirming the predominance of the α-Ti phase, while the enrichment of grain boundaries with V suggests the predominance of the β-Ti rich. Lastly, it is observed that the fraction of Al in the overall sample is below the SAE standard for aerospace Ti-6Al-4V alloy (5.5 wt.%), while V is within the standard requirements (3.5-4.5 wt.%). A significant variation of the fraction of Al in the grains and overall cross-section can also be observed when comparing Figure 4.34 (a) and Figure 4.43 (c), indicative of inhomogeneous distribution. However, in both cases the fraction of Al is higher compared to the Ti-6Al-4V pellets produced by the SPS method at 1200 and 1250°C.

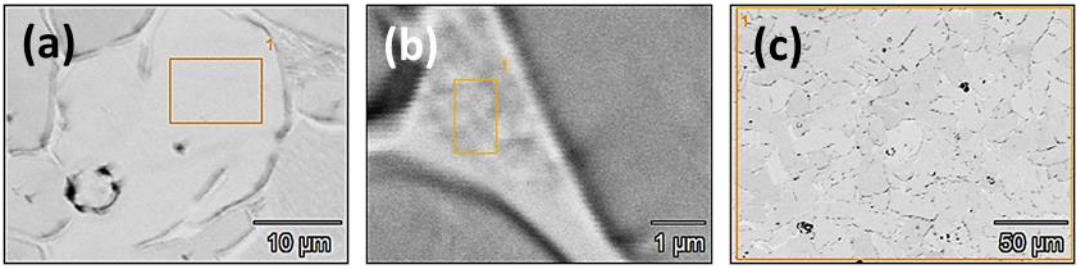

Element	Wt.%	Wt.% Error
Al K	5.73	±0.04
Ti K	92.61	±0.31
V K	1.66	±0.12

Element	Wt.%	Wt.% Error
Al K	3.27	±0.03
Ti K	80.5	±0.30
V K	16.23	±0.15

Element	Wt.%	Wt.% Error
Al K	5.25	±0.03
Ti K	90.77	±0.30
V K	3.98	±0.12

Figure 4. 34: EDS spot analyses of (a) grains, (b) grain boundaries and (c) overall cross-section of Ti-6Al-4V alloy rods produced by the CIP and pressureless sinter method

4.4 Rapid manufacturing of the Ti-6Al-4Valloy tensile specimens

Figure 4.35 shows the typical exterior appearance of the Ti-6l-4V alloy component fabricated by the rapid manufacturing method using the pre-alloyed Ti-6Al-4V powder as the starting material.

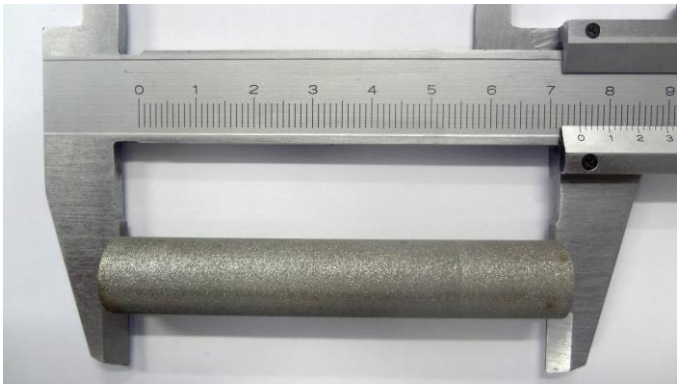

Figure 4.35: Outer appearance of the Ti-6Al-4V tensile sample fabricated by the rapid manufacturing route

The final densities of the Ti-6Al-4V tensile specimens, fabricated by the rapid manufacturing route, are shown in Table 4.8. The relative density is fixed at 98% for all the samples.

Table 4.8: Density of the laser fabricated Ti-6Al-4V tensile specimens

Sample ID	*Mass (g)*	*ρ(g/cm3)*	*ρ (%)*
LS0	43.141	4.41	98
LS1	43.188	4.42	98
LS2	43.148	4.41	98
LS3	43.156	4.41	98
LS4	43.166	4.42	98
LS5	43.207	4.42	98
LS6	43.164	4.41	98
LS7	43.098	4.42	98
LS8	43.105	4.42	98
LS9	43.112	4.41	98

The typical microstructure obtained on the transverse section of these tensile specimens is shown in Figure 4.36. Internal porosity is hardly perceivable, and the specimens predominantly consist of a very fine acicular α-Ti. Similar to the pressureless sintered plus HIP'ed alloy, the microstructure of the rapidly built tensile specimens appears homogeneous.

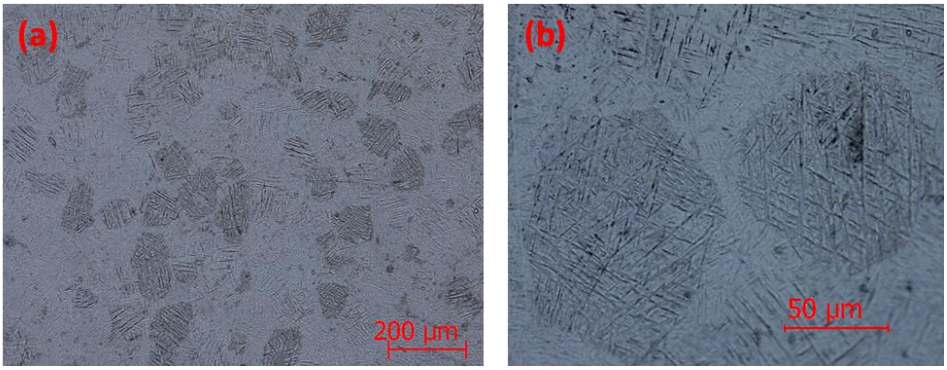

Figure 4.36: SEM microstructure of the Ti-6Al-4V tensile specimens fabricated by the rapid manufacturing method

The EDS spot analysis of the rapidly manufactured tensile specimen is shown in Figure 4.37. Similar to the SPS and pressureless sinter methods, it is evident that the fraction of Al in rapidly built specimens is below the SAE standard for the aerospace Ti-6Al-4V alloy (5.5-6.5 wt.%), while the vanadium is within the standard. It is also evident that the fraction of aluminium is comparable to that of the alloy produced by the pressureless sintering method, even though it is low compared to the starting pre-alloyed powder.

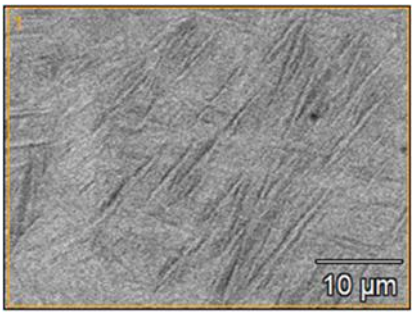

Element	Wt.%	Wt.% Error
Al K	5.28	±0.04
Ti K	90.48	±0.31
V K	4.24	±0.13

Figure 4. 37: EDS spot analysis of Ti-6Al-4V specimen produced directly from pre-alloyed powder using rapid manufacturing

4.5 Casting of pure titanium

Figure 4.38 shows the exterior appearance of a titanium tensile test specimen obtained by casting in a centrifugal field under an argon gas atmosphere. These specimens had a relatively sharp radius (region where the grip sections begin) and were therefore not suitable for tension testing. However, these samples were only used to study the microstructural features of titanium products produced under these conditions.

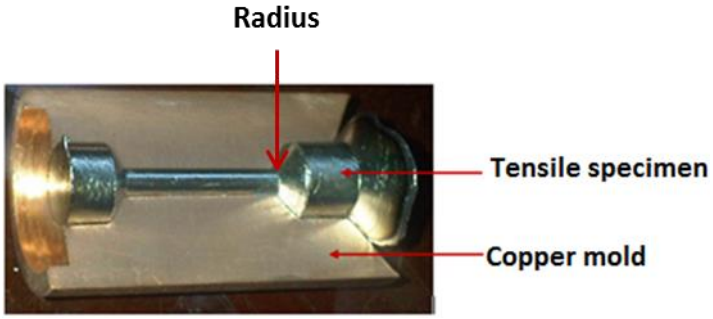

Figure 4.38: Titanium tensile specimen obtained by casting in a centrifugal field

Figure 4.39 shows the microstructure obtained at the centre of the reduced section of titanium tensile specimen produced by casting in a centrifugal field. The microstructure mainly consisted of individual α platelets and aligned α platelets.

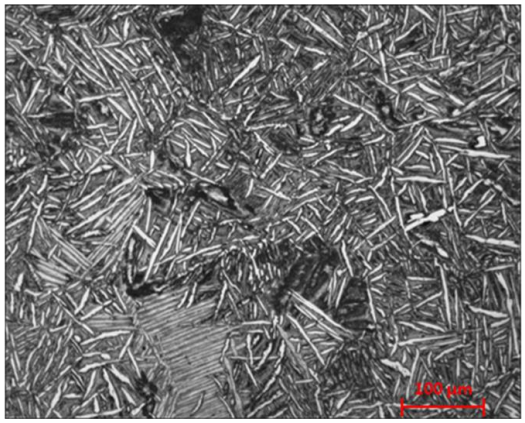

Figure 4.39: Optical micrographs of the titanium tensile specimen obtained by centrifugal casting

In contrast to centrifugal casting, a relatively homogeneous microstructure can be seen on the transverse section of a titanium specimen produced by vacuum casting (Figure 4.40). The microstructure primarily consists of colonies of α-Ti plates with different orientations. The microstructure resembles the basket-weave structure of titanium alloys.



Figure 4.40: Optical microscopic structure of CP-Ti obtained by conventional casting in a vacuum chamber furnace at (a) low magnification and (b) higher magnification

Table 4.9 shows the Leco gas analyses of the vacuum cast Ti ingot. It can be seen that the results are inconsistent and the first sample (W1) shows the oxygen content above that of the starting unalloyed titanium powder (0.45 wt. %), while the oxygen of the W2 sample is almost half. Therefore the average oxygen content of 0.84±0.62 was calculated, and this value is almost comparable to that of the CIP plus sintered alloy.

Table 4.9: Gas analysis of vacuum cast titanium

Sample label	*O_2% (<0.2)*	*H_2%(<0.0125)*	*N_2% (0.05)*
W1	1.45	0.0004	0.004
W2	0.22	0.0005	0.021

4.6 Casting of blended Ti-6Al-4V alloy

The optical micrographs of the blended Ti-6Al-4V alloy tensile specimen produced by centrifugal casting and vacuum casting and EDS spot analysis of vacuum cast Ti-6Al-4V are shown in Figure 4.41. Although evidence of residual porosity are observed in both castings, the size of the porosity appears smaller compared to the pressureless sintered alloy. The microstructure of the centrifugal casting exhibits homogeneous microstructural features, while the vacuum casting consists of prior β-grains and α-Ti phase of varying sizes. A martensitic microstructure is obtained by centrifugal casting, while a basket-weave structure can be observed in the vacuum cast alloy. The oxygen content of the vacuum cast alloy was determined as 1.04 wt.% by the gas fusion technique (Leco TCH 600), possibly due to the diffusion of oxygen from the ZrO_2 melting crucible. The oxygen analysis was consistent for all 3 samples analysed and appears high compared to vacuum casting of pure Ti and CIP plus sinter of the Ti-6Al-4V rods. The EDS analysis in Figure 4.41(c) shows traces of Zr, confirming the reactivity of the Ti-6Al-4V melt with the ZrO_2 melting crucible during vacuum casting. Furthermore, the fraction of Al in the vacuum casting is low compared to the master alloy used as alloying addition, while the V is comparable. Similar to the alloys produced by the SPS, pressureless sintering and rapid manufacturing methods, the concentration of V in the vacuum cast Ti-6Al-4V is also within the SAE aerospace specification.

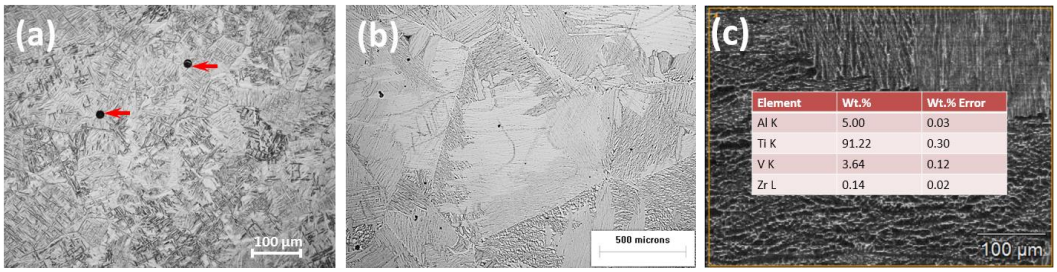

Figure 4.41: Microstructure of the Ti-6Al-4V tensile specimen produced by (a) centrifugal casting, (b) vacuum casting and (c) EDS spot analysis of vacuum cast Ti-6Al-4V alloy

4.7 HIP of Ti and Ti-6Al-4V tensile specimens

Figure 4.42 shows the microstructure obtained on the transverse section of the cold isostatically pressed and pressureless sintered titanium rods after HIP. The optical micrographs show that the use of a hydrostatic argon gas pressure of 1000 bar resulted in a fully dense sample, and the slow cooling of the rod from the HIP temperature of 950°C did not alter the original as-sintered microstructural features previously shown in Figure 4.32.

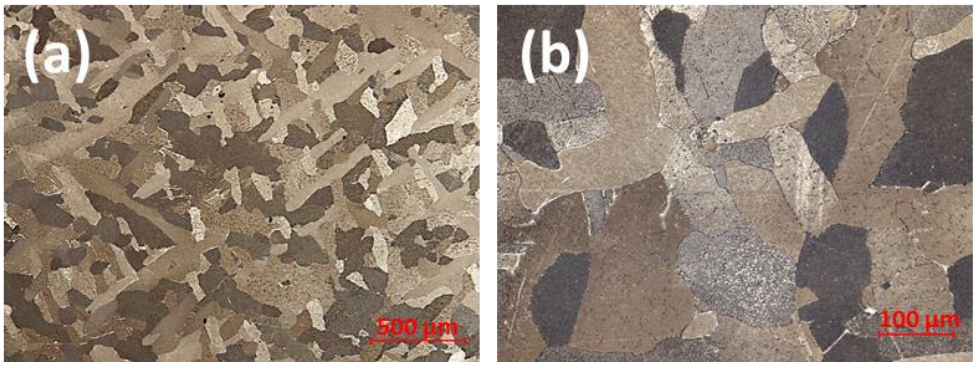

Figure 4.42: Microstructure of a pressed and sintered titanium rod in the HIP'ed condition

Figure 4.43 shows the microstructure observed on the cross-section of the CIP'ed and sintered Ti-6Al-4V after HIP. Similarly, Figure 4.43(a) shows that secondary densification at 950°C for 2 hours under a hydrostatic gas pressure of 1000 bar and heating resulted in a fully dense sample. It also appears that the microstructure is highly homogeneous compared to the as-sintered microstructure previously shown in Figure 4.33. The grains changed slightly to a semi-equiaxed shape as α-Ti grains

which are outlined by a thin layer of intergranular β (dark), as shown in Figure 4.43 (b). Comparing Figure 4.43(a) to Figure 4.33 reveals that HIP resulted in slight grain coarsening, and the microstructure appears more refined when comparing Figure 4.43 (b) to Figure 4.33(a). The grains are observed now exhibit a semi-equiaxed shape.

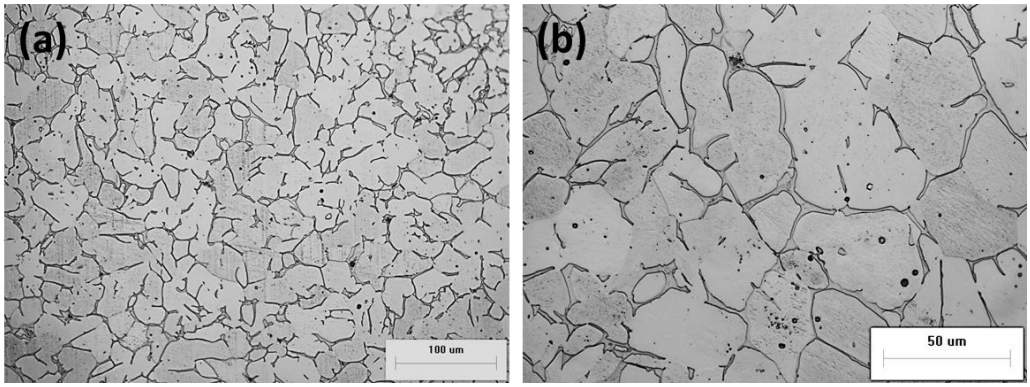

Figure 4.43: Microstructure of the pressed and sintered Ti-6Al-4V alloy in the HIP'ed condition

Figure 4.44 shows the optical micrograph of the vacuum cast titanium specimen in the HIP condition. It can be seen that the heating of the specimens at 950°C for 2 hours during HIP followed by slow cooling did not alter the starting lamellar microstructure of the vacuum cast titanium previously shown in Figure 4.40. However, it appears that the width of the α lamellae appears to have increased slightly.

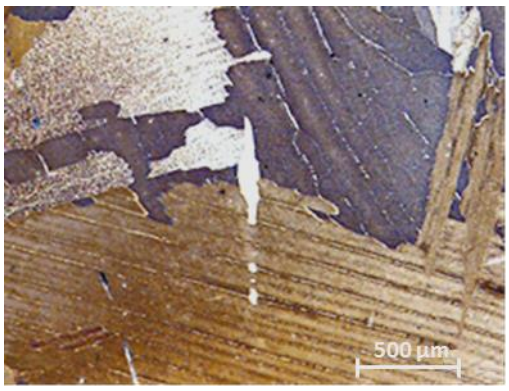

Figure 4.44: Microstructure of vacuum cast titanium in the HIP'ed condition

The microstructure obtained after the HIP of the Ti-6Al-4V produced by centrifugal casting is shown in the optical micrograph presented in Figure 4.45. Similarly, it can

be seen that HIP resulted in a fully dense material with a relatively homogeneous microstructure. The original martensitic α phase microstructure changed to a broken-up α+β structure (which almost resembles the basket-weave structure) as shown in Figure 4.45(b). The microstructure mainly consists of equiaxed grains which contain fine interlocked α platelets (light phase) in a matrix of the primary β-Ti phase (dark phase). The equiaxed gains are separated by a network of the grain boundary (GB) α-Ti phase. The coarsening of the α-Ti phase can also be seen in certain regions of the sample in Figure 4.45(a).

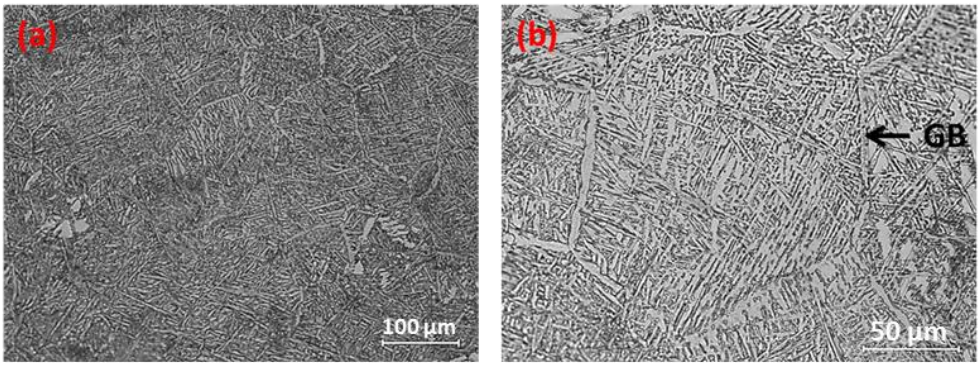

Figure 4.45: Microstructure of cast Ti-6Al-4V alloy in the HIP'ed condition

4.8 Heat treatment

The main aim for annealing was for the relief of residual stresses due to machining of sintered and cast materials into tensile specimens, and not to alter the microstructure. As expected, the annealing of the sintered and cast titanium specimens at 750°C for 2 hours followed by furnace cooling did not appear change the microstructure obtained by HIP, and will therefore not be presented. Figure 4.46 shows the exterior appearance one of the titanium specimens after annealing under vacuum and tensile testing. It can be seen that the sample has a brownish colour, which is usually associated with oxygen contamination for pure titanium. However, the Leco gas fusion analysis showed no evidence of oxygen or nitrogen pick-up in the annealed samples. The deformation observed on the test section is due to tensile testing.



Figure 4.46: Exterior appearance of the titanium specimen after annealing and tensile testing, showing a slight discoloration

Similarly, it was observed that the microstructure of the HIP'ed sintered and cast Ti-6Al-4V specimens remained unchanged after annealing at 750 and 850°C for 2 hours, and will therefore not be presented. The microstructures of the annealed rapidly built Ti-6Al-4V tensile specimens are compared to the as-fabricated microstructure in Figure 4.47. The optical micrographs in Figure 4.47(b) and Figure 4.47(c) show a slight coarsening after annealing at 750 and 850°C for 2 hours, respectively. It also evident that the microstructure of the specimen which was annealed at 750°C was the same as that obtained during annealing at 850°C.

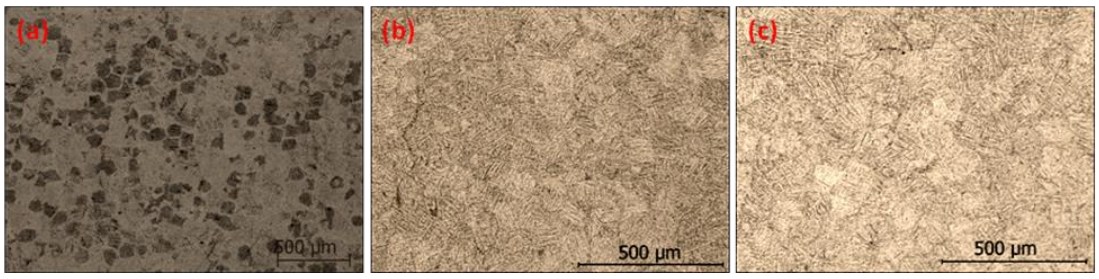

Figure 4.47: Microstructure of the rapidly manufactured pre-alloyed Ti-6Al-4V (a) in the as-fabricated condition, (b) after annealing at 750°C for 2 hours and (c) 850°C for 2 hour followed by furnace cooling

4.9 Tension testing

The pressureless sintered and vacuum cast Ti and Ti-6Al-4V specimens were subjected to tensile testing and the resultant properties are compared in this section. As stated earlier, the rapid manufacturing facility accessible during this time was only limited to using their own pre-alloyed Ti-6Al-4V powder. Therefore the pure Ti

specimens could not be fabricated and the blended elemental powder could not be used for this method. Hence the tensile properties of the rapidly built specimens are simply compared to the minimum requirements of wrought annealed and cast annealed Ti-6Al-4V reported in the literature to investigate the competence of the rapid manufacturing technology. While being aware that the as-received titanium powder used in this research already had high oxygen content, the sintered and vacuum cast materials are also compared to the minimum requirements of their commercial counterparts to see how significant the effect of oxygen is on the tensile properties. The materials produced by SPS and centrifugal casting were not tested for tensile properties due to the difficulty in producing large cylinders and bad design of the copper mould used, respectively.

4.9.1 Cast titanium tensile specimens

Table 4.10 shows the tensile properties of the vacuum cast titanium. The properties of the test samples are also compared to the typical properties of wrought annealed and cast titanium reported in the literature [2000Don]. It should be noted that the vacuum cast titanium specimens were subjected to HIP at 950°C for 2 hours followed by annealing at 750°C for 2 hours under vacuum after casting and machining respectively. The nomenclature FC represents furnace cooling. The nomenclature BO represents the samples which were cut out from the top half of the cast titanium ingot, while ON represents specimens which were cut out from the bottom section. It is evident that the tensile strength of the vacuum cast test specimens almost matched the minimum required for the wrought annealed titanium, while the elongation was 9-11% less. The strength and elongation were lower than that of the as-cast titanium (4-6 % and 80-97 MPa less, respectively). The tensile properties do not change much when comparing the samples extracted from the bottom and top section of the ingot.

Table 4.10: Tensile properties of vacuum cast unalloyed titanium

Specimen label	*Condition*	*Tensile stress at yield (Offset 0.2%) (MPa)*	*Modulus (GPa)*	*UTS (MPa)*	*Elongation (%)*	*Area reduction (%)*
BO 1.1	HIP+Anneal (750°C/2hr/FC)	479	116	549	13	27
BO 1.3	HIP+Anneal (750°C/2hr/FC)	482	112	557	11	23
BO 1.6	HIP+Anneal (750°C/2hr/FC)	476	113	558	17	25
Mean		**479**	**114**	**555**	**14**	**25**
BO 1.2	HIP (950°C/2hr)	456	112	543	15	31
BO 1.4	HIP (950°C/2hr)	462	115	536	13	25
BO 1.5	HIP (950°C/2hr)	485	122	552	16	24
Mean		**467**	**117**	**544**	**14**	**27**
ON 1.1	HIP+Anneal (750°C/2hr/FC	489	116	550	19	23
ON 1.3	HIP+Anneal (750°C/2hr/FC	470	120	543	15	19
ON 1.6	HIP+Anneal (750°C/2hr/FC	476	112	549	13	29
Mean		**478**	**116**	**547**	**16**	**24**
ON 1.2	HIP (950°C/2hr)	459	112	542	18	24
ON 1.4	HIP (950°C/2hr)	440	101	537	17	26
ON 1.5	HIP (950°C/2hr)	448	106	534	14	26
Mean		**449**	**106**	**538**	**16**	**25**
Wrought, annealed		*480*	*105-120*	*585*	*25*	---
Cast, as-cast		*510*	----	*635*	*20*	*31*

BO: samples cut out from the top section of the ingot
ON: samples cut out from the bottom section of the ingot

Figure 4.48 shows the variation of the mean strength and ductility (expressed in terms of elongation) with annealing temperature. It should be noted that the strength and elongation at an annealing temperature of 0°C represents the specimens which were tested in the cast+HIP condition. The mean strength (UTS and 0.2% yield strength) increased slightly after annealing at 750°C for 2 hours and the ductility seems to have remained unchanged.

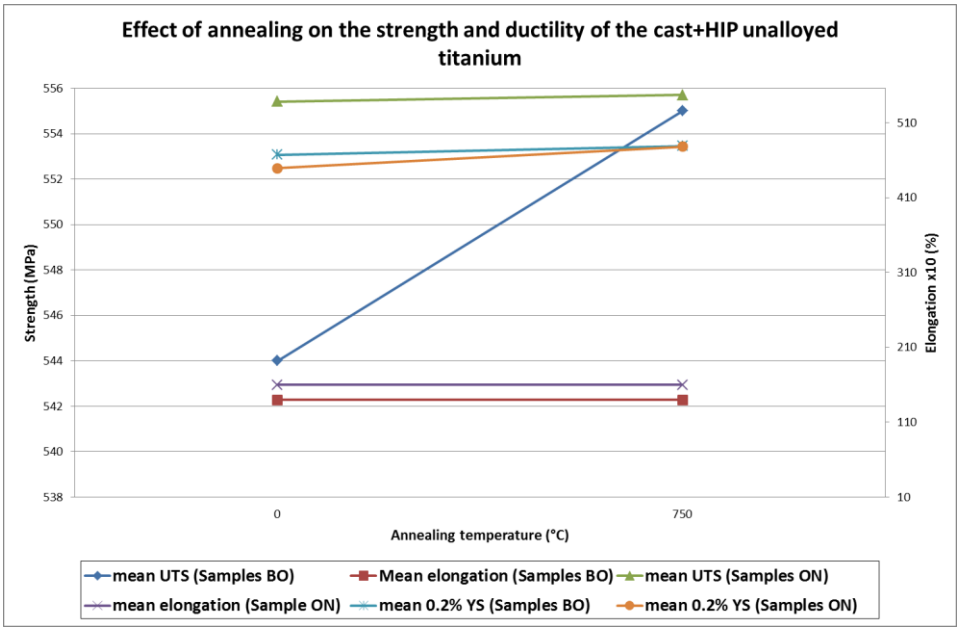

Figure 4.48: Effect of annealing on the mean strength and ductility of cast plus HIP'ed unalloyed titanium

Figure 4.49 and Figure 4.50 show the tensile stress-strain curves of vacuum cast titanium. It can be seen that the test specimens exhibited a relatively large degree of plastic deformation before fracture. A serrated stress-strain response is clearly observed at the horizontal portion of the curves.

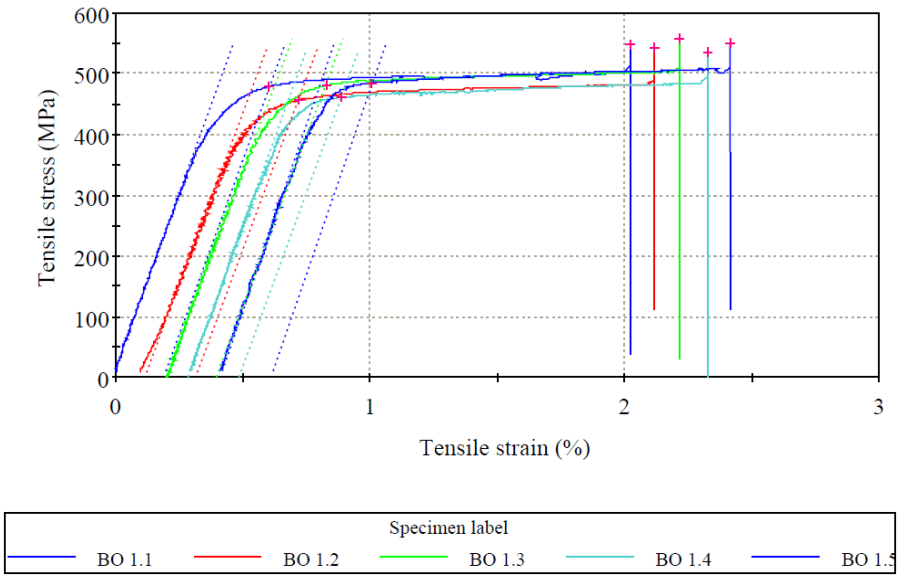

Figure 4.49: Tensile stress-strain curve of test specimens machined from the top section of the vacuum cast unalloyed titanium ingot

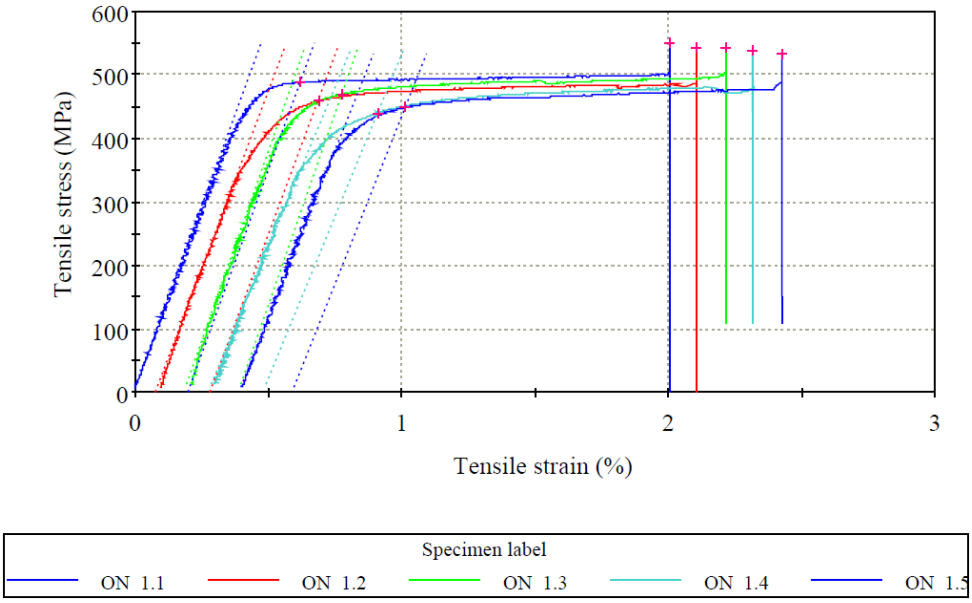

Figure 4.50: Tensile stress-strain curve of test specimens machined from the bottom section of the vacuum cast unalloyed titanium ingot

Figure 4.51 shows the gage length of a titanium specimen after loading to fracture. The deformation bands are seen to spread throughout the gage length of the test samples. Fracture finally occurred at the centre of the sample, making a 45 °angle with the tensile stress axis as shown in Figure 4.51(b).

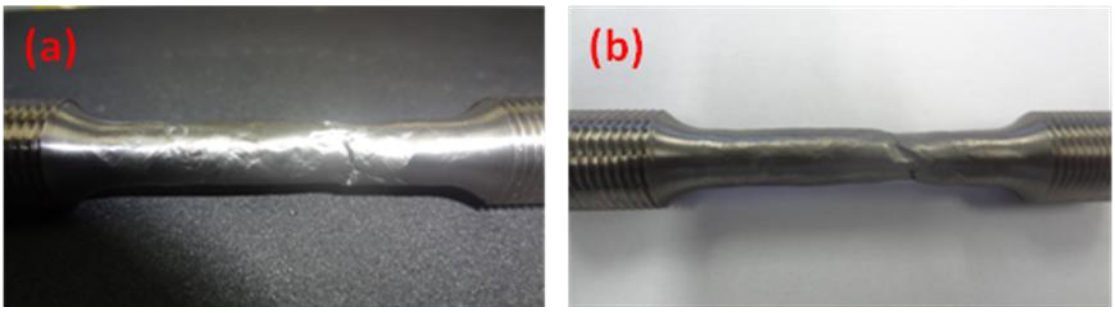

Figure 4.51: Exterior appearance of the gage length of a fractured unalloyed vacuum cast titanium tensile specimen

4.9.2 Pressed and sintered titanium tensile specimens

Most of the unalloyed titanium rods which were produced by cold isostatic pressing and sintering were severely bent, therefore only 3 proper samples could be machined from the rods. It should be remembered that the cold pressed unalloyed titanium rods

were also subjected to HIP at 950°C for 2 hours after sintering, followed by a annealing at 750°C for 2 hours under vacuum after the machining of tensile specimens. The resultant tensile properties are shown in Table 4.11 along with the minimum requirements of their commercial counterparts as cited from the literature [2000Don]. The test specimens generally exhibited poor tensile properties compared to the annealed wrought titanium and commercial P/M titanium compact. The elongation was lower by approximately 23% compared to that specified for wrought annealed titanium and 16% compare to annealed P/M titanium compacts. In contrast, the strength was comparable to that specified for wrought annealed Ti and 94 MPa higher than that of commercial annealed P/M titanium compact. The average strength is higher than that of vacuum cast titanium and the elongation is almost 14% less.

Table 4.11: Tensile properties of unalloyed titanium produced by CIP and sintering

Specimen label	***Yield stress (MPa)***	***UTS (MPa)***	***Elongation (%)***
CP-Ti2	---	610	2.358
CP-Ti7	---	543	1.881
CP-Ti9	---	568	1.903
Mean	---	**574**	**2.047**
Wrought, annealed	*480*	*585*	*25*
P/M compact, annealed	*370*	*480*	*18*

The complementary tensile stress-strain curves are shown from Figure 4.52 to Figure 4.54. In contrast to vacuum cast titanium, the sintered titanium specimens failed without showing any sign of plastic deformation prior to fracture.

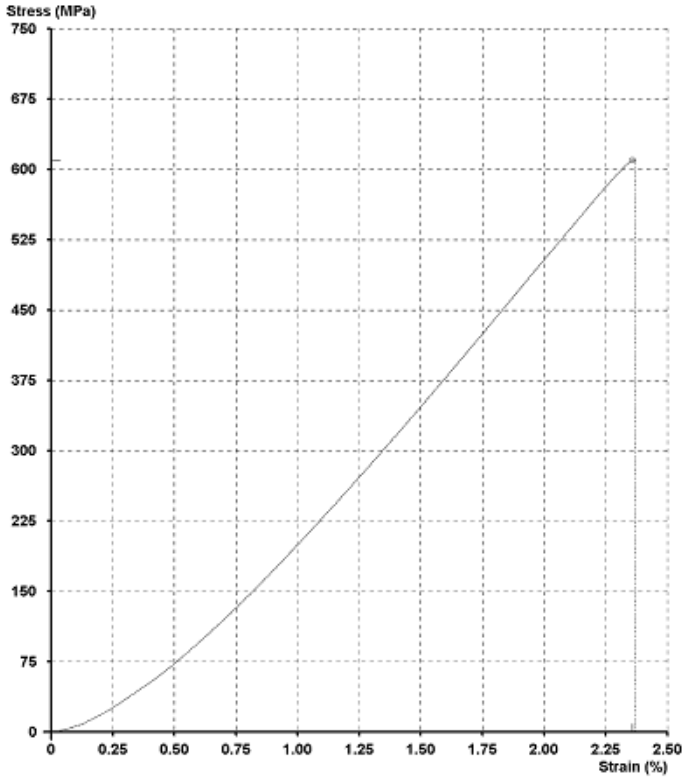

Figure 4.52: Tensile stress-strain curve of the pressed and sintered titanium test specimen CP-Ti2

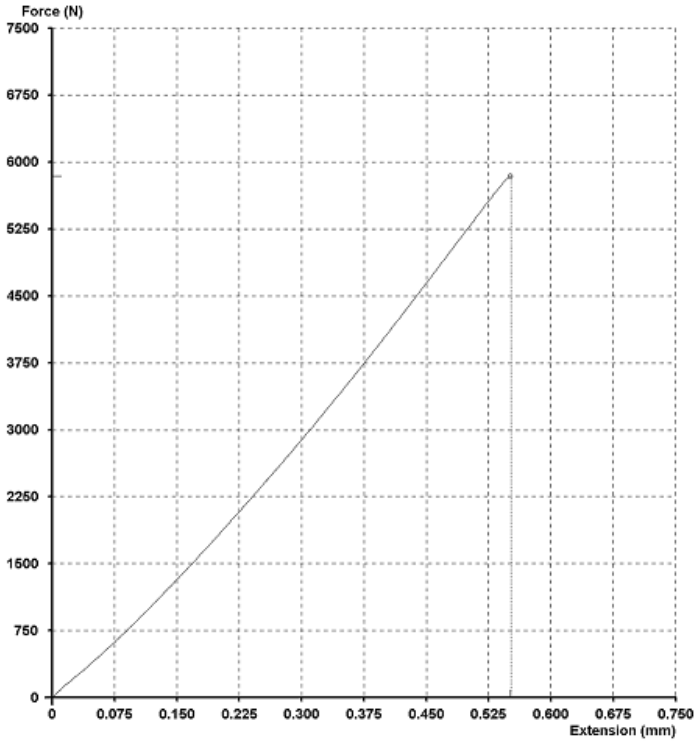

Figure 4.53: Tensile stress-strain curve of the pressed and sintered titanium test specimen CP-Ti7

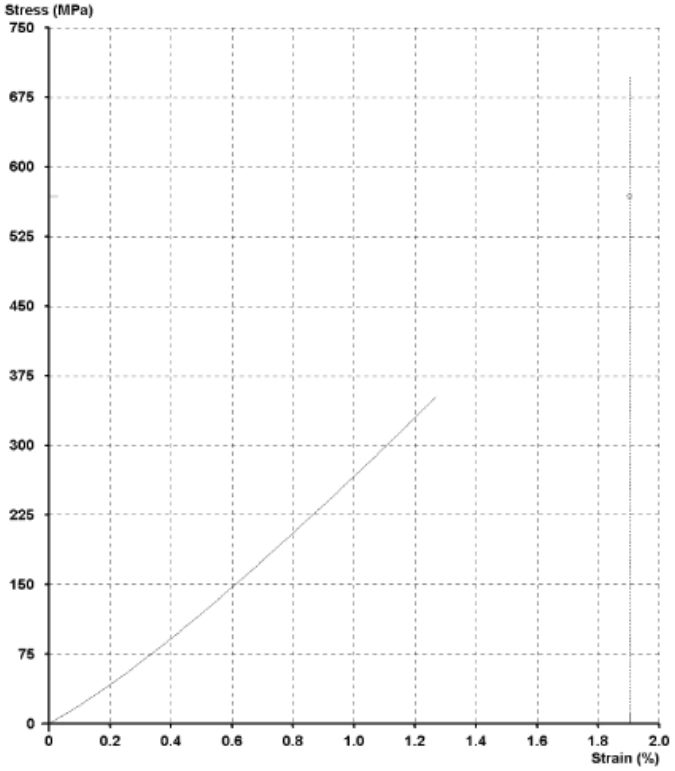

Figure 4.54: Tensile stress-strain curve of the pressed and sintered titanium test specimen CP-Ti9

4.9.3 Cast Ti-6Al-4V tensile specimens

The as-cast Ti-6Al-4V ingot was relatively hard, hence only three rods were machined into tensile specimens. Table 4.12 compares the tensile properties of the vacuum cast blended Ti-6Al-4V alloy test specimens to the typical properties of the wrought annealed and conventional cast annealed Ti-6Al-4V alloy as documented in the literature [1990ASM, 1996Cha, 2000Don]. Similarly, it should be noted that the all vacuum cast test Ti-6Al-4V alloy specimens were HIP'ed at 950°C for 2 hours and then subjected to conventional heat treatment at 850°C for 4 hours under vacuum using the parameters indicated in the second column of Table 4.12. The nomenclature FC stands for furnace cooling and 4 hr represents the annealing time. The tensile properties of the vacuum cast test specimens were very poor compared to the typical properties of the wrought and cast annealed Ti-6Al-4V alloy. The average elongation is almost 2% less than that of sintered pure titanium and the strength is significantly low (350 MPa less).

Table 4.12: Tensile properties of vacuum cast blended Ti-6Al-4V alloy

Specimen label	*Condition*	*Tensile stress at yield (Offset 0.2%) (MPa)*	*Modulus (GPa)*	*UTS (MPa)*	*Elongation (%)*	*Area reduction (%)*
SB1	HIP + Anneal (850°C/ 4hr/FC)	---	115.31	244.06	0.13	0.00
SB2	HIP + Anneal (850°C/ 4hr/FC))	---	118.96	228.92	0.17	0.00
SB3	HIP + Anneal (850°C/ 4hr/FC)	---	121.62	199.32	0.03	0.00
Mean		---	**118.63**	**224.10**	**0.11**	**0.00**
Wrought, annealed		*860*	*104 ± 2*	*955*	*9*	*21*
Ti-6Al-4V, Cast annealed		*885*	---	*930*	*12*	*20*

Figure 4.55 shows the resultant stress-strain curves of these samples. Similar to the pressed and sintered titanium, the vacuum Ti-6Al-4V specimens do not seem to have experienced plastic deformation prior to fracture.

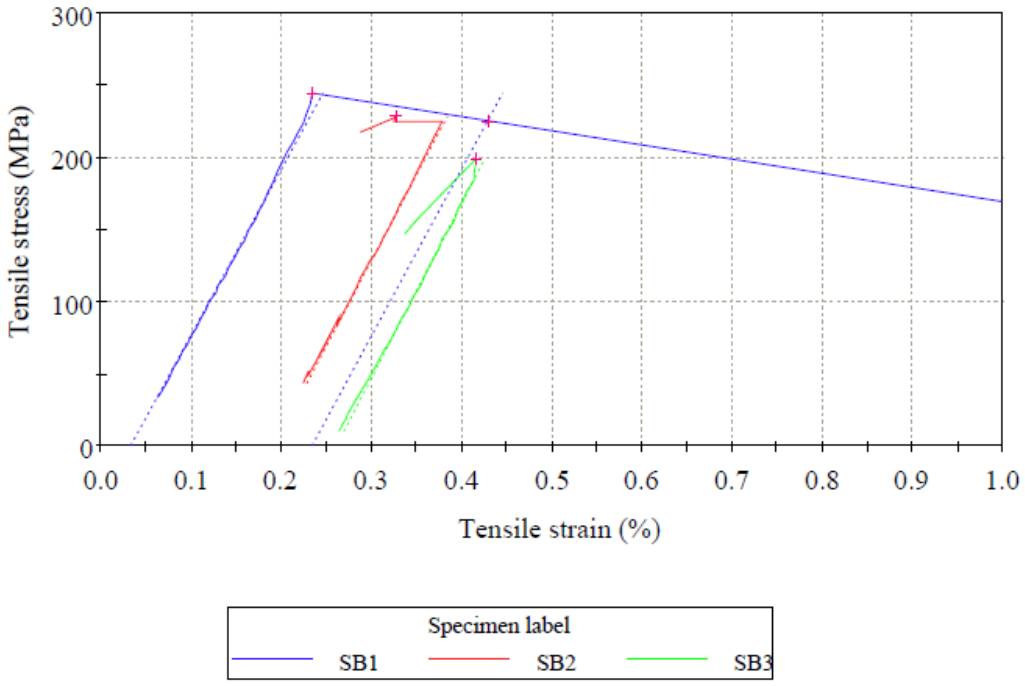

Figure 4.55: Tensile stress-strain curves of the HIP'ed and annealed vacuum cast Ti-6Al-4V alloy

4.9.4 Pressed and sintered blended Ti-6Al-4V alloy specimens

The tensile properties of CIP'ed plus sintered blended elemental Ti-6Al-4V alloy are presented in Table 4.13 and also compared to the typical properties of several

commercial Ti-6Al-4V alloy products reported in the literature [2000Don]. The specimens were HIP'ed at 950°C for 2 hours, machined and annealing at 750°C under vacuum for 2 hours followed by furnace cooling prior to tension testing. Although the ductility is lacking, the average strength (UTS) is higher compared to vacuum cast Ti-6Al-4V alloy. The strength of other specimens was even comparable to that of commercial counterparts.

Table 4.13: Tensile properties of the sintered, HIP'ed and annealed Ti6Al-4V tensile specimens

Specimen Label	***Condition***	***Yield stress (0.2%offset) (MPa)***	***Modulus (GPa)***	***UTS (MPa)***	***Elongation (%)***
CA1	HIP + Anneal (750°C/2h/FC)	----	119.42	887.71	0.06
CA2	HIP + Anneal (750°C/2h/FC)	----	121.21	948.88	0.50
CA3	HIP + Anneal (750°C/2h/FC)	----	126.09	965.36	0.56
CA4	HIP + Anneal (750°C/2h/FC)	----	123.94	700.65	0.06
CA5	HIP + Anneal (750°C/2h/FC)	----	116.68	788.01	0.38
CA6	HIP + Anneal (750°C/2h/FC)	----	117.95	875.08	0.31
CA7	HIP + Anneal (750°C/2h/FC)	----	118.22	902.10	0.50
CA8	HIP + Anneal (750°C/2h/FC)	----	119.51	964.93	0.56
CA9	HIP + Anneal (750°C/2h/FC)	----	120.22	887.83	0.50
Mean		----	**120.36**	**880.06**	**0.38**
Wrought, annealed		*860*	*104 ± 2*	*955*	*9*
P/M compact (~100% dense), forged and annealed		*840*	----	*925*	*12*
P/M compact, solution treat + age		*895*	----	*965*	*4*

Figure 4.54 shows the complementaryt tensile stress-strain curves of these specimens. Similar to the vacuum cast blended Ti-6Al-4V alloy specimens, the sintered Ti-6Al-4V alloy specimens appear to have not experienced any plastic deformation prior to fracture.

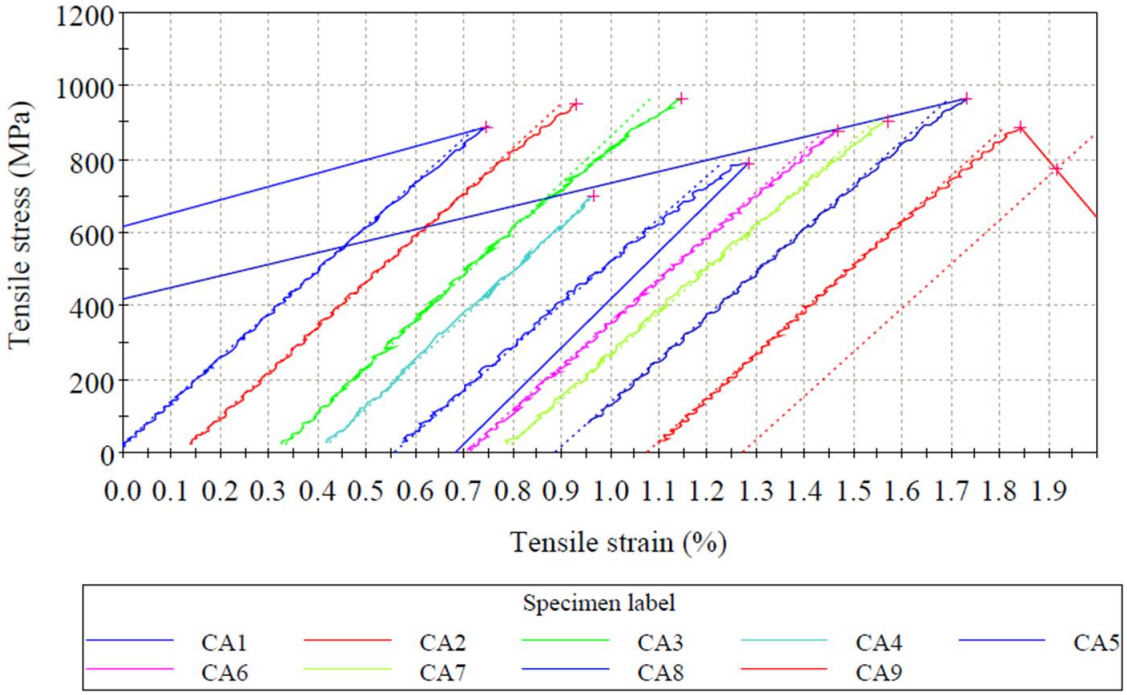

Figure 4.56: Tensile stress-strain curve of the of the HIP'ed and annealed sinteredTi6Al-4V alloy

4.9.5 Rapid manufactured Ti-6Al-4V tensile specimens

Table 4.14 compares the tensile properties of the rapidly built pre-alloyed Ti-6Al-4V specimens to the minimum requirements of wrought and cast annealed Ti-6Al-4V alloy reported in the literature [1990ASM, 1996Cha, 2000Don]. It is evident that the average elongation of the as-built specimens (LS0-LS3) was comparable to the typical elongation of wrought annealedTi-6Al-4V alloy, while the average strength (UTS and 0.2% yield strength) was extremely high. Additionally, the average strength was higher than the typical value specified for cast annealed Ti-6Al-4V alloy, while the average elongation was lower. Finally, the reduction-in-area of the rapidly built Ti-6Al-4V alloys was very high compared to wrought annealed and cast annealed Ti-6Al-4V alloys. A significant reduction of the cross-sectional area can be clearly seen on the fractured specimen shown in Figure 4.55. Furthermore, the rapidly built specimens exhibit superior tensile properties compared to the alloys produced by CIP and sinter and vacuum casting technologies. Annealing at 750 and 850°C for 2 hours does not appear to have a significant effect on the properties of the specimens obtained by rapid manufacturing.

Table 4.14: Tensile properties of the pre-alloyed Ti-6Al-4V alloy produced by rapid manufacturing

Specimen Label	***Condition***	***Tensile Stress at yield (0.2% Offset) (MPa)***	***UTS (MPa)***	***Elongation (%)***	***Reduction in area (%)***
LS0	As-fabricated	1180.8	1315.7	8.9	38.9
LS1	As-fabricated	1082.2	1269.8	9.5	43.8
LS2	As-fabricated	1127.5	1244.8	7.7	45.7
LS3	As-fabricated	1173.5	1303.5	9	7.1
Mean		**1141**	**1284**	**9**	**35**
LS4	Annealed (750°C/2h/FC)	1214.8	1258.6	7.5	23.8
LS5	Annealed (750°C/2h/FC)	1144.1	1193	8	38.8
LS6	Annealed (750°C/2h/FC)	1184.9	1234	8.3	35.4
Mean		**1181**	**1229**	**8**	**33**
LS7	Annealed (850°C/2h/FC)	1158.2	1199.3	7.8	43.8
LS8	Annealed (850°C/2h/FC)	1109.6	1151.7	8.1	23.4
LS9	Annealed (850°C/2h/FC)	1114.1	1156.5	8.3	45.3
Mean		**1127**	**1169**	**8**	**38**
Wrought, annealed		860	955	9	21
Ti-6Al-4V, Cast annealed		*885*	*930*	*12*	*20*



Figure 4.57: Pre-alloyed Ti-6Al-4V specimen showing a significant reduction in area and a cup and cone ductile fracture

It can be seen in Figure 4.56 that the percentage elongation appears to have decreased from 9 to 8% after annealing at 750°C for 2 hours, and remained constant at 8% when the annealing temperature was increased to 850°C. In contrast, it can be seen that the tensile strength (UTS) appeared to decrease with increasing annealing temperature.

The mean strength (UTS) decreased from 1284 to 1229 MPa. Increasing the annealing temperature to 850°C for 2 hours decreased the mean strength even further to 1169 MPa.

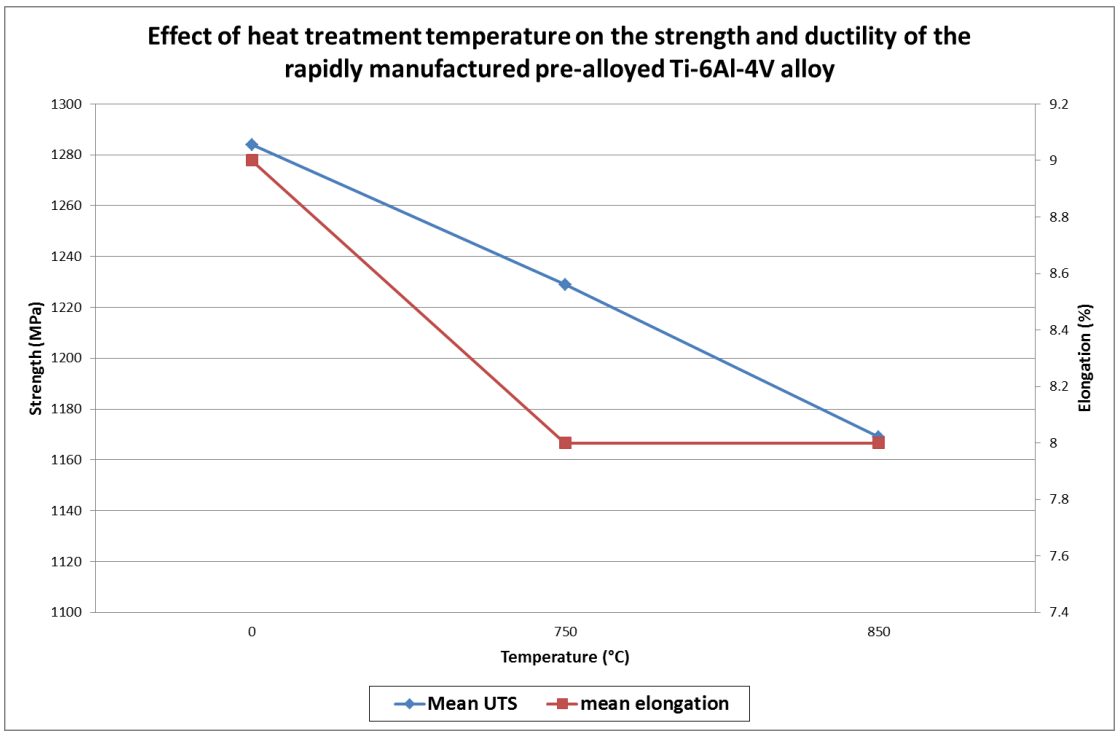

Figure 4.58: Effect of annealing temperature on the mean strength and ductility of the rapidly manufactured Ti-6Al-4V alloy

The tensile stress-strain curves of the rapidly built pre-alloyed Ti-6Al-4V alloy specimens are shown in Figure 4.57. It can be seen that these samples exhibited a large degree of plastic deformation prior to necking and fracture.

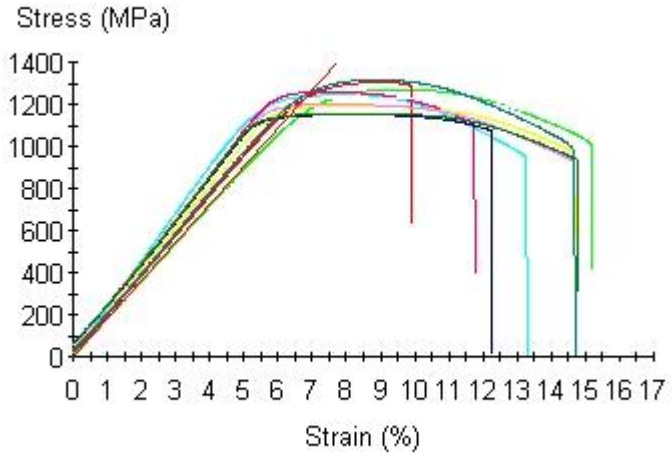

Figure 4.59: Tensile stress-strain curves of the laser formed Ti-6Al-4V specimens

CHAPTER 5: DISCUSION

5.1 Characterization of as-received powders

The particle size analyses revealed that all the as-received powders mainly consisted of micron-sized particles. As is evident from the SEM microphotographs in Figure 4.6, the master alloy and the pre-alloyed Ti-6Al-4V powders consist of spherical particles. The spherical particles are typical of powders produced using the atomization method [2008Nei, 2011Ger]. Spherical powder usually exhibits poor compactability and is seldom used in the conventional powder metallurgy method of pressing and sintering. In contrast, the unalloyed titanium consisted of irregular-blocky powder particles, making it ideal for cold press and sinter method due to the inter-locking of particles expected to result in permanently bonded particles during pressing. From the particle morphology analysis (Figure 4.6), it is also clear that the master alloy powder appears to contain a large fraction of fine particles compared to the pre-alloyed powder, which is in agreement with the particle size distribution results determined by the Mastersizer 2000.

The validation of alloying by EDS spot analysis showed that individual particles in the master alloy consisted of both Al and V elements (Figure 4.7). These were present in the form of V_5Al_8 and Al_3V intermetallics according to XRD pattern in Figure 4.9, which is in agreement with the Al-V equilibrium phase diagram presented in the work of others [2014Xu]. Furthermore, the EDS revealed that the average proportions of Al and V elements in individual particles were approximately 54 and 46 wt. % respectively, which is very close to the theoretical elemental composition of the 60Al:40V master alloy. Similarly, the EDS spectra in Figure 4.8 show the presence of the Ti, Al and V elements in individual particles of the pre-alloyed Ti-6Al-4V powder in proportions of 90, 5.8 and 4.2 wt. % respectively. These proportions are within the range specified by the ASTM B 265-08b standard for Grade 5 titanium (Ti-6Al-4V) [2008STA]. It should be noted that the Ti-6Al-4V alloy is classified as the α+β titanium alloy, and should ideally exhibit the coexistence of both the α and β phases at room temperature. In this work, the diffraction pattern of the as-received pre-alloyed

Ti-6Al-4V powder (Figure 4.10) revealed the presence of only the α-Ti phase. However a careful study of the diffraction pattern reveals a shift of the most intense α-Ti peak to a higher 2θ position. The shifting of the Bragg peaks is a common phenomenon in alloying, especially in non-equilibrium methods, and is usually indicative of the formation of a solid solution. The peaks also appear slightly broadened, usually typical of a strained crystal lattice and modification of lattice parameters. One possible cause for a modified crystal lattice is the diffusion of solute atoms (alloying elements) into the crystal lattice of the solvent material (major constituent).

The oxygen content of the as-received titanium powder, as determined by the Leco gas fusion technique (Table 4), was above the specification for all commercial grades of titanium according to the ASTM B265-08b standard. However, the powder was supplied as containing 0.377% O and can therefore be classified as the ASTM Grade 4 titanium. The content of oxygen in the pre-alloyed Ti-6Al-4V powder was below the specification for Grade 5 titanium alloy (Ti-6Al-4V) reported in the literature [2008STA]. The oxygen content of 0.13% indicates that this is possibly Grade 23 titanium, according to the ASTM B265-08b standard. Finally, the oxygen content of the 60Al:40V powder was very low compared to the maximum acceptable oxygen in Grade 5 titanium alloy (0.2%). As stated in the chapter 1, since the focus of this research is essentially to investigate the link between microstructure, tensile properties and processing of solid Ti and Ti-6Al-4V materials from powder. Therefore the high oxygen content of the Grade 4 titanium powder used is of less importance since the processes investigated are compared to each other based on the properties of solid materials produced from the same starting powder, except for the rapid manufacturing technique as explained in chapter 3. The comparison to properties of commercial parts is simply to show the extent to which the properties are affected by the high oxygen content of the starting powder and other contaminants.

5.2 Attrition milling of titanium powder and blended Ti-6Al-4V powder

As stated in chapter 3, the purpose for milling was particle size refinement and blending of Ti, Al and V elemental powders to form a homogenous Ti-6Al-4V

powder prior to sintering and casting experiments. The SEM micrographs accompanying the EDS spot analysis in Figure 4.12 reveal that the manually mixed Ti-6Al-4V powder mainly consists of Ti and Al, even though the V elemental powder was also added. The inability to detect V particles suggests inhomogeneity, which is expected in manual mixing. Milling both powders for 1 hour at a fixed speed of 1350 rpm resulted in the flattening of powder particles (Figure 4.15(b) and Figure 4.15(d)), similar to the observation by others [2007Dab]. The flattening of the powder particles results from the compression of ductile powder particles during collisions with hard WC balls and the milling jar. According to other researchers [2007Dab], this behaviour is usually observed in the initial stages during mechanical milling of ductile powders. Comparing Figure 4.15 (d) to Figure 4.15 (c)), it is evident that the particles of the milled powder are wider than the starting powder. The increasing width is confirmed by the D_{50} particle size, increasing from 31 µm to 34 µm for the titanium powder (Figure 4.1 vs. Figure 4.14) and 22 to 25 µm for the Ti-6Al-4V powder (Figure 4.11 vs. Figure 4.13). The failure to fracture the powder particles is attributed to the lower level of cold-working prominent during the 1 hour of milling, compared to durations in the range of 5−75 hours used by others [2007Dab]. The lower level of cold working simply resulted in what appears to be micro-forging, leading to a plate-like appearance of the powder particles. It was anticipated that particle size reduction would be significant after 1 hr since the high energy attritor mill was used compared to the low energy planetary ball mill (450 rpm rotation speed) used by others [2007Dab].

According to literature [2007Dab], the mechanical milling or alloying generally involves repeated welding, fracturing and re-welding of powder particles. In this work, it was observed that the powders had a tendency to form a thin coating on the side walls and a thicker layer at the bottom of the milling jar during milling. A large fraction of the milling balls were also embedded in the bottom layer. These events indicate two things; the ineffectiveness of the process control agent used (hexane) to reduce the effects of cold welding and agglomeration and the existence of a dead zone at the bottom of the attritor milling jar where no alloying takes place. The sticking of powder on the walls of the milling jar also increased the down-time between milling runs due time spent on scraping the powder off the milling jar. From Figure 4.16, it is

evident that the milled blended elemental Ti-6Al-4V powder contained a cold welded particle made of Ti, Al and V powder particles. These plate-like powder particles were cold welded into two distinct layers. The dark layer was rich in alloying elements, while the bright layer was titanium rich as determined by EDS spot analysis. The layering of the plastically deformed powder particles is common in the initial stages of mechanical alloying of ductile-ductile powders. The oxygen content of the milled powders almost doubled (see Table 4.2) due to the interaction of freshly exposed metal surfaces with normal atmosphere and a slight increase in the process temperature during high energy milling. The presence of the reflections due to pure Ti, Al and V in the diffraction pattern shown in Figure 4.17 indicates that the milling time was not long enough for alloying to take place. Milling was stopped when the process of mechanical alloying was still at early stages, mainly dominated by events of plastic deformation and cold welding as observed earlier during microscopic examination (Figure 4.15).

The Turbula mixer was chosen for preparing the powder mix due to its capability of blending small quantities of powders into larger volumes under dry conditions. The oxygen analysis obtained by the Leco gas fusion technique (Table 4.3) reveal that the Turbula mixer approach is more suitable for blending of materials with a high affinity for oxygen compared to the attritor mill used in this work. This is mainly due to the due to the ability to keep the powder at room temperature during mixing at 67 rpm compared to high energy milling at 1350 rpm, thereby significantly reducing the risk of oxidation. The oxygen content of the Ti-6Al4V powder obtained by the Turbula mixer approach was comparable to that of the as-received Grade 4 titanium powder, also indicative of the high purity of the master alloy used.

5.3 Cold compaction of titanium and blended Ti-6Al-4V powder

The as-received Grade 1 and Grade 4 titanium powders and the blended elemental Ti-6Al-4V powder were first subjected to compactability tests to trend their densification as a function of applied uniaxial pressure. No lubricant was applied on the die walls due to concerns of contamination. Similar to the observation made by Gronostajski et al. [2009Gro], the cold uniaxially pressed compacts based on the Grade 1 titanium

powder disintegrated upon removal from the die. It is known that spherical particles generally exhibit a small number of neighbouring contacts compared to irregular shaped powders, thereby resulting in compacts with particles which are not sufficiently bonded during cold compaction. Therefore the high purity powder could not be used further in this work.

Die pressing and cold isostatic pressing were used to make green compacts for sintering and casting experiments. A preliminary die pressing test was performed to trend the densification of Grade 4 Ti and Ti-6Al-4V powder prior to preparing actual green compacts for the SPS and centrifugal casting work. The compactability curves of the titanium powder and Ti-6Al-4V powder mix are shown in Figure 4.18 and Figure 4.19, respectively. These curves were studied to understand the interplay of mechanisms involved in the cold pressing. It is evident that the rate of densification is high in the early stages of compaction (region (a) in compaction curves). This initial rapid increase was also observed by others [1983Fis], and is believed to be caused by the rearrangement of particles in order to fill the large voids between loose powder particles, subsequently leading to initial contact between neighbouring particles at lower compaction pressures. The rate of densifications starts to decrease with continued application of uniaxial pressure due to the increasing number of interparticle contacts as indicated by region (b) in Figure 4.18 and Figure 4.19. This behaviour is also in agreement with the observation by Fischmeister and Arzt [1983Fis]. As the number of interparticle contacts increase, the particles undergo plastic deformation (flattening). The area of contact between particles increases with further pressing, leading to the closure of the voids between neighbouring contacts, thereby making further densification harder at higher pressures as indicated by the almost linear trend in region (c) of the compaction curves. The difficulty in powder compaction at higher pressures is also evident when comparing the green density obtained at the maximum die pressure (619MPa) and at a pressure of 700 MPa used during CIP. The compaction curve of the pure titanium powder (Figure 4.18) shows a maximum relative density of 88% at 619 MPa, while the average relative density of 87% was obtained at 700 MPa during the CIP as shown in Table 4.4. Similarly, a relative density of 90% and 85% was obtained for the Ti-6Al-4V powder mix during

die pressing (Figure 4.19) and CIP (Table 4.6) respectively. The slightly lower green density in CIP'ed compacts might also be due to pressing of large components compared to die pressing. The compaction behaviour and maximum green densities obtained in this work are comparable to those of other researchers [1981Smu, 2011Chen, 2011Ger].

5.4 Sintering of titanium powder and blended Ti-6Al-4V powder

As stated in chapter 3, the purpose for SPS was to investigate the densification behaviour and microstructural evolution of Ti and blended Ti-6Al-4V powders as a function of sintering temperature. Pressureless sintering was used to produce semi-finished rods from which tensile specimens can be machined. The rods were characterized for density, microstructure and chemistry and compared to the SPS materials. Figure 4.20 shows the influence of spark plasma sintering temperature on the linear shrinkage (height displacement) of Grade 4 titanium pellets at a fixed isothermal holding time and applied pressure. These SPS shrinkage curves are very similar to dilatometric curves obtained by other researchers during the sintering of micron-sized titanium powders at the temperature range of 650−1250°C [2006Dab, 2006Pan]. It can be seen that each shrinkage curve mainly consists of 4 distinct regions. In this work, the sintering behaviour is discussed with reference to the pellet which was sintered at 1250°C for the sake of simplicity.

The curve initially remained linear for a while during isothermal holding at 450°C and ultimately dipped as soon as constant heating at a rate of 250°C/min was started after approximately 5 minutes (see region (a) in Figure 4.20). This dipping behaviour was also observed by Dabhade et al. [2006Dab], and it is reported to be a result of linear expansion caused by the evolution of gasses/air absorbed or trapped in the green compact during cold pressing. As constant heating was continued, the height of the pellet started to shrink rapidly soon after a temperature of 600 °C was exceeded, as indicated by region (b) in Figure 4.20. This corresponds to the second sintering stage observed by Panigrahi et al. [2005Pan, 2006Pan]. The rapid shrinkage at this stage was possibly due to the melting/softening of Al powder particles which made the

consolidation of the pellet much easier compared to a constant heating at 450°C. The rapid shrinkage at higher temperatures of region (b) was possibly due to the transformation of α-Ti to β-Ti phase at approximately 882°C, since β-Ti is easy to deform compared to the room temperature hcp α-Ti phase. The sintering temperature of 1250°C was finally reached after approximately 9.1 minutes of constant heating, and the pellet was isothermally held for 10 minutes. It can be seen in region (c) that the linear shrinkage continued to increase rapidly but at a decreasing rate in the early stages of isothermal holding, and became almost linear towards the end of isothermal holding. Finally, the pellet was cooled at a constant rate of 250°C/min and the height decreased rapidly due to contraction as indicated by region (d). The overall sintering behaviour is in agreement with that described in dilatometric studies conducted by other researchers [2005Pan, 2006Dab, 2006Pan].

Furthermore, it can be seen that the total shrinkage and rate of linear shrinkage appears to increase with increasing temperature. For example, the pellets which were sintered at temperatures in the range of 600−850°C exhibited lower shrinkage, and the rate of shrinkage was slow compared to samples which were sintered at higher temperatures. A fast rate of shrinkage is observed for the samples which were sintered between 900 and 1250°C (rapid increase in the slope in region (b)), in agreement with the observation made by Panigrahi et al. [2005Pan]. It should be noted that the β transus temperature of unalloyed titanium is estimated at 882°C. Therefore the lower rate of linear shrinkage in the range of 600−850°C can be attributed to the close packed structure (hcp) of the α-Ti phase, while the higher shrinkage rate observed in the temperature range of 900−1250°C is due to the less packed structure (bcc) of β-Ti.

From the optical microphotograph in Figure 4.22, it is evident that the spark plasma sintering of the titanium pellets at 750°C appears to have resulted in a noticeable decrease in the fraction of internal porosity when compared to the pellet obtained at 600°C. However, not much sintering occurred at 750°C as the sample still mainly consisted of powder particle aggregates, which is indicative of the early stage of sintering also observed by Panigrahi et al. [2005Pan]. As seen in Figure 4.21, the relative density of this pellet increased to approximately 73% from a starting density of 71% relative to the theoretical density. The slight increase in density at 750°C is

possibly due to the fact that the sintering onset temperature of the titanium powder was exceeded, based on the formula $0.45T_m$; where T_m is the melting point of titanium [2006Dab]. This temperature was estimated as 747°C using this formula.

From Figure 4.23(a), it is evident that the Ti pellet produced by the SPS method further above the onset sintering temperature exhibited a significant decrease in the size and fraction of internal porosity. The significant densification observed from the optical micrograph of the the 800°C sample is in agreement with the linear shrinkage results, where an increase in sintering temperature from 750°C to 800°C resulted in a significant increase in the rate of linear shrinkage. From Figure 4.21, it is evident that more than half of the internal porosity observed in the 800°C pellet was completely closed after sintering at 1000°C .The microstructure also began to develop at this temperature due to the transformation of the high temperature β-Ti phase to α-Ti during intermediate cooling at 250 °C/min.

Eylon and Froes [1990Eyl] mention that, for titanium, a relative density above 99% is considered as full density. Similar to the findings by Shon et al. [2014Sho], it was demonstrated in this work that highly dense titanium pellets could be generated by spark plasma sintering method over a short duration. Figure 4.20 shows that the titanium pellets with a relative density of 99% were generated by the SPS method at 1200 and 1250°C. These sintered pellets exhibited a distict plate-like α-Ti morphology as shown by the optical micrographs in Figure 4.23(c) and Figure 4.23(d). According to Bolzoni et al [2012Bol[a]], the plate-like α-Ti morphology is typical of unalloyed titanium produced by pressure aided sintering, and is possibly caused by the use of an intermediate cooling rate from a temperature above the β-transus in this case. The plate-like morphology of the α-Ti also gives an indication that this phase was formed as a result of β transformation during cooling.

Temperatures in the range of 1000−1250°C were used during the spark plasma sintering of the Ti-6Al-4V pellets due to the reported [2012Bol[b]] sintering onset temperature of 820°C for the Ti-6Al-4V alloy. As can be seen in Figure 4.31, the sintering of the Ti-6Al-4V pellet at 1000°C using the SPS method resulted in 22.5% of shrinkage. According to Bolzoni et al. [2012Bol[b]], the presence of the more than

one phase region in the sintered blended elemental Ti-6Al-4V alloy (Figure 4.24(a)) is an indication of the incomplete diffusion of the alloying elements to stabilize both α-Ti and β-Ti phases and form a homogeneous microstructure. It is further reported [2012Bol[b]] that the co-existence of two phases (α+β) in the Ti-6Al-4V alloy indicates that complete diffusion of alloying elements has taken place, and the fraction of vanadium is high enough to stabilise the β-phase. Although the microstructural features of region 2 in Figure 4.24 could not be clearly distinguished at this point, it appears to exhibit a lamella structure which consists of α-Ti plates (dark phase) separated by a thin layer of the β phase (bright phase). In contrast, region 1 consists of a single phase, which is likely to be rich in α stabilizing element (aluminium). The XRD pattern in Figure 4.27 shows that α-Ti was the predominant phase in the sintered Ti-6Al-V alloy sample, possibly due to the incomplete diffusion of vanadium to stabilise the β-Ti phase.

Figure 4.26(a) shows the EDS elemental analysis of the pellet generated by the SPS method at 1000°C. It can be seen that the region which was analysed mainly consisted of Ti and Al, including Si and C impurities. Silicon probably came from the SiC abrasive paper or the colloidal silica suspension, both of which were used during metallographic preparation, while carbon originated from either SiC abrasive paper or bakelite on which the specimen was mounted on. It can also be seen from the EDS elemental composition that vanadium could not be detected in the analysed region. The inability to detect vanadium is probably due to incomplete diffusion. One other possible reason may be the inhomogeneous mixing of the Al and V alloying elemental powders into the titanium powder, thereby making the composition vary from pellet to pellet.

Looking at Figure 4.31, it can be seen that increasing the SPS temperature to 1100°C generated a Ti-6Al-4V pellet with a relative density of approximately 98.5%. Contrary to the observation by Bolzoni et al. [2012Bol[b]], it can be seen from the SEM micrograph in Figure 4.24(c) that the diffusion of the alloying elements was not yet complete as the microstructural features remained inhomogeneous. The micrograph shows that the fraction of region 2 increased at the expense of region 1, and the lamellar morphology of region 2 was clearer compared to the sample obtained at

1000°C. The presence of more α+β lamellae is an indication of improved diffusion of the alloying elements to stabilise both the α and β phases of titanium. The XRD pattern in Figure 4.28 shows that the sintered pellet predominantly consisted of the α-Ti phase, possibly due to the low volume fraction of the β-Ti phase.

The EDS spot analysis in Figure 4.26(a) shows that the pellet produced at 1100°C contained all mandatory constituents of the Ti-6Al-4V alloy and some carbon. Similarly, the carbon probably originates from the SiC abrasive paper or bakelite used in the metallographic preparation stage. It can also be seen that the elemental composition of the sample produced at 1100°C was not within the specifications of the Ti-6Al-4V alloy even though the alloying elements were added in appropriate proportions when preparing the ad-mix. Once again, this is evidence of the incomplete diffusion of alloying elements.

Similar to the observation by Nicula et al. [2007Nic], it was demonstrated in this work that a fully dense Ti-6Al-4V alloy compact could be produced by spark plasma sintering. The densification curve in Figure 4.31 shows that a maximum relative density of 99.8% was obtained by sintering at 1200 and 1250°C for 10 minutes under a uniaxial pressure of 10 MPa. It can also be seen from the SEM micrographs in Figure 4.25(a) and Figure 4.25(c) that these sintering temperatures lead to the complete closure of a significant fraction of internal porosity. The SEM micrographs in Figure 4.25(b) and Figure 4.25(d) show that both pellets consisted of a nearly homogeneous basket-weave microstructure. The basket-weave structure was obtained by an application of a high cooling rate (250°C/min) from a temperature above the β transus of the Ti-6Al-4V alloy, which is in agreement with the observation by other researchers [2002Din, 2006Lam]. The improved homogeneity of microstructural features indicates the near-complete diffusion of the alloying elements in the titanium matrix as reported by Bolzoni et al [2012Bol[b]]. The incomplete homogeneity of the microstructure also suggests that either a higher sintering temperature or prolonged sintering time at these temperatures is needed to ensure complete diffusion of alloying elements. The XDR patterns in Figure 4.29 and Figure 4.30 show that the resultant microstructure consisted of α-Ti as the predominant phase. The α phase detected by the XRD resulted from the β transformation during cooling, and exhibits a plate-like

morphology of varying width inside the equiaxed prior-β grains, as seen in Figure 4.25(b) and Figure 4.25(d). A thin layer of the β-Ti phase can be seen between the α-Ti phase plates, and the prior-β grains are outlined by a network of grain-boundary α-Ti (GB-α) of a non-uniform width. Since the width of the α platelets in the Ti-6Al-4V alloy is mainly influenced by the cooling rate from a temperature in the β phase field [1990Lam, 2000Don, 2001Gil, 2002Ding, 2003Lut], it is believed that the variation of the width of the α and GB-α phases may be caused by the fact that not enough time was allowed for all parts of the sample to be at an isothermal sintering temperature prior to cooling at a rate of 250°C/min.

Similar to the observation by Smugeresky and Dawson [1981Smu] and Ivasishin et al. [2002Iva], Table 4.5 and Table 4.7 show that the relative density of titanium and Ti-6Al-4V alloy rods which were sintered in the tube furnace hardly exceeded 95%. The densities obtained by pressureless sintering are also lower than that obtained by the SPS method. As stated earlier, the high density in SPS produced materials can be attributed to the simultaneous application of pressure during sintering. It can also be seen in Figure 4.32 that the microstructure of the pure titanium rods mainly consisted of a homogeneous plate-like morphology of the α-Ti phase, while Figure 4.33 shows that the Ti-6Al-4V rods exhibited a fully equiaxed α-Ti grains of different shades. The difference in the colour of the grains in the Ti-6Al-4V sample possibly indicates different degrees of etching. The homogeneity of materials obtained by pressureless sintering can be attributed to a prolonged isothermal holding time compared to spark plasma sintering.

It can be seen that the plate-like α-Ti in the titanium rods is coarser compared to the titanium compacts generated by the SPS method at 1250°C. The coarsening of the α-Ti plates was caused by a higher sintering temperature (1350°C), longer isothermal holding time (1 hour) and a slow cooling rate (5°C/min) compared to the SPS method, which is agreement with the literature [2000Don, 2003Lut, 2003Ley]. In agreement with the literature [2000Don], the fully equiaxed α microstructure in the pressureless sintered Ti-6Al-4V alloy rods was obtained by furnace cooling from a temperature above the β transus of the alloy. The equiaxed α grains are delineated by a thin dark layer of the intergranular β-Ti phase. Additionally, it can be seen that the

homogeneity of the microstructural features of the Ti-6Al-4V alloy rods was improved compared to the pellets generated by the SPS method at 1200 and 1250°C. This is because the Ti-6Al-4V rods were isothermally held for 1 hour compared to 10 minutes during the SPS method. It is reported [2012Mah] that the diffusion of vanadium in the titanium matrix to stabilize β-Ti phase is a very slow process which is significantly time dependent. Therefore, judging from the degree of microstructural homogeneity of the α+β equiaxed microstructure in the Ti-6Al-4V rods produced by the tube furnace sintering route, it appears that the diffusion of the vanadium was almost complete after 1 hour at 1350 °C. The overall chemical composition of the pressureless sintered Ti-6Al-4V rods is also very close to the specification compared to the SPS pellet obtained at 1250°C, still confirming that the diffusion of alloying elements is improved with increasing sintering temperature and isothermal holding time. It is also possible that some of the elemental Al was lost during spark plasma sintering, indicating the challenge of using elemental powders compared to the master alloy. The master alloy is known to have a higher melting temperature compared to elemental Al powder, hence the losses in Al are not so significant in the Ti-6Al-4V rods obtained by pressureless sintering. The reason for using elemental powders and the master alloy are highlighted in chapter 3 under the experimental procedures section.

5.5 Rapid manufacturing

Figure 4.34 shows that the surface finish of the Ti-6Al-4V alloy specimen fabricated by the rapid or layered manufacturing method appeared considerably rough compared to the sample obtained by the casting method (Figure 4.36). This appearance is typical of Ti-6Al-4V alloy components fabricated by layered or additive manufacturing as demonstrated by other researchers [2009Mur, 2011Koi, 2012Fra]. Table 4.8 shows that the layered manufacturing method is capable of producing materials which are denser compared to cold isostatic pressing and sintering, possibly due to high local temperatures of the laser beam during the sintering of each layer of powder compared to sintering of the large size Ti-6Al-4V rod. It can also be seen that the density was consistent for all nine samples, unlike the pressureless sintered rods, which demonstrates the accuracy of the rapid manufacturing technique. It evident in Figure 4.35 that the pre-alloyed Ti-6Al-4V specimens obtained by rapid manufacturing had a

very fine microstructure compared to the cold isostatically pressed and sintered and spark plasma sintered alloys. With reference to the same work by other researchers [2009Mur, 2011Koi], the as-built specimens exhibited a typical fine acicular α microstructure. The fine microstructure is believed to be due to the reported [2012Gu] high heating and cooling rate of the rapid manufacturing technology (10^3-10^8 K/s) compared to the lower cooling rates used in spark plasma sintering and the cold isostatic press and sinter techniques used in this work. The content of Al in the rapidly built Ti-6Al-4V also lower than the minimum required for the commercial alloy, similar to the cold isostatically pressed and sintered alloy. It is also possible that some of the Al was lost during laser sintering, given the high local temperature of the laser beam during rapid building of each layer.

5.6 Casting

5.6.1 Centrifugal casting

Although several fully dense tensile specimens were successfully produced by centrifugal casting, it was observed that the radius of the dumbbell shaped tensile specimens was very sharp. A sharp radius is considered as a metallurgical notch and acts as a stress concentrator thereby causing the specimen to fail at that notch rather than within the test section. Therefore these specimens were only analysed for microstructural features.

Figure 4.36 shows that the exterior appearance of the as-cast unalloyed titanium specimen was smooth and shiny due to the smooth surface of the copper mould used for casting. However a close look at the outer surface revealed deep furrows, which may be evidence of the poor flow-ability of the melt during pouring into the copper mould under a centrifugal field. The optical micrographs in Figure 4.37 show that the centrifugally cast titanium specimen consisted of a finer microstructure compared to the vacuum cast titanium. It should be noted that a copper mould was used in both centrifugal casting and vacuum casting. Therefore the fine microstructure in centrifugally cast specimens may be attributed to the high heat losses through the copper mould during solidification compared to vacuum casting. The microstructure appears to primarily consist of a combination of α-Ti morphologies (mostly individual

α-Ti platelets and aligned α plates in this case), which is common for commercial purity titanium castings according to Ibrahim et al [2011Ibr].

By contrast, the casting of Ti-6Al-4V alloy under a centrifugal field resulted in a relatively homogeneous needle-like microstructure, which is characteristic of the ά martensite (see Figure 4.39). Literature [2000Don, 2001Gil, 2002Din, 2003Lut] mention that a martensitic microstructure in titanium and titanium alloys is usually obtained by quenching or rapid cooling. The martensitic structure obtained during centrifugal casting implies that the copper mould used was capable of cooling the titanium alloy melt at a rate comparable to quenching. Evidence of spherical internal pores can also be seen in Figure 4.39, indicating incomplete densification. The microstructure of centrifugally cast Ti-6Al-4V alloy is also finer compared to vacuum cast Ti-6Al-4V, indicating fast solidification compared to vacuum casting.

5.6.2 Vacuum casting

Similar to the observation by Ibrahim et al. [2011Ibr], it can be seen in Figure 4.38 that the conventional casting of pure titanium under vacuum resulted in a microstructure mainly consisting of equiaxed prior-β grains in which aligned α plates having a width of approximately 12 μm could be identified. The aligned α-Ti plates in the as-cast titanium ingot are possibly due to a slow solidification rate from a temperature in the β phase field [2000Don, 2002Din, 2006Lam, 2011Ibr] compared to centrifugal cast titanium. As it can be seen in Figure 4.38(b), solidification caused the nucleation of the α-Ti phase along the grain boundaries which subsequently grew parallel to each other to form colonies inside the prior-β grains. Similar to the vacuum casting of pure titanium, the vacuum cast Ti-6Al-4V alloy resulted in a basket weave structure. This structure is indicative of a slower solidification rate compared to the centrifugal casting of the Ti-6Al-4V alloy.

The gas fusion analysis in Table 4.9 show that the oxygen content of the vacuum cast titanium ingot was in the range of 0.2−1.45 wt. %. It can be seen that the upper limit of this range is extremely high compared that of the raw titanium powder (0.45 wt. %), suggesting that the casting suffered from severe oxygen contamination. However,

the oxygen is unlikely to come from the normal atmosphere due to the fact that a high vacuum pressure of $1x10^{-5}$ mbar was maintained inside the melting chamber during casting. The only possible reason would be the diffusion of oxygen from the ZrO_2 crucible used during melting. The oxygen content of the vacuum cast Ti-6Al-4V alloy was also determined as 1.04 wt.% and traces of Zr could also be detected by EDS, confirming the reactivity of the melt with the ZrO_2 crucible. It is noteworthy that the oxygen contamination was higher compared to alloy produced by the cold isostatic press and sinter method.

5.7 Hot isostatic pressing

Similar to the observation by Smugeresky and Dawson [1981Smu] and Lapovok et al. [2008Lap], it can be seen in Figure 4.40 and Figure 4.41 that the hot isostatic pressing of titanium and Ti-6Al-4V powder green compacts at 915°C for 2 hours under a hydrostatic pressure of 1000 bar appears to have completely eliminated the residual subsurface porosity. It can also be seen that the hot isostatic pressing did not alter the original microstructure of the pressed and sintered titanium and Ti-6Al-4V rods. The sintered titanium rods retained the plate-like α-Ti microstructures, while the fully equiaxed microstructure of the pressureless sintered Ti-6Al-4V rods remained unchanged. The HIP also appears to have refined the microstructure of the pressed and sintered Ti-6Al-4V alloy. Furthermore, it can be seen in Figure 4.42 that the lamellar structure of the vacuum cast titanium did not change after hot isostatic pressing. However, it was observed that the width of the α lamellae increased from approximately 12 µm to approximately 100 µm after HIP. This is expected since it is reported that titanium suffers from grain growth with an increasing heat treatment temperature and time, and HIP can be technically considered as a heat treatment process [1995Gil, 2000Don]. The Ti-6Al-4V rods retained their equiaxed α microstructure due to the fact that the HIP temperature (915°C) was below the β transus temperature of the alloy, and slow cooling was applied after HIP. This is also supported by the literature [1990ASM]. Similarly, the aligned plate-like α structure of the titanium rods did not change due to slow cooling.

It is reported [1990ASM] that the as-cast and cast + HIP microstructures of the Ti-6Al-4V alloy look similar due to the fact that the HIP temperature is generally below the β transus temperature. However, it is believed that this only applies to the typical lamellar microstructure usually obtained by conventional casting. To confirm this, it can be seen in Figure 4.43 that the ά martensite structure of the Ti-6Al-4V alloy specimen which was obtained by centrifugal casting was completely transformed to form equiaxed prior-β grains consisting of fine interlocked α platelets surrounded by residual β during HIP. The equiaxed prior-β grains are delineated by a network of grain-boundary α (GB-α). In this case the hot isostatic pressing is observed to resemble the tempering process, which usually results in the complete decomposition of ά martensite to form equilibrium α and β phases at temperatures above 800°C as demonstrated by Gil et al. [1996Gil].

5.8 Heat treatment

All titanium tensile specimens were subjected to treatment at 750°C for 2 hours, while the Ti-6Al-4V alloy specimens were annealed at 750 and 850°C for 2 hours. However, it was observed that the HIP and annealed microstructures were the same for both titanium and Ti-6Al-4V alloy specimens. The literature [2000Don] confirms that the microstructure of the hot isostatically pressed α+β titanium alloys cannot be altered by heat treating in the α+β phase field followed by furnace cooling. Figure 4.44 shows that the exterior surface of some of the cast unalloyed titanium specimens exhibited a brownish colour after annealing at 750°C for 2 hours in the vacuum furnace, which is usually indicative of an oxide layer. This colour was also observed during the preliminary sintering and heat treatment of titanium samples in the tube furnace prior to the installation of oxygen traps. However, the Leco gas fusion analysis conducted on one such sample indicated no excess oxygen or nitrogen after heat treatment. Therefore the discoloration could not be explained.

5.9 Tension testing

5.9.1 Cast and sintered titanium

As can be seen in Table 4.10, the tensile properties of the cast+HIP titanium specimens were similar to those of the specimens tested in the cast+HIP+annealed condition. The comparable properties are believed to be due to the similarity of the cast+HIP and cast+HIP+annealed microstructures. As mentioned in the preceding section, the application of a slow cooling rate (furnace cooling) from a heat treatment temperature below the β transus was not sufficient to alter the microstructure of the hot isostatically pressed titanium. It also appears that there is no significant difference between the tensile properties of samples extracted from the bottom and top sections of the titanium ingot. This was possibly due to the fact that the microstructural features and chemical composition of the specimens which were extracted from both sections were the same.

The tensile properties in Table 4.10 reveal that the average ductility (expressed in terms of percentage elongation) for both the cast+HIP and cast+HIP+annealed titanium tensile specimens was below that of the wrought annealed and as-cast titanium. It should be noted that wrought titanium is usually supplied in the mill-annealed condition [2011Dob]. In the mill-annealed condition, wrought titanium usually exhibits an equiaxed microstructure. This microstructure is characterized by a better balance of room temperature strength and ductility compared to the lamellar microstructure [2011Mar]. As can be seen in Table 4.10, the low ductile nature of the lamellar microstructure of the cast annealed titanium specimens was confirmed. Furthermore, it is reported that the increment of the content of oxygen content in titanium based materials usually leads to reduced ductility [2003Lut, 2006Lam]. It should be understood that the titanium powder used in this work had a higher content of oxygen (0.45 wt. %), which explains the lower values of ductility obtained during tension testing compared to commercial wrought annealed and as-cast titanium.

The tensile properties of titanium and titanium alloys are primarily affected by the microstructural features and chemical composition [2000Don, 2003Lut]. For the lamellar structure, the strength increases with a decreasing size of the α lamellae, while the increase of oxygen content generally leads to reduced ductility [2000Don,

2003Lut, 2006Lam, 2011Dob]. Therefore the lower ductility of the titanium specimens is mainly attributed to the high oxygen content of the starting powder (0.45 wt. %). It was also mentioned in the preceding sections that the HIP and annealing did not alter the vacuum cast lamellar structure of the titanium specimens, but appeared to coarsen the α-Ti phase from a width of approximately 12 to 100 μm during HIP. This is in agreement with the findings of the work by Gil et al. [1995Gil] on the heat treatment of unalloyed titanium at a temperature range of 700−1100°C for 3−120 minutes. In agreement with the literature [2009Fac], the coarsening of the lamellar structure during HIP decreased the tensile strength while the ductility did not change much as shown in Figure 4.46. Therefore it is apparent that the post HIP annealing treatment does not offer any improvement of the tensile properties.

Figures 4.47 and 4.48 show the typical stress-strain curves of unalloyed titanium, which is characterized by a significant plastic deformation. It can be seen that the specimens exhibited a serrated flow in the region of plastic deformation. The literature [1989Her, 2008Pra] mentions that the serrated stress-strain response is typical of unalloyed titanium and other hexagonal close packed metals, and it is normally associated with audible clicks emitted from within the sample as elongation proceeds. In this work, a repetitive clicking sound was emitted from the specimens after the yield stress was exceeded, and the deformation bands (which are believed to be due to twinning deformation) were observed to propagate along the gage length of the fractured specimens as shown in Figure 4.49. The specimens failed by ductile fracture.

By contrast, the sintered unalloyed titanium tested in the HIP+annealed condition suffered a brittle fracture before even reaching the yield strength and without any plastic deformation as shown by the stress-strain curves in Figures 4.50 and 4.52. The very poor ductility, compared to wrought annealed titanium, was caused by the high oxygen content of the starting Ti-6Al-4V powder mix (0.6 wt.%). This finding is in agreement with the literature [2003Lut, 2006Lam]. Finally, it can be seen that for the same chemical composition, the cast+HIP titanium specimens exhibited better tensile properties compared to the pressed and sintered titanium specimens tested in the annealed condition.

5.9.2 Cast and sintered blended elemental Ti-6Al-4V alloy

It was shown earlier that the HIP of the cold pressed and sintered Ti-6Al-4V alloy rods appeared to result in a complete elimination of residual porosity. Work by Božić et al. [2006Bož] demonstrated that the strength of the equiaxed microstructure of the powder metallurgy Ti-6Al-4V is dependent on the amount of residual porosity, with an increase in residual porosity causing a decrease of the tensile strength. From Figure 4.41 and Table 4.13, it can be seen that even though a fully dense equiaxed Ti-6Al-4V specimen was obtained by the HIP of pressed and sintered specimens, the tensile properties were very poor compared to wrought annealed and commercial powder metallurgy Ti-6Al-4V compacts. The poor ductility is attributed to the high oxygen content of the blended Ti-6Al-4V powder (0.6 wt. %). The conventional casting and HIP of the Ti-6Al-4V alloy usually results in a lamellar microstructure, and work by Božić et al. [2006Bož] demonstrated that this structure exhibits better tensile strength compared to the equiaxed α microstructure. In contrast, it can be seen in Table 4.12 that the tensile strength of the vacuum cast and HIP'ed Ti-6Al-4V specimens produced in this work was very low compared to that of the pressed and sintered specimens with a fully dense equiaxed microstructure (Table 4.13). It was observed that a lot of gas was evolved during the vacuum casting of the Ti-6Al-4V billet; which possibly resulted in a lot of surface and subsurface porosity. It is suspected that the evolved gas possibly originated from the master alloy since the melting of pure titanium powder billet during vacuum casting did not release any gases. Similar to the observation by Liu and Welsch [1988Liu], the tensile stress-strain curves in Figures 4.50 to 4.52 confirm that the oxygen concentration of 0.6 wt. % resulted in the brittle fracture of the Ti-6Al-4V alloy specimens before the yield strength could be reached.

5.9.3 Rapidly manufactured pre-alloyed Ti-6Al-4V alloy

As can be seen in Table 4.14, the ductility (elongation) of the as-built tensile specimens was similar to that of wrought Ti-6Al-4V alloy (9%) due to the high purity (0.13% O) of the pre-alloyed powder used as the starting powder. The elongation was also within the range of 4.4−25% found by Murr et al. [2009Mur] during the rapid-layer manufacturing of the Ti-6Al-4V alloy. The reduction-in-area was 67% higher than that of the commercial cast annealed Ti-6Al-4V alloy. The high level of area

reduction is evident when looking at the fractured specimen, which appears to have underwent a significant localized deformation as shown in Figure 4.55. The higher strength of 1284 MPa was possibly caused by the very fine acicular α microstructure of the as-built specimens as shown in Figure 4.35. The strength (UTS and 0.2% yield strength) was also within the range of 900−1450 MPa found in the work by Murr et al. [2009Mur].

Table 4.14 and Figure 4.56 show that the mean UTS decreased by 4% at the annealing temperature of 750°C, while the mean elongation decreased from 9% to 8%. The increment of the annealing temperature to 850°C decreased the mean UTS by 9%, while the mean elongation remained constant at 8%. The decreasing strength was probably caused by the slight coarsening of the acicular α during heat treatment for 2 hours, which is in agreement with the literature [2000Don, 2003Ley, 2003Lut, 2009Fac].The tensile stress-strain curves in Figure 4.57 show that the specimens exhibited a low plastic deformation compared to the unalloyed titanium specimens, which is typical of the Ti-6Al-4V alloy according to Facchini and Molinari [2009Fac].

CHAPTER 6: CONCLUSIONS AND RECOMMENDATIONS

The conclusions drawn from the evaluation of the microstructural features, tensile properties, density, oxygen pick-up and chemistry of pure titanium and Ti-6A-4V alloy produced by spark plasma sintering (SPS), cold pressing and sintering, casting and rapid manufacturing are presented in this section. A decision is then made on the most promising approach for producing titanium-based materials based on the superiority of the properties obtained.

6.1 Conclusions

The evaluation of the materials produced by SPS, CIP and sinter, rapid manufacturing, centrifugal casting and vacuum casting led to the following conclusions

- Attrition milling at 1350C could not reduce the particle size of Ti and Ti-6Al-4V powders due to a shorter milling time
- The fabrication of pure Ti using the SPS and CIP and sinter methods at 1250°C and 1350°C, respectively, results in a homogeneous plate-like α microstructure.
- The SPS produced Ti materials are denser compared to CIP and sintered Ti materials due to pressure aided sintering during the SPS method.
- In contrast, Ti-6Al-4V materials obtained by the CIP and sintered at 1350°C consist of a homogeneous equiaxed α+β microstructure compared to the basket-weave structure of the Ti-6Al-4V alloy produced by the SPS method at 1250°C. The homogeneity is attributed to a higher sintering temperature and prolonged isothermal holding time compared to the SPS method.
- Similar to the pure Ti materials, the Ti-6Al-4V alloy materials obtained by the SPS method are fully dense compared to the CIP and sintered materials due to pressure aided sintering.
- The rapidly manufactured Ti-6Al-4V tensile specimens are highly dense compared to CIP and sintered Ti-6Al-4V materials, and similar to the CIP and sinter method, they also consist of a homogeneous microstructure. The high

density may be attributed to the high power of the laser beam, which translates to high local sintering temperatures during the scanning of layers of powder compared to pressureless sintering at 1350°C. The homogeneity of the rapidly built Ti-6Al-4V tensile specimens may be attributed to the use of pre-alloyed powder, resulting a shorter path for the diffusion of Al and V in α-Ti and β-Ti during laser scanning.

- The density of the Ti and Ti-6Al-4V alloys produced by the CIP and sinter method could be increased further to full density using HIP at 915°C for 120 min under 1000 bar of Ar pressure, and no change in as-sintered microstructural features could be observed due to HIP'ing below the β-transus and slow cooling
- In contrast, the Ti-6Al-4V alloys produced by the SPS method at temperatures in the range of 1200 and 1250°C are denser compared to the rapidly built specimens, confirming the benefits of pressure aided sintering for the SPS method.
- The alloys fabricated by the SPS, CIP and sinter, additive manufacturing all appear to exhibit a deficiency in Al compared to the starting powders and standard requirements for the Ti-6Al-4V alloy for aerospace applications. The deficiency is believed to be due to the evaporation of some of the Al during processing at high temperatures.
- The heat treatment of all as-fabricated materials at temperatures of 750 and 850°C also did not result in changes in the microstructures obtained after HIP heating below the β-transus temperature
- The vacuum cast Ti shows better elongation compared to both CIP and sintered Ti, possibly due to limited absorption of oxygen due to melt-ZrO_2 crucible interaction. The poor tensile ductility is attributed to inherent oxygen and oxygen picked up during high temperature processing of the Ti-6Al-4V materials
- Severe oxygen pick-up and contamination by Zr was confirmed during the vacuum casting of Ti-6Al-4V alloy, which explains the low ductility compared to the alloy produced by the CIP and sinter method.

- The tensile properties are very poor for the materials produced by the CIP and sinter and vacuum casting routes compared to their counterparts reported in the literature.
- Rapid manufacturing results in the Ti-6Al-4V alloy with better ductility compared to all alloys produced in this work. This is due to the high purity of the pre-alloyed Ti-6Al-4V powder used as a starting material compared to the Grade 4 Ti powder used to prepare the blended elemental Ti-6Al-4V powder.
- Therefore, based on microstructural homogeneity, superior tensile properties, low oxygen pick-up and density very close to that required for practical applications, the rapid manufacturing route appears to be the most promising technique for producing solid Ti-based components directly from powder in a single step.

6.2 Recommendations

Based on the results obtained and discussed, the following recommendations are made:

(1) Optimise the attrition milling process to improve particle size reduction and mechanical alloying of the Ti with the Al and V elemental powders

(2) Hydrogenate the spherical Grade 1 titanium powder and mill the hydride powder under an inert atmosphere followed by dehydrogenation at 500°C to obtain a fine irregular shaped titanium powder with a low content of oxygen.

(3) Produce unalloyed titanium specimens directly from the Grade 1 titanium powder using the rapid manufacturing method and compare tensile properties to wrought titanium.

(4) Anneal the as-cast titanium specimens at various temperatures within the recommended range of 650−760°C to clearly establish the effect of annealing temperature and time on the tensile properties.

(5) Anneal the rapidly manufactured TI-6Al-4V specimens slightly above the β transus temperature under an inert atmosphere followed by furnace cooling to obtain a lamellar structure with a better ductility compared to the as-built fine acicular α microstructure.

REFERENCES

[1974Avn] S.H. Avner, Introduction to physical metallurgy, Tokyo: McGraw-Hill, 1974

[1981Smu] J.E. Smugeresky and D.B. Dawson, New titanium alloys for blended elemental powder processing, Powder Technology, 30 (1981) 87-94

[1983Fis] H.F. Fischmeister and E. Arzt, Densification of powders by particle deformation, Powder Metall. 26 (1983) 82-88.

[1983Ram] P. Ramakrishnan, History of powder metallurgy, Indian journal of history of science , Vol. 18, No. 1, (1983) 109-114

[1986Fro] F.H. Froes and J.C. Williams, Titanium Alloys: Powder Metallurgy, Encyclopaedia of Materials Science and Engineering, (M. B. Bever, ed.), Pergamon Press, Oxford, England, (1986) 5089-5094

[1988Liu] Z. Liu and G. Welsch, Effects of oxygen and heat treatment on the mechanical properties of alpha and beta titanium alloys, Metallurgical Transactions A, Vol. 19A, (1988) 527-542

[1989Her] R.W. Hertzberg, Deformation and fracture mechanics of engineering materials: 3rd edition, John Wiley & Sons, (1989) 29

[1990ASM] ASM Handbook: Properties and selection: nonferrous alloys and special-purpose materials, ASM International, Vol. 2, (1990) 594-1898

[1990Eyl] D. Eylon and F.H. Froes, Titanium P/M products, tenth Ed., ASM Handbook, Vol. 2, (1990) 647-660

[1990Lam] S. Lampman, Wrought Titanium and Titanium Alloys: tenth ed., ASM Handbook, vol. 2. (1990) 592-633.

[1991ASM] ASM Handbook, Heat treatment, ASM international, Vol. 4, (1991) 916

[1991Kru] J-P. Kruth, Material incress manufacturing by rapid prototyping techniques , Annals of the CIRP, Vol. 40, No. 2, (1991) 603-614

[1994Hen] S. D. Henry, Fatigue Data Book: Light Structural Alloys, ASM International, Technology & Engineering, (1994) 207

[1995Gil] F.X. Gil, D. Rodriguez and J.A. Planell, Grain growth kinetics of pure titanium, Scripta Metallurgica et Materialia, Vol. 33, No. 8, (1995) 1361-1366

[1996All] P. Allen, Titanium alloy development, Advanced Materials & Processes, 10 (1996) 35-37

[1996Cha] H. Chandler, Heat Treater's Guide: Practices and Procedures for Nonferrous Alloys, ASM International, Materials Park, OH, USA, (1996)

[1996Fuj] T. Fujita, A. Ogawa, C. Ouchi and H. Tajima, Microstructure and properties of titanium alloy produced in the newly developed blended elemental powder metallurgy process, Materials Science and Engineering A, 213 (1996) 148-153

[1996Gil] F.X. Gil Mur, D. Rodríguez and J.A. Planell, Influence of tempering temperature and time on the ed-Ti-6A1-4V martensite, Journal of Alloys and Compounds, 234 (1996) 287-289

[1996Her] R.W. Hertzberg, Deformation and fracture mechanics of engineering materials: 3rd edition, J. Wiley & Sons, (1996) 22

[1998Lut] G. Lütjering, Influence of processing on microstructure and mechanical properties of (α+β) titanium alloys, Materials Science and Engineering A, 243 (1998) 32-45

[1999Ede] L. Ederer, The effect of zinc stearate on the compaction and sintering characteristics of a Ti-6Al-4V hydride-dehydride powder, Master of Engineering Thesis, Department of Mining and Metallurgical Engineering, McGill University, Montreal Canada,(1999) 21-24

[1999Lar] D. Larsen and G. Colvin**,** Vacuum-die casting titanium for aerospace and commercial components, JOM, (1999) 26-27

[1999Lee] W.W. Lee, D.B. Lee, M.H. Kim and S.C. Ur, High temperature oxidation of an oxide-dispersion strengthened NiAl, Intermetallics, 7 (1999) 1361-1366

[2000Don] M.J. Donachie, Titanium: A Technical Guide, Second Ed., ASM International, (2000)

[2000Yas] K. Yasue, G.L. Yu, C.E. Wen and Y. Yamada, Elemental blended powders semisolid forming of Ti-Al based alloys, Journal of Materials Science, 35 (2000) 5927-5932

[2001Chr] J. Chrapoński and W. Szkliniarz, Quantitative metallography of two-phase titanium alloys, Materials Characterization, 46 (2001) 149-154

[2001Dab] V.V. Dabhade, T.R. Rama Mohan, and P. Ramakrishnan, Synthesis of nanosized titanium powder by high energy milling, Applied Surface Science, 182 (2001) 390-393

[2001Ger] S.J. Gerdemann, Titanium process technologies, Advanced Materials Processes, (2001) 41-43

[2001Tos] J.P.V. Tosetti, F.B. Neto and D. Rodrigues, Evaluation of HDH process of Ti-6Al-4V alloy, Third International Latin-American Conference on Powder Technology, (2001) 26-28

[2002Bie] S.G. Ivanova, R.R. Biederman, and R.D. Sisson Jr., Investigation of fatigue crack initiation in Ti-6Al-4V during tensile-tensile fatigue, Journal of Materials Engineering and Performance, Vol. 11, No. 2, (2002) 226-231

[2002Din] R. Ding, Z.X. Guo and A. Wilson, Microstructural evolution of a Ti–6Al–4V alloy during thermomechanical processing, Materials Science and Engineering A, 327 (2002) 233-245

[2002Iva] O.M. Ivasishin, D.G. Savvakin, F. Froes, V. C. Mokson, and K. A. Bondareva, Synthesis of alloy Ti-6Al-4V with low residual porosity by a powder metallurgy method, Powder Metallurgy and Metal Ceramics, Vol. 41, No. 7-8, (2002) 382-390

[2002Kim] M.-G. Kim, S.K. Kim, and Y.-J. Kim, Effect of mold material and binder on metal-mold interfacial reaction of investment castings of titanium alloys, Materials Transactions, Vol. 43, No. 4, (2002) 745-750

[2002Nal] R.K. Nalla, B.L. Boyce, J.P. Campbell, J.O. Peters and R.O. Ritchie, Influence of microstructure on high-cycle fatigue of ti-6al-4v: bimodal vs. lamellar structures, Metallurgical And Materials Transactions A, Vol. 33A, (2002) 899-918

[2002Kat] I. Katzarov, S. Malinov, and W. Sha, Finite element modelling of the morphology of β to α phase transformation in Ti-6Al-4V alloy, Metallurgical and materials transactions A, Vol. 33A, (2002) 1027-1040

[2003Cha] M. Chandrasekaran and Z.S. Xia, Effect of alloying time and composition on the mechanical properties of Ti alloy, Materials Science and Engineering A, 394 (2005) 220-228

[2003Fil] R. Filip, K. Kubiak, W. Ziaja and J. Sieniawski, The effect of microstructure on the mechanical properties of two-phase titanium alloys, Journal of Materials Processing Technology, 133 (2003) 84-89

[2003Lut] G. Lütjering and J.C. Williams, Titanium, Springer-Verlag Berlin Heidelberg, (2003)

[2003Ley] C. Leyens and M. Peters, Titanium and titanium alloys: Fundamentals and Applications, Wiley-VCH Verlag GmbH& Co. KGaA, Weinheim, (2003)

[2004Alm] D.E. Alman and S.J. Gerdemann: Powder Metall. Sci. Technol. Briefs, Vol. 6 (1), (2004), 11-14.

[2004AST] Standard test methods for tension testing of metallic materials [Metric], ASTM international, United States (2004)

[2004Don] D. F. Heaney and R. M. German, Advances in the Sintering of Titanium Powders, PM Lightweight and Porous Materials Euro PM, (2004)

[2004Hun] C.-C. Hung, G.-L. Hou, C.-C. Tsai and C.-C. Huang, Pure titanium casting into zirconia-modified magnesia-based investment molds, Dental Materials, Vol. 20, No. 9, (2004) 846-851.

[2004Žit] M. Žitňanský and L. Čaplovič, Effect of the thermomechanical treatment on the structure of titanium alloy Ti6Al4V, Journal of Materials Processing Technology, Vol. 157-158, (2004) 643-649

[2005Zhe] A. Zhecheva, W. Sha, S. Malinov and A. Long, Enhancing the microstructure and properties of titanium alloys through nitriding and other surface engineering methods, Surface & Coatings Technology, Vol. 200, Issue 7, (2005) 2192-2207

[2005Pan] B.B. Panigrahi, M.M. Godkhindi, K. Das, P.G. Mukunda and P. Ramakrishnan, Sintering kinetics of micrometric titanium powder, Materials Science and Engineering A, 396 (2005) 255-262

[2006Bož] D. Božić, I. Cvijović, M. Vilotijević and M. T. Jovanović, The influence of microstructural characteristics on the mechanical properties of Ti6Al4V alloy produced by the powder metallurgy technique, J. Serb. Chem. Soc., Vol. 71, Nos. 8–9, (2006) 985-992

[2006Dab] V. V. Dabhade, B.B. Panigrahi, M.M. Godkhindi, T.R. Rama Mohan and P. Ramakrishnan, Dilatometry of attrition milled titanium powders, Materials Research Bulletin, 41 (2006) 2111-2122

[2006Han] D. Handtrack, F. Despang, C. Sauer, B. Kieback, N. Reinfried and Y. Grin, Fabrication of ultra-fine grained and dispersion-strengthened titanium materials by spark plasma sintering, Materials Science and Engineering A, Vol. 437, Issue 2, (2006) 423-429

[2006Jov] M.T. Jovanovic´, S. Tadic´, S. Zec, Z. Miškovic´ and I. Bobić, The effect of annealing temperatures and cooling rates on microstructure and mechanical properties of investment cast Ti–6Al–4V alloy, Materials and Design, Vol. 27, Issue 3, (2006) 192-199

[2006Lam] M. Lamirand, J.-L. Bonnentien, G. Ferrière, S. Guérin and J.-P. Chevalier, Effects of interstitial oxygen on microstructure and mechanical properties of ti-48al-2cr-2nb with fully lamellar and duplex microstructures, Metallurgical and Materials Transactions A, Vol. 37A, (2006) 2369-2378

[2006Liu] Y. Liu, L. Chen, W. Wei, H. Tang, B. Liu, and B. Haung, Improvement of ductility of powder metallurgy titanium alloys by addition of rare earth element, J. Mater. Sci. Technol., Vol.22, No.4, (2006) 465-469

[2006Pan] B.B. Panigrahi and M.M. Godkhindi, Dilatometric sintering study of Ti–50Ni elemental powders, Intermetallics, Vol. 14, Issue 2, (2006) 130-135

[2007Ber] M.J. Bermingham, S.D. McDonald, M.S. Dargusch and D.H. StJohn, Microstructure of cast titanium alloys, Materials Forum, Vol. 31,(2007) 84-89

[2007Dab] V.V. Dabhade, T.R. Rama Mohan and P. Ramakrishnan, Nanocrystalline titanium powders by high energy attrition milling, Powder Technology, 171 (2007) 177-183

[2007Kru] J.-P. Kruth, G. Levy, F. Klocke and T.H.C. Childs, Consolidation phenomena in laser and powder-bed based layered manufacturing, CIRP Annals - Manufacturing Technology, Vol. 56, Issue 2, (2007) 730-759

[2007Nag] CH. RVS. Nagesh and C. S. Ramachandran, Electrochemical process of titanium extraction, Transactions of Nonferrous Metals Society of China, 17 (2007) 429-433

[2007Nic] R. Nicula, F. Lüthen, M. Stir, B. Nebe and E. Burkel, Spark plasma sintering synthesis of porous nanocrystalline titanium alloys for biomedical applications, Biomolecular Engineering, 24 (2007) 564-567

[2007Sui] Y.-W.Sui, B.-S Li, A.-h. Liu, H. Nan, J.-J. Guo and H.-Z. Fu, Microstructures and hardness of Ti-6Al-4V alloy staging castings under centrifugal field, Transactions of Nonferrous Metals Society of China, 18 (2008) 291-296

[2008Lap] R. Lapovok, D. Tomus and B.C. Muddle, Low temperature compaction of Ti-6Al-4V powder using equal channel angular extrusion with back pressure, Materials Science and Engineering A, 490 (2008) 171-180

[2008Nei] O.D. Neikov, S.S. Naboychenko, I.V. Murashova, V. G. Gopienko, I.V. Frishberg and D.V. Lotsko, Handbook of non-ferrous metal powders: Technologies and Applications, Elsevier Ltd. (2008) 314-323

[2008Pra] K. Prasad and V. K. Varma, Serrated flow behavior in a near alpha titanium alloy IMI 834, Materials Science and Engineering A, 486 (2008) 158-166

[2008STA] Standard specification for titanium and titanium alloy strip, sheet, and plate: Designation: B 265 – 08b, ASTM International (2008)

[2009Alc] J. Alcisto, A. Enriquez, H. Garcia, S. Hinkson, T. Steelman, E. Silverman, P. Valdovino, H. Gigerenzer, J. Foyos, J. Ogren, J. Dorey, K. Karg, T. McDonald and O.S. Es-Said, Tensile Properties and Microstructures of Laser-Formed Ti-6Al-4V, Journal of Materials Engineering and Performance, Vol. 20, No. 2, (2011) 203-212

[2009AST] ASTM B 265 – 08b, Standard specification for titanium and titanium alloy strip, sheet, and plate, ASTM International, United States, 2009

[2009Fac] L. Facchini, E. Magalini, P. Robotti and A. Molinari, Microstructure and mechanical properties of Ti-6Al-4V produced by electron beam melting of pre-alloyed powders, Rapid Prototyping Journal, Vol. 15, Issue 3, (2009) 171-178

[2009Geb] A. Gebert, F. Gostin, U. Kühn and L. Schultz, Corrosion of a Zr-based bulk metallic glass with different surface finishing states, ECS Transactions, Vol. 16, No. 32, (2009) 1-7

[2009Gro] Z. Gronostajski, P. Bandoła and T. Skubiszewski, Influence of cold and hot pressing on densification behaviour of titanium alloy powder Ti6Al4V, Archives Of Civil And Mechanical Engineering, Vol. 9, No. 2, (2009) 48-57

[2009Hua] T. Hua, C. Jing, Z. Fengying, L. Xin and H. Weidong, Microstructure and mechanical properties of laser solid formed ti-6al-4v from blended elemental powders, Rare Metal Materials and Engineering, Vol. 38, No.4, (2009) 0574-0578.

[2009Jov] M. T. Jovanović, I. Bobić, Z. Mišković and S. Zec, Precision cast Ti-based alloys – microstructure and mechanical properties, Metalurgija-Journal of Metallurgy, Scientific Journal, Vol. 15, No. 1-4, (2009) 53-69

[2009Mur] L.E. Murr, S.A. Quinones, S.M. Gaytan, M.I. Lopez, A. Rodela, E.Y. Martinez, D.H. Hernandez, E. Martinez, F. Medina and R.B. Wicker, Microstructure and mechanical behavior of Ti–6Al–4Vproduced by rapid-layer manufacturing, for biomedical applications, Journal of the mechanical behavior of biomedical materials, Vol. 2, (2009) 20-32

[2009Rob] I. M. Robertson and G.B. Schaffer, Some Effects of particle size on the sintering of titanium and a master sintering curve model, Metallurgical and Materials Transactions A, Vol. 80, Issue 8, (2009) 1968-1979

[2009Soe] S. Seong, O. Younossi, B.W. Goldsmith, T. Lang and M. Neumann, Titanium: Industrial base, price trends, and technology initiatives, Rand Corporation, (2009)

[2009Vin] A. Vinicius and R Henriques, Titanium production for aerospace applications, Journal of Aerospace Technology and Management, Vol. 1, No. 1, (2009) 7-17

[2009Wil] M. de Wild, R Schumacher, S. Fabbri, A. Yildiz and E. Schkommodau, Analysis and Surface Modification of Rapid Prototyped Titanium Structures, European Cells and Materials, Vol. 17, Suppl. 1, (2009) 6

[2009Zha] S. Zhang, X. Lin, J. Chen and W. Huang, Heat-treated microstructure and mechanical properties of laser solid forming Ti-6Al-4V alloy, Rare Metals, Vol. 28, Issue 6, (2009) 537-544

[2010Fac] L. Facchini, E. Magalini, P. Robotti, A. Molinari, S. Höges and K. Wissenbach, Ductility of a Ti-6Al-4V alloy produced by selective laser melting of pre-alloyed powders, Rapid Prototyping Journal, Vol. 16, No. 6, (2010) 450-459

[2010Ger] S.J. Gerdemann and P.D. Jablonski, Compaction of titanium powders, Metallurgical and Materials Transaction A, Vol. 42, No. 5, (2011)-1325-1333

[2010Rob] I. M. Robertson and G. B. Schaffer, Swelling during sintering of titanium alloys based on titanium hydride powder, Powder Metallurgy, Vol. 53, No. 1, (2010) 27-33

[2010Yua] B.G. Yuan, C.F. Li, H.P. Yu and D.L. Sun, Influence of hydrogen content on tensile and compressive properties of Ti–6Al–4V alloy at room temperature, Materials Science and Engineering A, 527 (2010) 4185-4190

[2011Chen] W. Chen, Y. Yamamoto , W.H. Peter , S.B. Gorti, A.S. Sabau, M.B. Clark, S.D. Nunn, J.O. Kiggans, C.A. Blue, J.C. Williams, B. Fuller and K. Akhtar, Cold compaction study of Armstrong Process Ti-6Al-4V powders, Powder Technol. (2011)

[2011Dob] R. Dobeson, N. Petrazoller, M. Dargusch and S. McDonald, Effect of thermal exposure on the room temperature tensile properties of Grade 2 titanium, Materials Science and Engineering A, 528 (2011) 3925-3929

[2011Ger] S. J. Gerdemann and P. D. Jablonski, Compaction of titanium powders, Metallurgical and Materials Transactions A, Volume 42 A,(2011) 1325-1333

[2011Gos] X .Goso, and A. Kale, Production of titanium metal powder by the HDH process, The Southern African Institute of Mining and Metallurgy, Advanced Metals Initiative, Light Metals Conference, Misty Hills, Muldersdrift, Johannesburg, South Africa, (27-29 October 2010). pp. 292-305.

[2011Ibr] K. M. Ibrahim, M. Mhaede and L. Wagner, Mechanical characterization of cp-Ti produced by investment casting, Trans. NonFerrous Met. Soc. China, Vol. 21, (2011) 1735-1740

[2011Koi] M. Koike, P. Greer, K. Owen, G. Lilly, L. E. Murr, S. M. Gaytan, E. Martinez and T. Okabe, Evaluation of titanium alloys fabricated using rapid prototyping technologies-electron beam melting and laser beam melting, Materials, Vol. 4, (2011)1776-1792

[2011Mar] P.E. Markovskya and S.L. Semiatin, Tailoring of microstructure and mechanical properties of Ti–6Al–4V with local rapid (induction) heat treatment, Materials Science and Engineering A, 528 (2011) 3079-3089

[2011Oos] S.J. Oosthuizen, In search of low cost titanium: the Fray Farthing Chen (FFC) Cambridge process, The Journal of The Southern African Institute of Mining and Metallurgy, Vol. 111, (2011) 199-202

[2011Zha] W. Zhang, Z. Zhu and C.Y. Cheng, A literature review of titanium metallurgical processes, Hydrometallurgy, 108 (2011) 177-188

[2011Zhu] Z. Zhu, W. Zhang and C. Y. Cheng, A literature review of titanium solvent extraction in chloride media, Hydrometallurgy, 105 (2011) 304-313

[2012Bol] L. Bolzoni, E.M. Ruiz-Navas, E. Neubauer and E. Gordo, Mechanical properties and microstructural evolution of vacuum hot-pressed titanium and Ti–6Al–7Nb alloy, Journal of The Mechanical Behavior Of Biomedical Materials, 9 (2012) 91-99

[2012Bol[a]] L. Bolzoni, E.M. Ruiz-Navas, E. Neubauer and E. Gordo, Inductive hot-pressing of titanium and titanium alloy powders, Materials Chemistry and Physics, 131 (2012) 672-679

[2012Bol[b]] L. Bolzoni, P.G. Esteban, E.M. Ruiz-Navas and E. Gordo, Mechanical behaviour of pressed and sintered titanium alloys obtained from master alloy addition powders, Journal of the Mechanical Behavior of Biomedical Materials,15 (2012) 33-45

[2012Chen] W. Chen, Y. Yamamoto, W.H. Peter, M.B. Clark, S.D. Nunn, J.O. Kiggans, T.R. Muth, C.A. Blue, J.C. Williams and K. Akhtar, The investigation of die-pressing and sintering behavior of ITP CP-Ti and Ti-6Al-4V powders, Journal of Alloys and Compounds, 541 (2012) 440-447

[2012Gu] D. Gu, Y.-C. Hagedorn, W. Meiners, G. Meng, R. J. S. Batista, K. Wissenbach and R. Popraw, Densification behavior, microstructure evolution, and wear performance of selective laser melting processed commercially pure titanium, Acta Materialia, Vol. 60, Issue 9, (2012) 3849-3860

[2012Mah] A.M. Soufiani, F. Karimzadeh and M.H. Enayati, Formation mechanism and characterization of nanostructured Ti6Al4V alloy prepared by mechanical alloying, Materials and Design, 37 (2012) 152-160

[2012Sar] S. Pattnaik, D.B. Karunakar and P.K. Jha, Developments in investment casting process-A review, Journal of Materials Processing Technology, Vol. 212, Issue 11, (2012) 2332-2348

[2012Vra] B. Vrancken, L. Thijs, J.-P. Kruth and J. Van Humbeeck, Heat treatment of Ti6Al4V produced by selective laser melting: Microstructure and mechanical properties, Journal of Alloys and Compounds, 541 (2012) 177-185

[2012Wan] R. Wanhill and S. Barter, Fatigue of beta processed and beta heat-treated titanium alloys, Springer Briefs in Applied Sciences and Technology, (2012)

[2013Qiu] C. Qiu, N.J.E. Adkins and M.M. Attallah, Microstructure and tensile properties of selectively laser-melted and of HIPed laser-melted Ti–6Al–4V, Materials Science & Engineering A, 578 (2013) 230-239

[2013Red] R. Red, A.A. Nofal and A.-H.A. Hussein, Effect of quenching temperature on the mechanical properties of cast Ti-6Al-4V Alloy, Journal of Metallurgical Engineering, Vol. 2, Issue 1, (2013) 48-54

[2013Sie] J. Sieniawski, W. Ziaja, K. Kubiak and M. Motyka, Titanium Alloys - Advances in Properties Control: Chapter 4, InTech, (2013) 69-80

[2014Sho] J. H. Shon, I.-B. Song, K.-S. Cho, Y.-I Park, J.-K. Hong, N.-K. Park and M.-H. Oh, Effect of particle size distribution on microstructure and mechanical properties of spark plasma sintered titanium from CP-Ti powders, International Journal of Precision Engineering and Manufacturing, Vol. 15, Issue 4, (2014) 643-647

[2014Xu] X. Xu G. L. Nash and P. Nash, Sintering mechanisms of blended Ti6Al4V powder from diffusion path analysis, J Mater Sci, Vol. 49, (2014) 994–1008